UNIVERSITY OF CALIFORNIA,

IRVINE

Optimization of a microfluidic tissue dissociation platform with incorporation of an acoustic cell elution module

DISSERTATION

submitted in partial satisfaction of the requirements

for the degree of

DOCTOR OF PHILOSOPHY

In Chemical and Biomolecular Engineering

by

Marzieh Aliaghaei

Dissertation Committee:

Professor Jered Haun, Chair

Professor Tayloria Adams

Professor Abe Lee

Professor Kai Kessenbrock

2021

DEDICATION

To

my beloved parents and siblings

in recognition of their worth

TABLE OF CONTENTS

LIST OF FIGURES

LIST OF TABLES

ACKNOWLEDGEMENTS

I would like to express the deepest appreciation to my advisor and committee chair, Dr. Jered B. Haun for all his guidance and mentorship over the past five years through every step of my research. Your endless help and support throughout my graduate work has made me a better researcher. This work would not have been possible without his constant inspiration, enthusiasm, encouragement, patience, and passion. I would like to thank my committee members for providing me with their insight and expertise on various projects and collaborations. I am grateful to all their advice and guidance that I received through our fruitful discussions. I would also like to thank my other qualifying exam committee members for their critiques during my advancement exam. My sincerest gratitude to all members of the Haun lab. I would like to thank my mentor Jeremy Lombardo for introducing me to the world of microfluidic tissue processing, my lab mates for their help at various stages of my work, and my undergraduate students for their passion and willingness to learn from me. Special thanks to the Fleishman lab for animal work involved in my projects. Lastly, I would like to extend my gratitude to the Center for Advanced Design & Manufacturing of Integrated Microfluidics (CADMIM), National Cancer Institute.

CURRICULUM VITAE

Marzieh Aliaghaei

EDUCATION

University of California, Irvine

Ph.D., Chemical and Biomolecular Engineering Jan 2021

Dissertation: "Development of integrated microfluidic devices platform and protocol optimization for digestion, dissociation and filtration of Tissues and organs into Single Cells."

Amirkabir University of Technology

M.Sc., Polymer Engineering June 2010

Thesis: "Development of an injectable drug delivery chitosan hydrogel based on rheological characteristics."

Amirkabir University of Technology

B.Sc., Polymer Engineering June 2008

Journal Publications

M. Aliaghaie, et al., "**Investigation of gelation mechanism of an injectable hydrogel based on chitosan by rheological measurements for a drug delivery application**", *Soft Matter, 2012,8, 7128-7137.*

M. Aliaghaie, et al., "**Microfluidic platform accelerates tissue processing into single cells for molecular analysis and primary culture models**", *Nat Communs, 2021, 12, 2858.*

Podium Tasks

M. Aliaghaei, J. Lombardo and J. B. Haun. Microfluidic Tissue Processing Platform for Single Cell Analysis and Primary Cell Isolation. Presented at Biomedical Engineering Society virtual meeting. Oct 2020.

Poster Presentations

M. Aliaghaei, J. Lombardo and J. B. Haun. Scaling up microfluidic digestion for high throughput processing of tissue into single cells. Presented at Center for Advanced Design and Manufacturing of Integrated Microfluidics industry advisory board meeting. Irvine, CA. Feb 2020.

M. Aliaghaei, J. Lombardo and J. B. Haun. Integrated Microfluidic Tissue Processing Platform for Single Cell Analysis. Presented at Center for Advanced Design and Manufacturing of Integrated Microfluidics industry advisory board meeting. Irvine, CA. Feb 2019.

ABSTRACT OF THE DISSERTATION

Optimization of microfluidic tissue dissociation platform with incorporation of an acoustic cell elution module for new applications

By Marzieh Aliaghaei

Doctor of Philosophy in Chemical and Biomolecular Engineering

University of California, Irvine,

2021

Professor Jered B. Haun, Chair

Single cell analysis studies have dramatically increased in the past decade, transforming our understanding of cellular heterogeneity in healthy and diseased tissues. However, the dissociation of tissues as the first step in single cell analysis procedure continues to introduce artifacts to the result. Conventional dissociation methods include manual processing steps that make this process time consuming, laborious, and erroneous. Cell aggregation causes underestimation of single cell concentration. Moreover, chemical, and enzymatic treatments can damage cellular protein expression in long exposure times. Therefore, it is crucial to develop a universal approach for single cell preparation with minimum processing time. Microfluidic devices propose various options to make single cell preparation, hands-free, accurate, and predictable. Our lab has developed a microfluidic platform including Digestion, Dissociation, and Filtration devices for tissue dissociation to

single cells to automate the single cell preparation while optimizing single cell yields and maintaining cell viability. Each device has its standalone function whereas it can be integrated with other devices in the platform. I optimize the processing conditions for the dissociation of heat and liver tissue as two soft and rigid tissues to achieve highest viability and cell yield. In the next step, dissociation of aggregates with the Integrated Dissociation/Filtration (IDF) device is studied to understand the involved dissociation mechanisms of each module and their connection with cell-cell and cell-ECM interactions to improve cell yield for each cell type. This study will help us to optimize processing condition toward higher cell yield while reducing the processing time. Then, the effect of pulsatile flow versus the steady shear flow is studied on performance of IDF in tissue dissociation. Next, Digestion device is added before IDF device to study the effect of flow rate on cell liberation rate. Finally, a new device will be developed to be integrated with this platform. This device will continuously separate cells from our platform with acoustic forces to increase the overall efficiency in terms of cell yield and functionality.

CHAPTER 1: Introduction

1.1. Single cell analysis

Traditional cell assays provide an average response of a cell population. However, it cannot be representative of each cell inside the population because of cellular heterogeneity[1]. It also prevents us from access to important information about a small subpopulation of cells that may determine the behavior of the whole population[2]. For example, in regenerative medicine, specific stem cell population in a tissue is of interest since it is responsible for regeneration in response to injury [3].Full understanding of individual cells and cell-to-cell variation in a population is important for precision medicine, too[4-6]. Single cell analysis will tackle these problems while it facilitates obtaining an insight into the interaction between the environment and cellular activities[7]. Also, Recent cell atlasing efforts, like the Human Cell Atlas Initiative, have also begun cataloguing cellular heterogeneity in tissues and organs in order to assemble comprehensive cell reference maps. These maps then serve as a basis for further research and for guiding disease diagnosis and treatment[8-10]. Moreover, single cell analysis can identify the role of specific cell types and their molecular events on development of diseases[1, 11-13]. As a result, over the past several years, tissues are increasingly being analyzed at the single cell level.

Single cell analysis is a measurement of transcription, translation, regulatory, and signaling events within individual cells at the molecular level[14]. It enables us to understand how cell events link to the behavior of tissue, organs, and whole organism[15]. Cell-based analysis platforms such as flow cytometry, mass cytometry, and single cell

sequencing are ideally positioned to assess cellular heterogeneity[16-18]. Flow cytometry has been able to examine complex cellular systems using parameters like size, granularity and fluorescent features of the cells derived from antibodies or dyes to analyze and differentiate cells. Mass cytometry has leveraged the ability of cytometry by combining flow cytometry and mass spectrometry and adding metal-conjugated antibodies to overcome spectral limits of fluorescent proteins[19]. Flow cytometry and mass cytometry both characterize cells in a high throughput manner using protein-specific antibodies and dyes for up to ~50 parameters per cell, based on known surface or intracellular markers present on cell types of interest. As an alternative, qPCR can be used for quantification of single cell mRNA levels. It offers rapid and highly quantitative assay for single-cell gene expression in the absence of specific antibodies. However, it also requires measurement of a pool of genes which limits its potential for detection of new genes and proteins[20]. As a result, there has been substantial focus on development of new methods for unbiased molecular profiling of single cells based on next-generation sequencing. Next generation sequencing and recent advances in single cell omics technologies have enabled the study of the genome, transcriptome, epigenome, and proteome at the level of individual cells. Single cell RNA sequencing (scRNA-seq) provides a particularly powerful method for unbiased grouping of 2 cell types and subpopulations, without prior knowledge of marker proteins or genes of interest, and has led to discoveries of new cell types, cellular states, and cell-type specific markers[21]. These technologies, however, all require single cell suspensions to analyze, and are thus hindered by the difficulty of dissociating tissues to the single cell level.

1.2. Single cell preparation

To study biology at the resolution of single cell, different steps must be done including tissue dissociation, cell sorting, isolation, lysis, and analysis. The first step toward single cell analysis is breaking down the tissue to single cells. This process must disrupt extracellular matrix (ECM) which holds the cells together in a 3D structure. Different tissues vary in ECM composition and stiffness. Therefore, dissociation protocol should be optimized for each specific tissue of interest. Optimization of this process is of high importance since any error can propagate to the downstream assay and impact the data. It is vital to choose a process for single cell preparation that ends up with cells as true representatives of their origin[14].

In conventional methods, mechanical and enzymatic processes are used for tissue dissociation. The intact tissue is obtained via biopsy and then it is incubated with enzymes such as collagenase to digest ECM. Exposure to chelating agents such as Ethylenediaminetetraacetic acid (EDTA) disrupts cell junctions regulated by cadherin proteins though binding to Ca^{2+}. After chemical exposure, a cell suspension can be achieved via mechanical agitation. A lot of studies have been done to optimize cell yield and viability in these protocols for different tissues empirically by changing parameters like enzyme type and concentration, incubation time and temperature, agitation methods, etc.[22-24]. It is also important to know that these parameters need optimization for different tissue types based on their clinical method of preservation[25].

This process is time and labor-consuming and increases the contamination risk, operator error, and variability. Mechanical dissociation is usually done through repeated pipetting which can be poorly controlled and results in variations among different samples

in different laboratories. Furthermore, the digestion process may result in a loss of cell surface protein expression which impacts the sorting via Fluorescent activated cell sorting (FACS). It can also affect the gene expression and phenotype. In summary, the process of single cell preparation is the greatest source of unwanted technical variations and errors in single cell analysis[26]. Therefore, the method should be optimized to introduce the least possible artifact[27]. The optimum protocol yields the highest number of viable cells in the shortest duration with the least effect on cellular phenotype and expression[28]. Currently, there are few commercially available tissue dissociation platforms. The GentleMACs system by Miltenyi is one frequently referenced in literature. It consists of a disposable conical that is filled with minced tissue and enzymatic solution, heated, and blended using a rotating screw to generate shear forces to break apart tissue. This technology is a Rotor/stator homogenizer which runs at 2700 rpm with a gap of 300-500 which will expose the tissue to high level of shear of 310-45000 Pa which can damage the cells[29]. IncellPrep by IncellDx is a system that uses rotating blades to mechanically break apart small pieces of tissue without the use of enzymes. Also, tissue dissociation based on applying pestle array to grind tissues against the side walls of standard microtiter plates have been developed[30]. However, these systems are costly (~$1000-$5000), only allow for semi-automated tissue dissociation in poorly defined shear environments, and still require an additional cell straining step before downstream single cell analyses. More importantly, this approach can damage the cells and cause stress-induced genomic transcription. As a result, there remains a critical need for technologies that can further standardize and automate the complete dissociation of tissues into single cell suspensions. Microfluidics has emerged in this field and shown good potential which will be discussed in the next section.

1.3. Microfluidics

Application of microfluidic devices has the potential to minimize unwanted variations in tissue dissociation for single cell analysis[26, 31]. Small length scales and laminar flow in microfluidics provide benefits like diffusion dominant transport, portability, disposability, lower cost, automation, and precision. On the other hand, miniaturization of single cell separation ends up with higher compatibility to downstream microfluidic steps and increases the possibility of integration to one platform and less variability because of operator error.

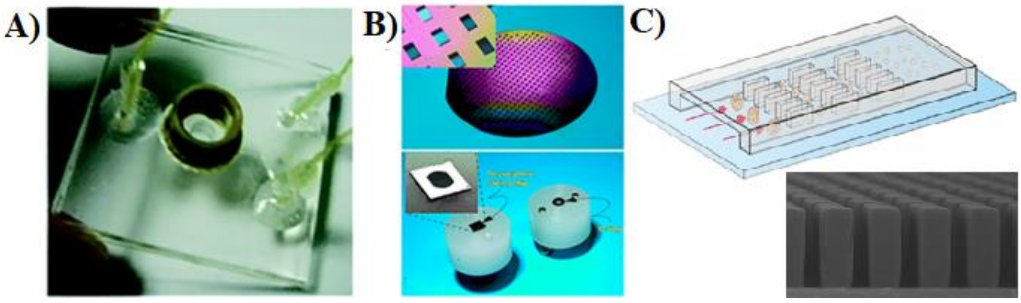

Figure 1-**Microfabricated devices for tissue dissociation**. A) a chip comprised of an open tissue chamber for whole tissue culture and dissociation. reproduced from [32]. B) dissociation grid assembled into the silicon wafer. Reproduced from [33] c) schematic illustration of μ-CDC for neurosphere dissociation. Reproduced from [34]

Although microfluidic devices have been broadly studied in single cell analysis field including cell purification, sorting, and lysis, little attention has been given to tissue dissociation. Toward this goal, Hattersley et al. developed a microfluidic device for tissue perfusion with collagenase (Figure 1A). Although this process minimizes the contamination risk and results in a desirable yield, it lasts for about 2 hours, which is unsuitable for gene

expression analysis[32]. Another microfluidic device called Biogrid was introduced by Wellman et al. for the dissociation of neurospheres (Figure 1 B). Neurospheres are aggregates of neural stem and progenitor cells isolated from the embryonic and adult central nervous system (CNS), grown in a suspension. Biogrid, an array of micrometer silicon knife edges provided a non-enzymatic method for dissociation of neurospheres. However, dissociation into single cells was not achieved[33]. Toward the same goal, Lin et al. developed μ-CDC containing a microchannel with arrayed micropillars (Figure 1 C). However, cell viability and sphere reformation after μ-CDC dissociation are lower than chemical treatment[34].

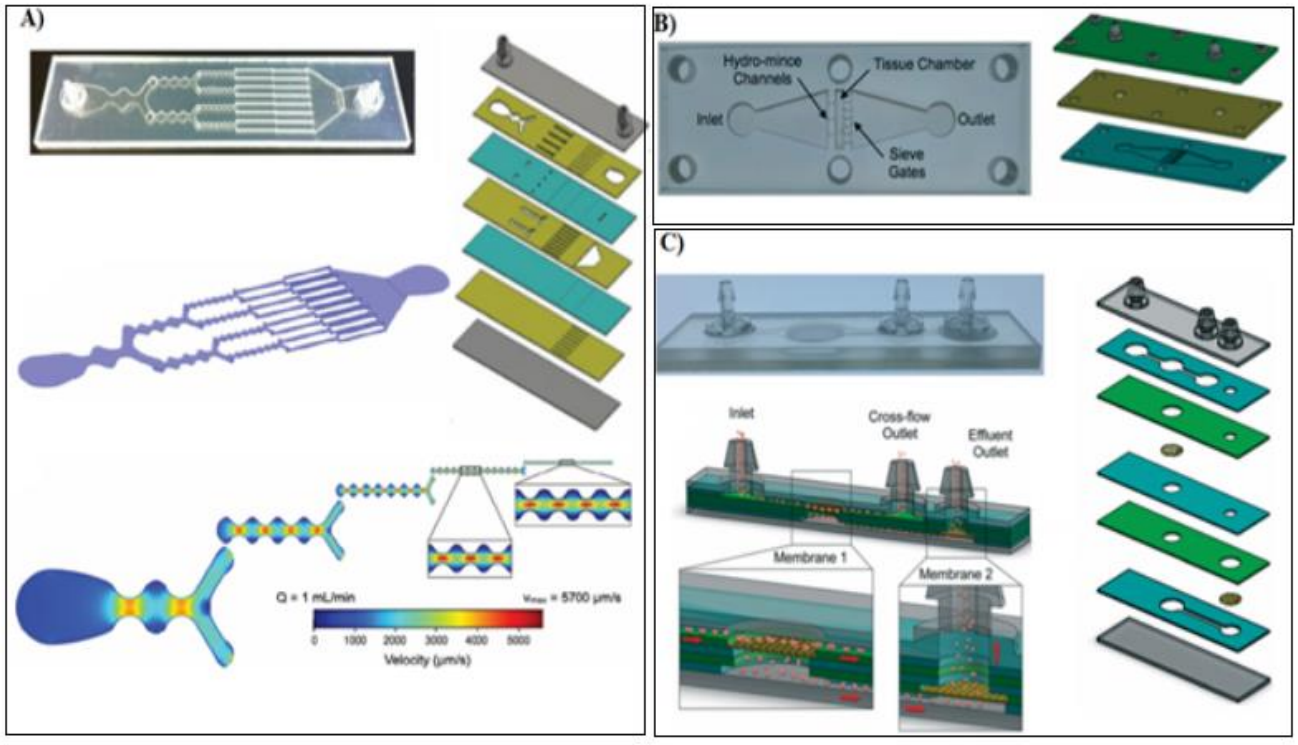

Figure 2- **Picture, schematic and exploded view of the pressure lamination fabrication** A) Dissociation Device B) Digestion Device C) Filtration Device [35-37]

Qiu et al. introduced a microfluidic device for dissociation of tumor tissue for the first time. The device channels narrow down in 5 steps from millimeters to hundreds of microns while constriction and expansion along each channel called hydrodynamic micro-scalpels, provide fluid jet for breaking down the tissue into single cells. It is shown that the cell yield is significantly augmented while still maintaining viability. Furthermore, the processing time goes down to ten minutes which is critically important for commercialization and retaining cellular functionality[35]. It is also beneficial since shorter processing time will reduce the risk of stress induced gene transcription which was mentioned in our recent work[38].

Upstream the Dissociation device, Digestion device is required where the tissue can be loaded, and cell suspension will be collected from the output. This technology offers higher cell yield compared to traditional method with significantly shorter processing time. More importantly, it exposes cells to well defined laminar flow with shear stresses in range of 50 Pa in opposite to commercially available systems like Miltenyi GentleMACS, for this application[39]. One cm long tissue with a 1 mm diameter circular cross-section (Similar to needle biopsy sample) is loaded into the tissue chamber on the device. A series of fluidic channels upstream of the chamber provides the high-velocity fluid jet directed into the tissue called “hydro-mincing”. Then, fluidic channels located downstream of the chamber act as a sieve to retain the tissue and large aggregates while allowing single cells and enzyme to be recirculated. This device applies pulsatile flow provided by a peristaltic pump to recirculate the enzyme over the tissue embedded device[37].

Downstream the Dissociation device, the Filtration device has been designed to offer a label-free, cost-effective, simple, and rapid approach for single cell filtration by embedding one/two nylon mesh membranes into laser cut laminated devices[36, 40].

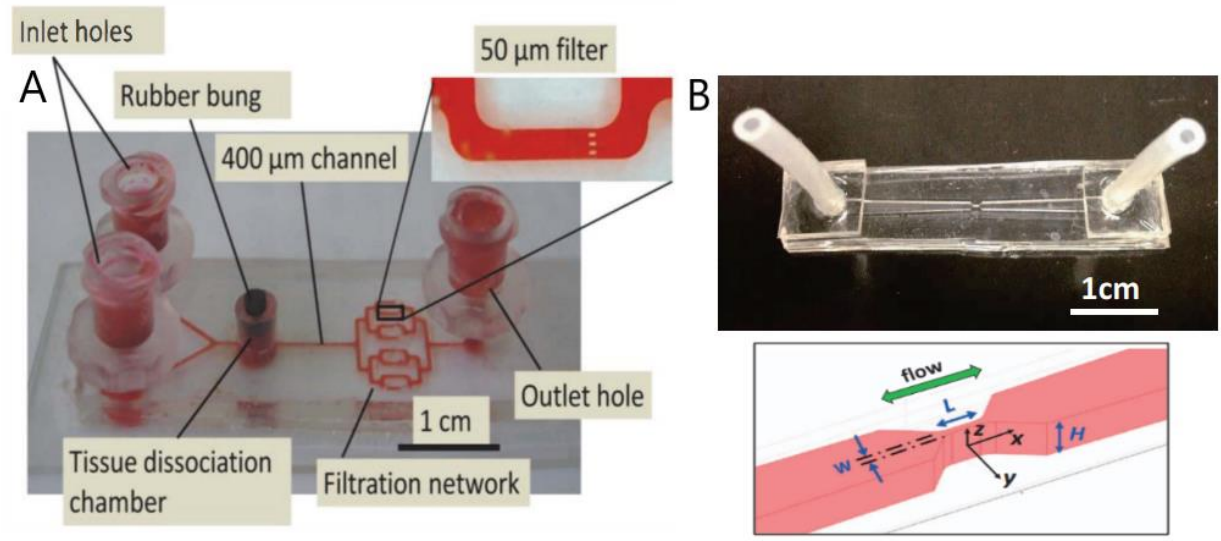

Figure 3- **Other tissue dissociation devices**. A) A photograph of dissociation device for dissociation of endometrial tissue to isolate stem cells with a chamber for loading tissue, filtration network, inlets for enzyme and culture medium and outlet[41] B) A photograph and drawing of the microfluidic device for dissociation of brain tissue into viable single neurons featuring a constriction at its center[42].

It is worth mentioning that some attempts for development of tissue dissociation microfluidic devices have been done in parallel with other groups. Al-Mofty et al proposed a microfluidic platform for tissue dissociation in clinical applications which lacks competitiveness in flow rate and efficiency compared to our platform. Also, the cell yield is not enough for downstream single cell analysis[43]. Another group have proposed a miniaturized platform for endometrial tissue to isolate endometrial stem cells suitable for

various stem cell-based therapies[41]. This study doesn't provide quantitative results and comparison with current manual methods. Another microfluidic device has been offered for brain tissue dissociation under oscillatory flow field[42]. This technology needs a long-time processing which is not favorable for single cell preparation.

While more studies are required for optimization of tissue dissociation platform, our studies showed a necessity for continuous isolation of cells from the system. Our solution was development of an acoustic device which can be integrated with other modules in our platform. Since our final aim is proposing an acoustofluidic device for cell isolation, the final section of the background will be dedicated to acoustofluidics.

1.4. Acoustofluidics

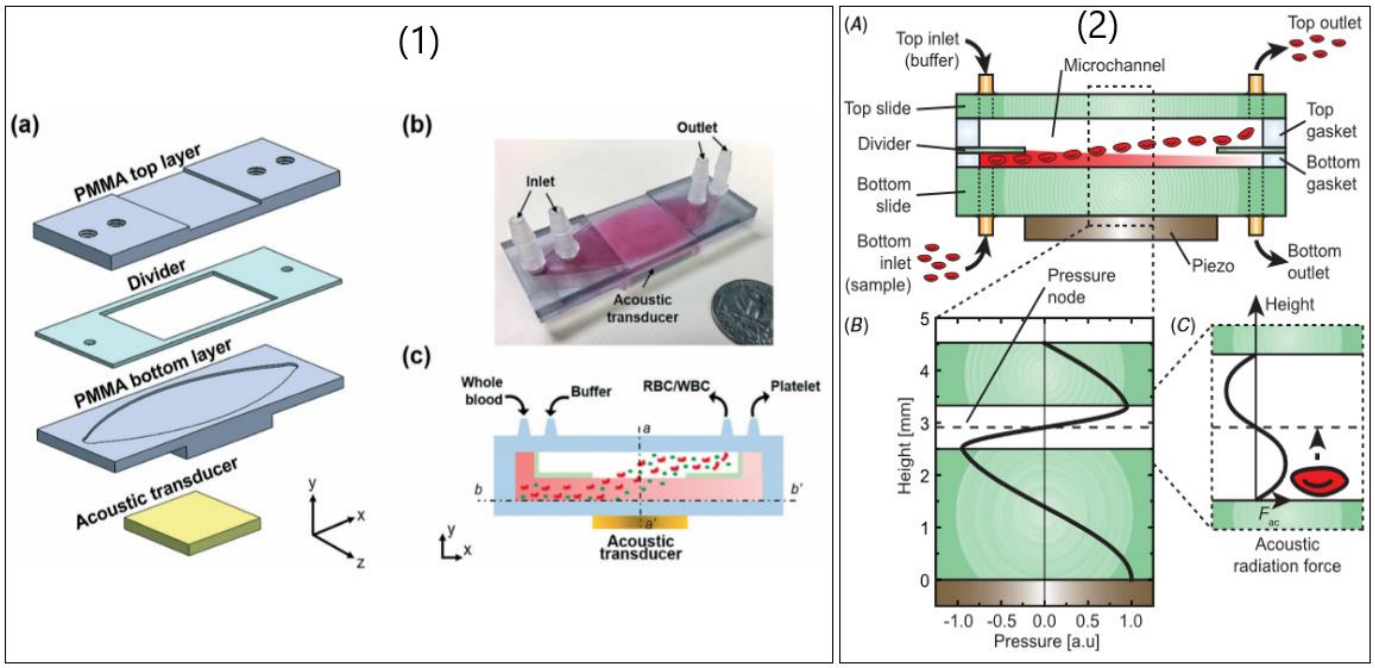

Figure 4-**Acoustofluidic devices for cell transfer to new buffer.** (1)Exploded view of the device(a), picture(b), and schematic view(c) of the device developed by Gu et al.[44].(2) Schematic view(A), pressure field(B), and acoustic force(C) for the device developed by Adams et al.[45].

Acoustofluidics is the field of ultrasound handling of fluids and particles in microfluidic systems. For frequencies less than 1.5 MHz, the sound wavelength in water matches well with dimensions of microfluidic systems and results in the formation of standing acoustic waves [46]. Acoustophoresis has been used for cell manipulation in cell concentration, filtration, separation, and buffer exchange in a flow-through or batch mode using bulk acoustic wave (BAW) or surface acoustic wave (SAW)[47, 48]. The methods rely on the formation of standing acoustic waves and offer a powerful means for label-free separation of cells in biology research, diagnostics, and clinical studies. BAW are defined as compressional waves in a solid that propagate through the bulk materials whereas SAW propagate along the surface of a materials. Although a lot of studies have been done on using acoustic field for cell separation, they have not been practical due to relatively low sensitivity and efficiency[49]. In a standing acoustic wave, particles populating the fluid are pushed toward minimal acoustic radiation pressure region which are called pressure nodes.

For high throughput applications, BAW is preferred as compared to SAW due to higher acoustic energy[50]. It leads to the capability of cell manipulation in a high flow rate that can fulfill many biomedical applications. Therefore, our focus will be on BAW technology. In BAW acoustophoresis, an ultrasonic standing wave is generated in a fluid-filled channel by a bulk piezoelectric transducer. The piezoelectric transducer excites bulk waves and resonance in channels within an acoustically hard material. Another

consideration is that SAW devices are fabricated in soft materials since the wave propagates into fluidic compartment via substrate with similar acoustic impedance such as PDMS. However, BAW devices are made of rigid materials since the relies on reflection between channel walls and hence it needs high Q-value materials like silicon or glass. On the other hand, Challenges like fluid relocation because of poor impedance match between fluid and device, challenges in the manipulation of small particles because of acoustic streaming, perfect adhesion of layers, and difficulties in fabrication method are some barriers toward the development of industrial applications of acoustofluidics[48]. Therefore, it is important to consider these challenges in device design to achieve the final goal which is cell transfer from one buffer to another.

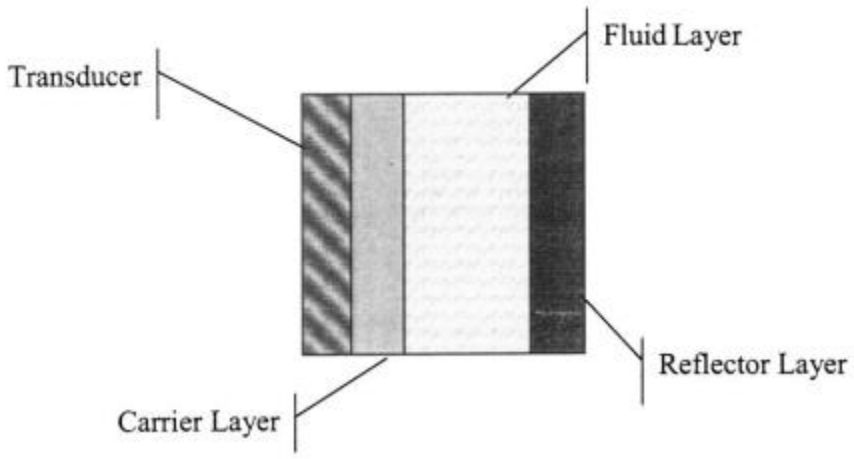

Figure 5- Schematic diagram of layered resonator. The layered resonator requires perfectly matched reflection and matching(carrier) layers with high Q-value.

First, different design principles are presented here. There is a range of acoustofluidic device architectures including layered resonator which is composed of different layers with specific roles to build the resonance (Figure 5). The transducer generates the sound, and the

coupling layer transmits it into the system. The matching layer provides a barrier between fluid and transducer. The fluid layer contains the liquid and cells/beads. The reflector layer is responsible for reflecting the incoming wave back into the fluid layer giving rise to the standing wave. The layered resonator is quite complex as the different layers required precise control of thicknesses to achieve a strong resonator. As the main reflection occurs between the air backed reflector layer and the transducer, some losses in supporting layers with using materials like polymers can be acceptable. The attenuation in polymers can also be a benefit as it leads to larger bandwidth for resonator[51].

Among the studies in the application of acoustofluidic for cell separation, we focused on application of BAW. Adams et al. developed a broad channel high throughput BAW device made of glass based on layered resonator principles[45]. However, their fabrication was expensive and not applicable for point of care. Gu et al. introduced the first plastic BAW device for the separation of platelets from whole blood with high throughput(Figure 4)[44]. This study gave us the inspiration to develop an acoustofluidic device for integration with our microfluidic platform. This device design fulfilled the requirements for our purpose to continuously isolate cells from enzyme at high flow rates. Dimensions of a layered resonator can be selected based on model transfer impedance model described by Hill et al[52]. If we assume a very high impedance at the transducer boundary, the fluid layer will resonate when the impedance looking into the reflector matches the impedance at the boundary with reflector[53].

$$k_f - t_f = tan^{-1}\left(\frac{r_f\left(r_r^2 + r_0^2 tan^2(k_r t_r)\right)}{r_r \tan(k_r t_r)\left(r_r^2 - r_0^2\right)}\right) \quad (1)$$

Where r is the impedance, k is the wavenumber, t is the thickness, r index refers to reflector and f index refers to fluid. This criterion can be fulfilled at different ratios of reflector thickness and channel heights. A quarter wave chamber with half wave reflector is one of the solutions which has been used by Gu et al. as shown in Figure 6. This design was chosen for our device, as well.

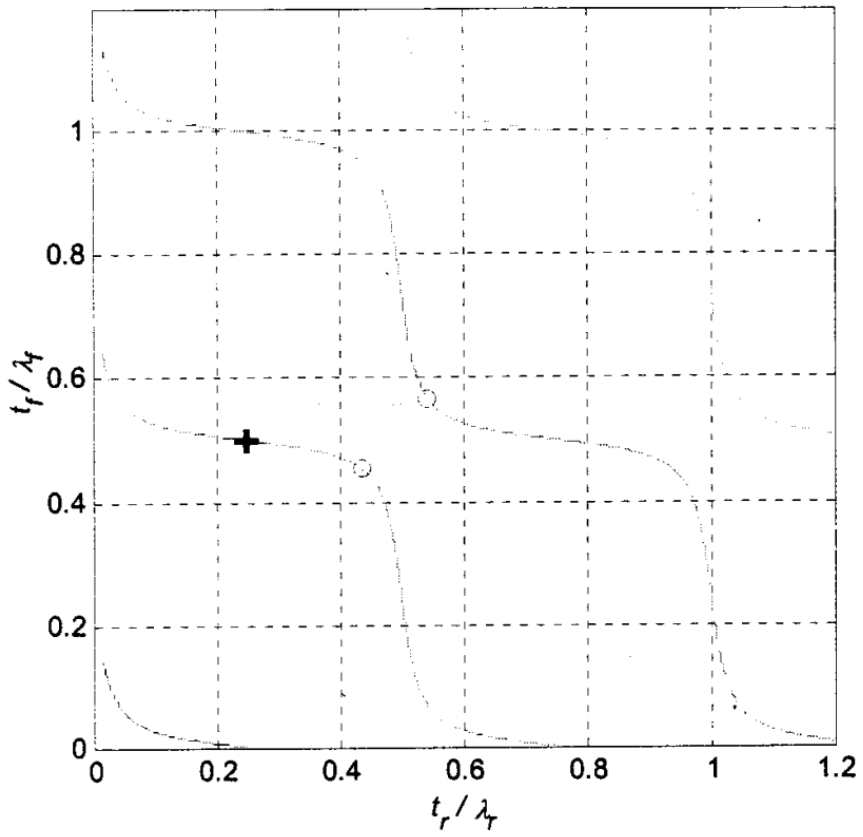

Figure 6- The first four solutions to equation for balance between impedance at the boundary with the reflector and impedance looking into the reflector.

The nearly identical specific acoustic impedances for plastic and water does not allow localized resonances in the water domain that are decoupled from the solid domain, as is usually the case in acoustically hard systems such as silicone-glass devices. Instead, the acoustic fields in the two domains are strongly coupled, and given its large volume compared to that of fluid, the solid domain largely determines the resonance behavior[54]. Moreover, in plastic devices, rigid wall approximation is insufficient and hence, the selection of operating frequency remains partially empirical. Therefore, frequency sweep around the fundamental resonance frequency can be used for finding the optimum resonance [55-57].This information provides the required background for development of acoustic device.

1.5. Structure of the dissertation

The remainder of the dissertation is organized as follows: In chapter 2, optimization of our tissue dissociation microfluidic platform for heart and liver was done toward in order to evaluate our platform for tissues with different stiffnesses. This study led to understanding the significance of collecting the isolated cells in different time intervals during the process. In chapter 3, the integrated dissociation and filtration (IDF) device was explored in more depth for understanding the governing mechanisms of tissue dissociation and cell line disaggregation with two integrated modules. This study led to shortening digestion time and exposure to physiological temperature. Also, it was found that different cell types have different responses to IDF processing. In chapter 4, the effect of pulsatile flow versus steady shear flow on tissue dissociation and cell line disaggregation was studied. Most

cell types show higher cell yield with steady shear flow provided by syringe pump although endothelial cells showed higher cell yield in pulsatile flow. These findings reflect the unique characteristics of each cell type and their ECM in tissue. After studying the IDF device with different flow types, the platform including IDF, and Digestion device was studied at different flow rates. It shows that we can reduce the processing time at higher flow rate with comparable cell yield while it also demonstrates how cell liberation vary by flow rate and cell type. In chapter 5, an acoustically driven microfluidic device was developed for continuous elution of cells from the digestion device. This acoustofluidic device can be integrated to the digestion device to transfer liberated cells to a parallel stream of buffer to prevent over exposure of cells to stresses during the digestion process. This device fabrication and proof of concept was done. Further studies will be continued. Chapter 6 summarizes the major outcomes of this dissertation and future directions.

CHAPTER 2: Optimization of microfluidic dissociation platform for heart and liver tissue

2.1. Introduction

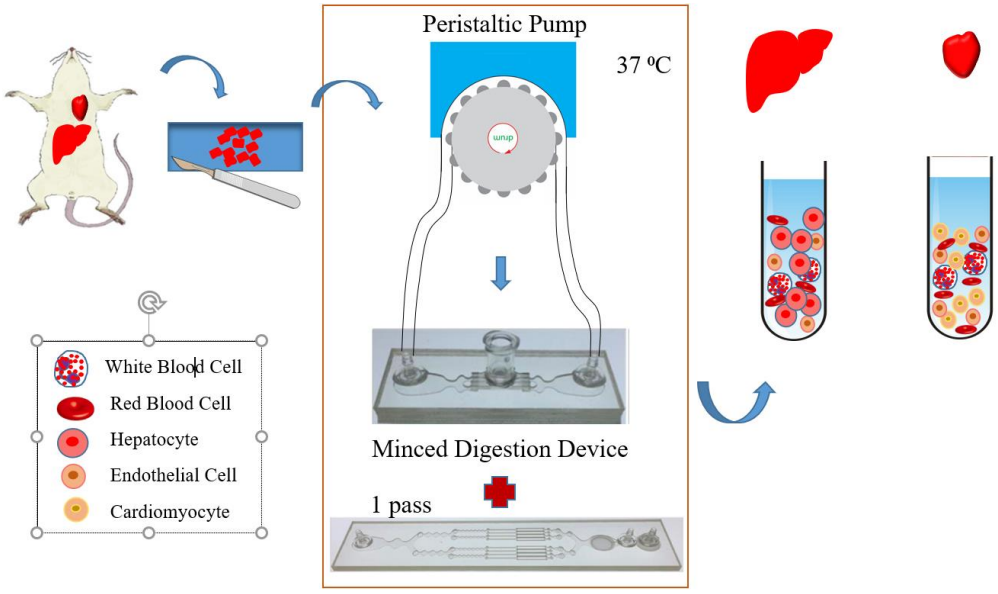

Figure 7- **Schematic view of tissue dissociation process**. First, the tissue is minced to 1mm^3 pieces. Then, it is recirculated through the Minced Digestion Device (MTD) followed by one path through the Integrated Dissociation/Filtration Device. After this process, the population of each cell type and its viability will be assessed by flow cytometry.

Traditional methods for dissociation of tissue into single cells are based on handling digestion with enzyme, dissociation through pipetting up and down, and filtration steps which are time-consuming and laborious while they cause a lot of lab-to-lab variations stemming from the nuances in processing method and the operator skills. It is crucial to minimize these variations in single cell preparation process to have reliable data for single cell RNA sequencing. Typical workflow for generating single-cell data incorporate single-cell

preparation, single cell isolation, library construction, and sequencing. Error in the first step which is tissue dissociation to single cells will cause artifacts in final results which means wasting a lot of time, effort, and cost[58]. Therefore, our group has developed a microfluidic platform to operate single cell preparation process in a cheap, fast, and automated way. Our platform is comprised of three parts including Digestion, Dissociation, and Filtration devices. Each device is designed to be a substitute for one major step of the manual dissociation process. Digestion device can substitute the mincing and enzymatic digestion process. Dissociation device can be a replacement for pipetting up and down the digested tissue in enzyme. Filtration device can be used instead of traditional filters. It has been shown that these devices can shorten the tissue dissociation process, significantly. It optimizes the mechanical and chemical stresses on tissue to maximize the cell yield while keeping the viability in an acceptable range.

It is highly valuable to develop a universal platform for breaking down the tissue to single cells that can be applied for different tissue types. Each tissue is a heterogeneous population of cells attached with its unique ECM to carry out a specific function. Therefore, it is crucial to factor in different tissue properties, characteristics of ECM and each cell type functionality in optimization of tissue dissociation platform. Our platform has been used for kidney and tumor before. Here, our goal is to optimize this platform for liver and heart tissue (Figure 7).

Liver is the largest organ in the body and has functions including synthesis and metabolism of carbohydrates, proteins and lipids, clearance of toxins and regulation of immune responses[59]. Liver plays a major role in drug metabolism and therefore, in vitro

screening of drugs against primary liver tissue is a critical component of preclinical testing. There are at least four major types including hepatocytes, liver sinusoidal endothelial cells (LSECs), Kupffer cells (KCs) and hepatic stellate cells (HSCs). Hepatocytes are aligned into cellular plates separated by narrow sinusoids lined with endothelial cells. A gap called the space of Disse is formed between the endothelium and hepatic plate in this structure, allowing the immune response as well as other metabolic functions.

Hepatocytes account for approximately 80% of the liver mass with a diameter of 20-30 micron. LSECs are second most abundant cell type in the liver, positioned between blood and hepatocytes that permit the passive transport of solutes and regulate trafficking between the blood supply and the hepatocytes. KCs constitute around 80% of the tissue macrophages and about 15% of all liver cells. KCs are the first macrophage population to encounter endotoxin (LPS) and antigens by expressing scavenger receptors such as CD163, toll like receptors (TLRs) and Fc receptors[60]. HSCs comprise 5-8% of liver cells and reside in Disse space.

It is desirable to recover all these cell types in dissociation process while retaining their functionality. Our goal is to optimize our dissociation platform to recover these cell types with highest yield and viability. In future, the cell functionality will be studied to ensure that the dissociation process has the minimal effect on cellular phenotype. So, it can be proved that our platform can be used for preparation of liver cells in liver modeling for drug screening. It is worth mentioning that immortalized hepatocytes can be applied for toxicity testing, but they display abnormal levels of liver-specific function, and they are not necessarily a good representative of liver tissue for a specific patient. Therefore, primary

hepatocytes recovered from liver tissue are considered the best choice for drug evaluation[61]. While liver is a soft tissue with stiffness in range of 400-600 Pa based on rheometry[62], , hepatocytes are well known to be fragile and thus liver presents a unique challenge for dissociation process In another study stiffness of 150 Pa was reported for normal liver by AFM[63]. The maximum shear stress in our Digestion device is 106 Pa based on following equation.

$$\tau = 6Q\eta/h^2w$$

So, tissue will be in the elastic region when exposed to shear in the Digestion device. However, this will not be enough to ensure about the integrity of cell membrane and phenotype. Since cells are detected based on proteins expressed on their surface in flow cytometry, it can be a reliable method to ensure about retaining cell integrity.

It has been previously shown that at shear stresses above 0.2 Pa cells experience phenotypical changes and at shear stresses above 0.5 Pa, cells start to die[64]. Therefore, physiological shear stress used in perfusion culture systems is 0.2 Pa for hepatocytes[65-67]. It should be emphasized that in these studies, cells were attached to a surface. The maximum shear stress expressed by cells is approximately three times higher than free cell in the same geometry[68]. To the best of our knowledge, there has been no study on effect of maximum shear stress on free cells. It is crucial to ensure that our Digestion device is not exposing cells to unsafe level of stress. Therefore, flow cytometry will be used to find the cell yield based on the specific surface markers on cells to ensure that cell yield reflect population of cells with intact surface proteins.

The next step is evaluation of our platform for heart tissue. Heart is composed of cardiomyocytes, fibroblasts, endothelial cells (ECs) and perivascular cells. Cardiomyocytes occupy around 70-85% of the heart volume and they are essential for vascular supply, providing the intracellular communication and homeostasis. Both myocytes and nonmyocytes respond to physiological and pathological stress. Therefore, it is necessary to dissociate the heart tissue while not promising their functionality[69]. It is crucial to dissociate the heart tissue to its components and study them individually to understand cellular signaling and functions for the final application in tissue regeneration. On the other hand, heart failure is a leading cause of drug withdrawal from the market. Therefore, liberation of cardiomyocytes from heart tissue is high of significance in drug development. It is notable that cardiomyocytes have been shown to be highly sensitive to mechanical and enzymatic dissociation techniques[70]. It highlights the importance of development of a tissue processing method for isolation of cardiomyocytes with high cell yield and viability without compromising cellular functionality.

In clinical studies of drugs, studying drug toxicity to liver and heart is crucial and hence, our device should provide the highest cell yield, viability, and functionality that can be used in the generation of tissue models, specifically for each patient to develop personalized medicine. Our platform is going to be optimized toward this goal.

2.2. Materials and methods

2.2.1. Device design and fabrication

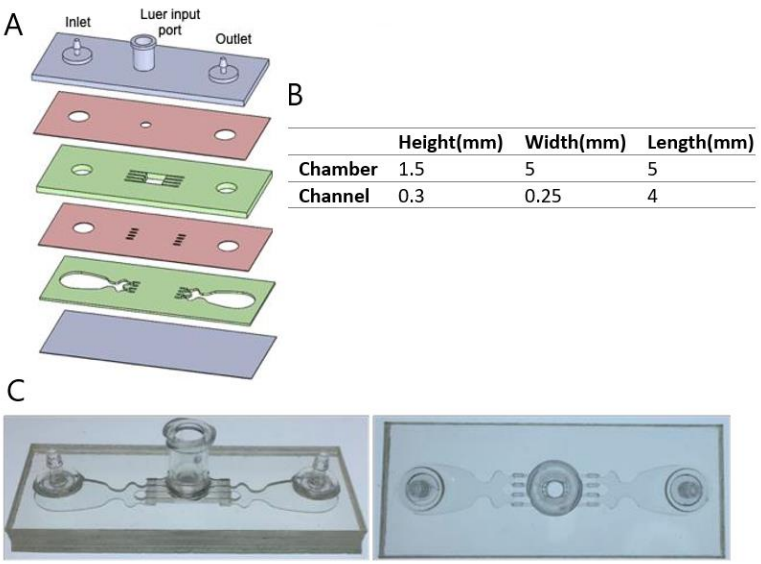

	Height(mm)	Width(mm)	Length(mm)
Chamber	1.5	5	5
Channel	0.3	0.25	4

Figure 8- **Minced tissue digestion (MTD) device design.** It consists of a tissue chamber in the middle, upstream channels to agitate the tissue and downstream channels to prevent tissue pieces from leaving (A) Exploded view of minced Digestion device (B) Chamber and channel dimensions (C) Top and side view of fabricated minced Digestion device

The Minced tissue digestion (MTD) device was designed to process ~1mm^3 pieces of tissue into cellular suspensions that can be integrated with downstream Integrated Dissociation and Filtration (IDF) device including branching channel array and filter modules. The MTD device is composed of 3 primary components. The first component is a luer input port centered directly above the tissue chamber. This port provides an access point where minced tissue can be easily and quickly loaded into the tissue chamber and then closed off with a stopcock during device operation. The second component is a ~5 mm x 5 mm tissue chamber, which retains the pieces of minced tissue while proteolytic enzyme solution is pumped through the chamber. These chamber dimensions were designed to be easily filled by loading tissue through the ~2.5 mm diameter input port above it. The

chamber height is 1.5 mm, slightly larger than the pieces of tissue to prevent clogging. The third and final component is a series of upstream and downstream fluidic channels. The upstream channels were designed to focus the enzymatic solution into high velocity fluidic jets directed at the pieces of tissue, agitating the pieces. The downstream channels function as a sieve to prevent large pieces of tissue from leaving the chamber, while single cells and small aggregates can exit the chamber for collection or further microfluidic processing. Channel widths entering and leaving the tissue chamber were chosen to be 250 μm. Channel height is 300 μm like the other devices. Channels were separated by 1 mm to allow reliable fabrication by laser cutting and pressure lamination, and four channels could comfortably be accommodated across the sides of the tissue chamber. The channel length is 4 mm to avoid clogging. The device was fabricated using pressure lamination method which includes laser cutting features in polymeric sheets and attach them together with pressure-sensitive adhesive (PSA) under pressure (Figure 8). This device will be used in series with previously discussed Integrated Dissociation/Filtration (IDF) device with 50 and 15 μm filters. This platform has been optimized for kidney and tumor in our research group and we will focus on optimization for liver and heart tissues.

2.2.2. Digestion process

B6J mice were euthanized with CO2 asphyxiation. Next, heart or liver tissue was harvested and uniformly minced with a scalpel to ~1 mm^3 pieces. For the control sample, minced tissue samples were then digested while immersed in 0.25% collagenase type I in microcentrifuge tubes on a shaking incubator at 37 ^{0}C under shaking for a specified period.

Then, the suspension was pipetted repetitively to dissociate the cell aggregates, mechanically. Finally, the suspension was filtered through a 100 μm filter.

For the device digestion process, MTD device was prepared by affixing 0.05" ID tubing to the device inlet and outlet hose barbs. Then, the device was washed with PBS+ to reduce cell binding to channel walls. Freshly dissected tissue was minced into 1 mm^3 pieces and then loaded into the device through the luer input port and the channels were primed with collagenase type I. In the next step, the enzyme filled tubing was connected to make a close circuit between the device and peristaltic pump. Then, circulation of enzyme was done inside an incubator at 37 ^{0}C at flow rate of 20 ml/min for specified time. After that, the cell suspension was collected in a conical tube. Next, tubing was connected from the outlet of the MTD device to the inlet of the IDF device. The crossflow outlet was closed off with a stopcock, and sample was pumped at 20mL/min and collected from the integrated device effluent outlet into a conical tube. Then, devices were washed with 2 mL PBS+ to flush out and collect any remaining cells. For time interval collection condition, at the end of each time interval, the effluent was collected, and the device was washed with 2 ml PBS+. Then, the device and tubing were primed with collagenase solution and the outlet of the MTD device was reconnected to the peristaltic pump for recirculation until the next interval collection. Finally, cell suspensions were treated with 100 Units of DNase I for 10 min at 37°C and washed by centrifugation into PBS+. Cell suspensions were then ready for flow cytometry analysis.

2.2.3. Flow cytometry analysis

Table 1- flow cytometry probe panel

Assay	Antibody		Fluorophore			Positive cells
	Clone	Dilution (µg/mL)	Tumor	Liver	Heart	
EpCAM	G8.8	7	PE	N/A	N/A	Epithelial cells
TER-119	TER-119	5	AF647	AF647	AF647	Red blood cells
CD45	30-F11	5 (AF488) or 12.5 (BV510)	BV510	BV510	BV510	Leukocytes
Viability	N/A	3.33 (7-AAD) or 1:1000 (ZV)	7-AAD	7-AAD	Zombie Violet	Dead cells
CD31	MEC13.3	8	AF488	AF488	AF488	Endothelial cells
ASGPR1	8D7	10	N/A	PE	N/A	Hepatocytes
Troponin T	REA400	0.15	N/A	N/A	PE	Cardiomyocytes

Cell suspensions were analyzed using developed tissue-specific flow cytometry panels (Table 1). For liver tissue, cell suspensions were stained with antibody cocktail based on the flow cytometry panel for 30 minutes considering the manufacturer dilution ratio. Samples were then washed twice using PBS/1%BSA and stained with the viability dye, 7-AAD (BDB559925, Thermo Fischer) on ice for at least 10 minutes before flow cytometry.

Since Troponin T is an intracellular marker[71], so intracellular staining protocol was required for heart tissue. First, cells were stained with Fixable viability Dye, Zombie Violet (423114, Biolegend). After washing cells, fixation and permeabilization with Fix Buffer 1 (55787, BD Biosciences) was done for 20 minutes at 4 ^{0}C, protected from light. In the next step, the cells were washed with 1X Perm/Wash buffer (554714, BD Biosciences) two times. After that, cells were stained with pre-determined amount of antibody for 30 minutes at 4 ^{0}C protected from light. This step, staining for surface markers were done like the protocol mentioned for liver. Finally, cells were washed with Perm/Wash buffer two times to start flow cytometry.

Samples were analyzed on a flow cytometer (Novocyte 3000, ACEA Biosciences). Flow cytometry data was compensated using single stained cell samples or compensation

beads. Gates encompassing the positive and negative subpopulations within each compensation sample were inputted into FlowJo to automatically calculate the compensation matrix. Appropriate isotypes were used to assess nonspecific background staining with each antibody. Data was analyzed using a sequential gating scheme (

Figure 9). Gate 1 used FSC-A vs. SSC-A to exclude debris near the origin. Gate 2 used FSC-A vs. FSC-H to select single cells. Gate 3 used CD45- BV510 vs. TER119-AF647 to distinguish leukocytes (CD45+TER119-) and red blood cells (CD45-TER119+). Gate 4 was applied to the CD45-TER119- subset and used PE channel to identify epithelial cells via EpCAM (kidney and tumor), hepatocytes via ASGPR1 (liver), or cardiomyocytes via Troponin T (heart). Gate 5 was applied to the EpCAM/ASGPR1/Troponin T negative cell subset and used CD31-AF488 to identify endothelial cells. Finally, gate 6 used 7- AAD (kidney, tumor, liver) or Zombie Violet (heart) to distinguish live and dead cells.

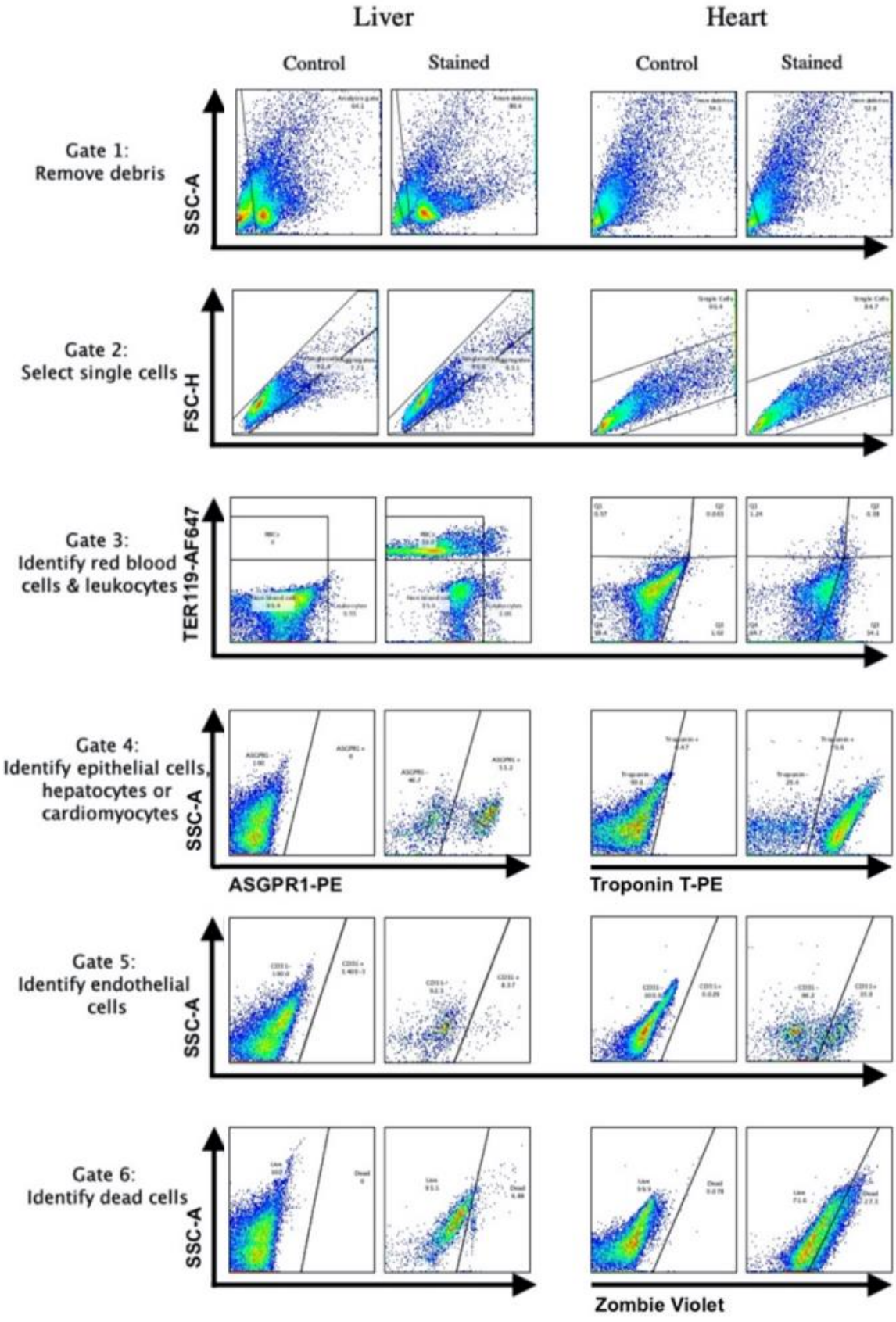
Liver
Heart
Control
Stained
Control
Stained
Gate 1:
Remove debris
SSC-A
Gate 2:
Select single cells
FSC-H
Gate 3:
Identify red blood
cells & leukocytes
TER119-AF647
Gate 4:
Identify epithelial cells,
hepatocytes or
cardiomyocytes
SSC-A
ASGPR1-PE
Troponin T-PE
Gate 5:
Identify endothelial
cells
SSC-A
Gate 6:
Identify dead cells
SSC-A
Zombie Violet

Figure 9- **Flow cytometry gating schemes.** Cell suspensions obtained from tissue samples were stained with the fluorescent probes and analyzed using flow cytometry. Acquired data was compensated and assessed using a sequential gating scheme. Gate 1, based on FSC-A vs. SSC-A, was used to exclude debris near the origin. Gate 2 was used to select single cells based on FSC-A vs. FSC-H. Gate 3 distinguished leukocytes based on CD45-BV510 positive signal and TER119-AF647 negative signal and identified red blood cells based on TER119-AF647 positive signal and CD45-BV510 negative signal. Gate 4 was applied to the CD45-, TER119- cell subset to identify epithelial cells in kidney based on positive EpCAM-PE signal, to identify hepatocytes in liver samples based on positive ASGPR1-PE signal, and to identify cardiomyocytes in heart samples based on positive Troponin T-PE signal. Gate 5 was applied to the EpCAM- cell subset in kidney and tumor samples, to the ASGPR1- cell subset in liver tissue, and to the Troponin T- cell subset in heart tissue to identify endothelial cells based on positive CD31-AF488 signal. Finally, gate 6 was used to identify live cells in epithelial, hepatocyte, cardiomyocyte, leukocyte, and endothelial cell subsets based on negative 7-AAD signal. Appropriate isotype controls were initially used to assess nonspecific background staining, and appropriate fluorescence minus one (FMO) controls were used to determine positivity and set gates.

2.3. Results

2.3.1. Digestion platform optimization for liver tissue

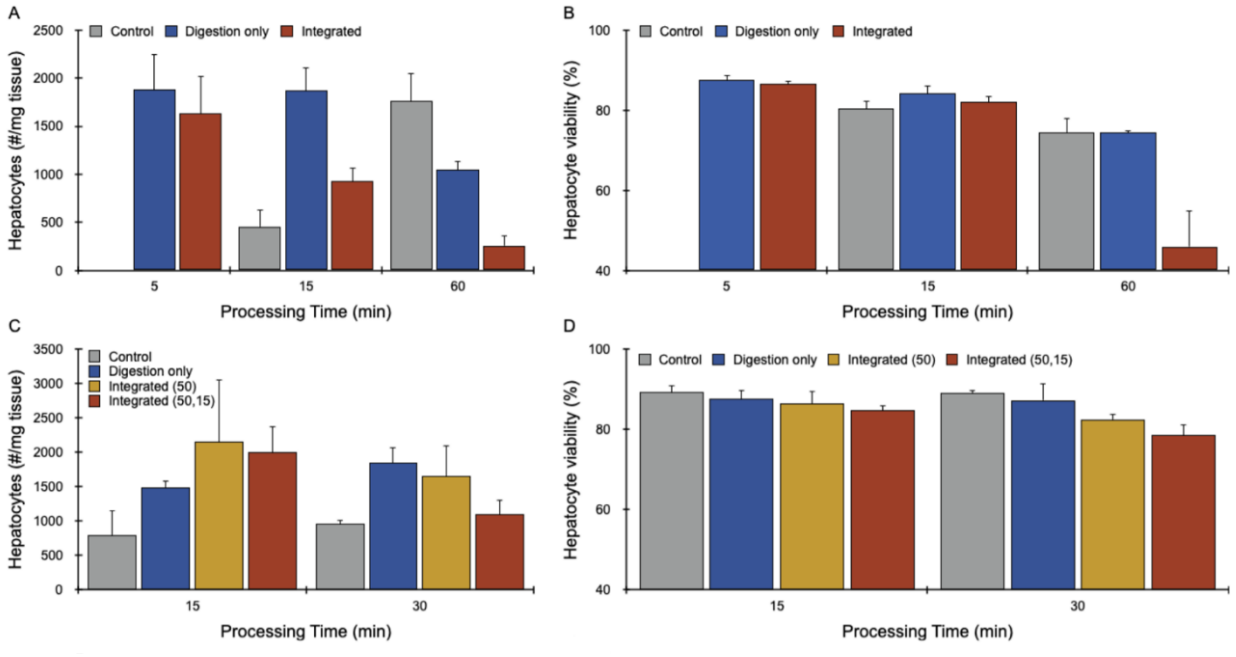

Figure 10- **Optimization of the platform for liver tissue.** hepatocyte number (A) and viability (B) when murine liver tissue was processed for 5, 15, and 60 minutes for control(gray), MTD device only(blue) or MTD device plus 1 pass through the integrated device with 50 and 15 μm filters (red). Hepatocyte number (C) and viability (D) when murine liver tissue was processed for 15 and 30 minutes with different device configurations of MTD and IDF device. Control refers to tissue processed with traditional method(gray), "Digestion only" refers to recirculation of enzyme through the MTD device(blue), "Integrated (50)" refers to recirculation through MTD device followed by one pass through the 50 μm filter(yellow), and "Integrated (50,15) refers to recirculation of enzyme through the MTD device followed by one pass through the 50,15 μm filters(red).

Tissue processing was done with enzyme recirculation through MTD device," Digestion only" condition or MTD device followed by one pass through the IDF device, "Integrated" condition for specified time. Flow cytometry was used to compare the number of recovered cells from the device effluent with control condition. Four antibodies specific to cell types in liver including erythrocyte, endothelial, hepatocyte and leukocyte cells were

used. Hepatocyte count and viability was used to assess the device efficiency. Processing tissue with MTD device only for 5 or 15 minutes has the same yield as 60 minutes digestion in control condition (Figure 10A). In addition, viability is higher than 80% and close to control conditions. Our platform is significantly reducing the processing time without losing the yield or viability. It is of high importance for clinical applications. It can also reduce the risk for stress induced genomic transcriptions. It is notable that number of recovered cells will drop significantly when processing the tissue in MTD device for long times (60 minutes) which shows that long term processing will damage the hepatocytes and decrease the cell yield. Also, the cell yield is slightly lower when the MTD device processing is followed by passing through the IDF device which can be because of large size of hepatocytes compared to second filter in filtration module of IDF device.

In addition, the effect of passing effluent through the IDF device was studied. In general, IDF device with 50-micron filter, "Integrated (50)" leads to higher cell yield and viability compared to the IDF device with 50 and 15 μm filters, Integrated (50,15) (Figure 10 C). Since hepatocytes have a diameter around 25-50 microns, it can be implied that filters of the IDF device can damage the hepatocytes when their mesh size is smaller than cell diameter. Therefore, IDF device with 50 μm filter only was used for the next experiment. IDF device with 50 μm filter has a positive effect in increasing the cell yield for shorter times. Therefore, this version of IDF device was chosen for the next stage. In addition, cell viability results confirm that IDF device negatively affects the cell viability. Also, passing the effluent through IDF device with two filters causes lower viability than the IDF device with one 50 μm filter. Since IDF device would eliminate the need for cell straining, it was kept in series with Digestion device in final platform but with 50 μm filter only.

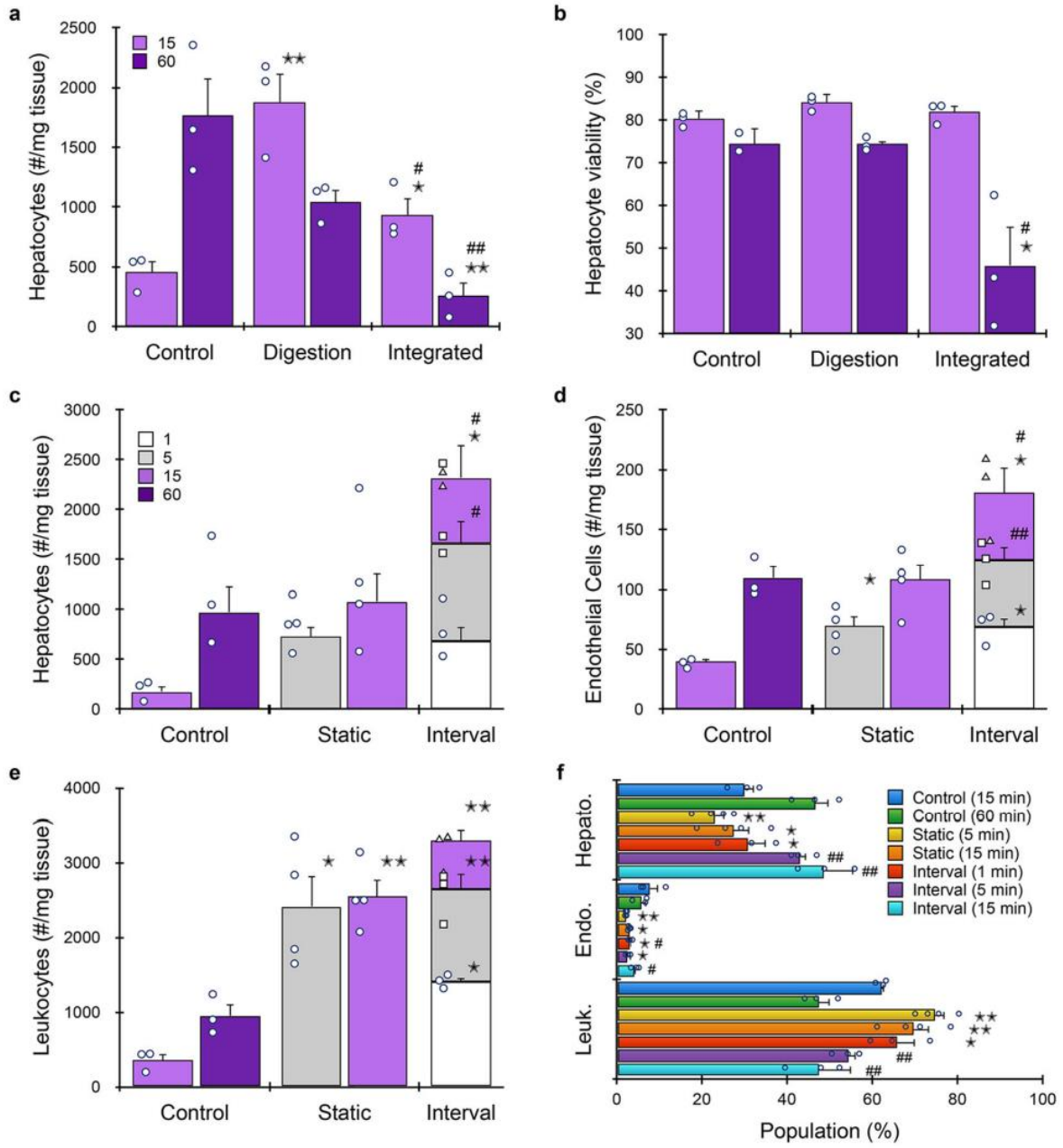

Figure 11- **Studying different configurations of MTD and IDF devices.** Liver was harvested, minced, and evaluated with the minced digestion device alone, named "Digestion "and in combination with the IDF device, named "Integrated". Hepatocytes were identified and quantified by flow cytometry. a) Comparison of Control, Digestion, and Integrated conditions. b) Hepatocyte viability. The digestion device increased hepatocyte recovery at 15 min. c–f) Results using shorter digestion

times and a single pass with a dissociation/filtration device containing only the 50 μm filter. c) Epithelial cells d) Endothelial cells, e) Leukocytes. f) Population distributions obtained for each processing condition. After only 5 min of microfluidic processing, four-fold more cells were obtained than the 15 min control. Interval condition enhanced hepatocyte yield by ~2.5-fold relative to the 60 min control and 15 min static conditions. Circles indicate values for experimental replicates. For stacked plots, experimental replicates are indicated by circles at 15 min, squares at 30 min, and triangles at 60 min. Two-sided T test was used for statistical testing. Stars indicate $p < 0.05$ and double stars indicate $p < 0.01$ relative to the 60 min control. Crosshatches indicate $p < 0.05$ and double cross-hatches indicate $p < 0.01$ relative to the static condition at the same digestion time. p values for all comparisons are presented in the Source Data file.

We used another operation method to improve the device efficiency in improvement of cell yield and viability. Our studies directed us toward the hypothesis that long period of circulation through MTD device could expose liberated cells to more hydrodynamic pressure and damage the cells, irreversibly which leads to reduction of cell yield. To verify our hypothesis, the effluent was removed from the device in specified time intervals and fresh enzyme was loaded into the device for the next time interval. This condition is named as Intervals and was designed to collect effluent at different time intervals including 1,5 and 15 minutes. This condition leads to significantly higher hepatocyte cell yield than the control condition in the same period, 2400 versus 100 hepatocytes/mg tissue (15 minutes). The cell count in one minute is higher than processing the tissue for 15 minutes in control condition or with MTD device in static condition (Figure 11). Also, hepatocyte yield with Interval operation for 15 minutes is 2.5 times higher than control condition in 60 minutes. Similar response was observed for endothelial cells and leukocytes. Viability was always in

acceptable region and did not change, dramatically (Figure 12). However, viability reduces at longer times which highlights the importance of shorter tissue processing method. It proves our hypothesis that long circulation time in MTD device will cause cell damage and eventually lysis. Extraction of dissociated cells in short time intervals rises the cell yield and reduces the potential cell damage.

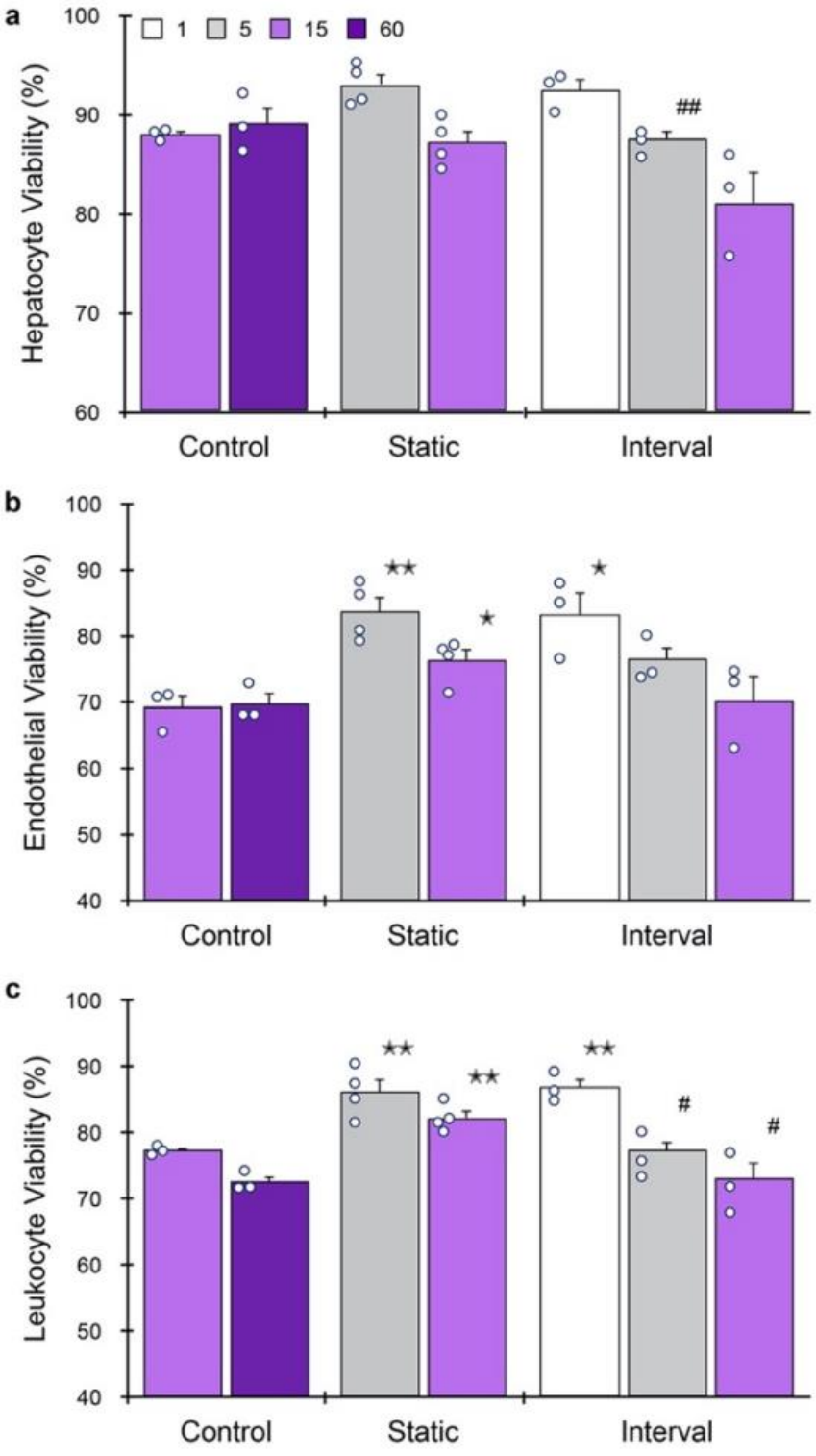
a
1
5
15
60
Hepatocyte Viability (%)
100
90
80
70
60
##
Control
Static
Interval
b
Endothelial Viability (%)
100
90
80
70
60
50
40
★★
★
★
Control
Static
Interval
c
Leukocyte Viability (%)
100
90
80
70
60
50
40
★★
★★
★★
#
#
Control
Static
Interval

Figure 12- **Cell viability from final microfluidic platform studies using murine liver.** a) Hepatocyte viability remained ~90% for all conditions except the 60 min interval, which decreased to ~85%. b) Endothelial cell and (c) leukocyte viabilities were generally between ~70% and 85% and increased with device processing at the early time points.

2.3.2. Digestion platform optimization for heart tissue

In the next step, evaluation of our platform efficiency in terms of cell yield and viability was planned for heart tissue since its mechanical properties and functionality is significantly different from liver. Heart tissue rigidity is significantly higher than liver. Cardiomyocytes rigidity is 4 KPa and it's dynamic activity depends on matching with the environment[72]. It is a valuable candidate for our dissociation platform optimization with significantly different mechanical properties compared to liver.

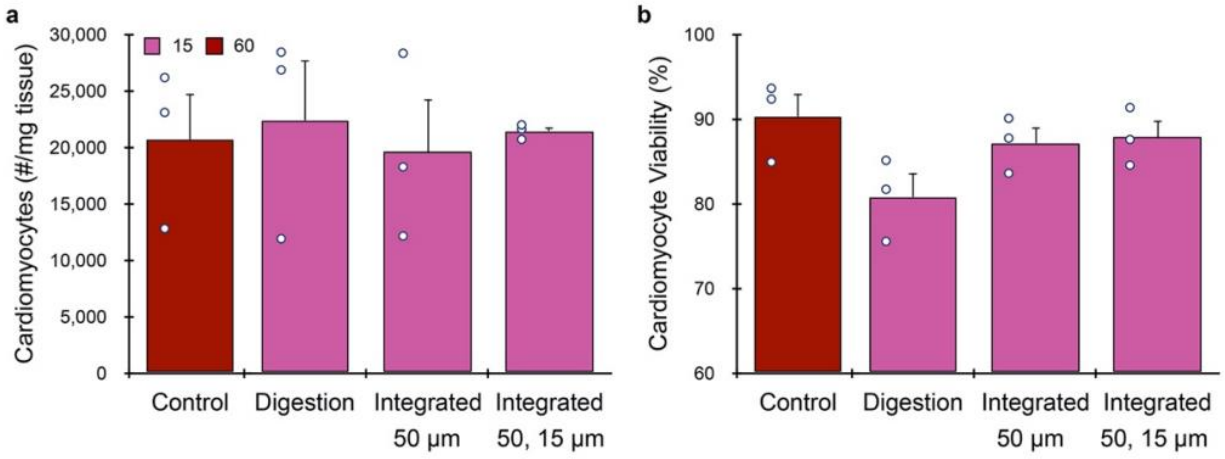

Figure 13- **Optimization of device configuration in tissue platform using heart**. Heart was processed with the MTD device for specified time and passed through the IDF device with different formats. Digestion device (MTD device only), Integrated 50 µm (IDF device with 50 µm filter), Integrated 50,15 µm (IDF device with 50 and 15 µm filters) and control condition. a) Cardiomyocyte

cell count b) Cardiomyocyte viability. Control refers to tissue processed with traditional method(red), “Digestion” refers to recirculation of enzyme through the MTD device, “Integrated (50 μm)” refers to recirculation through MTD device followed by one pass through the 50 μm filter, and “Integrated (50,15 μm) refers to recirculation of enzyme through the MTD device followed by one pass through the 50,15 μm filters.

To optimize our platform for heart tissue, different configurations of Digestion device and IDF device were set up. Digestion device processing in 15 minutes and control processing for 60 minutes show similar cell yield and viability. Digestion device significantly decreases the processing time with slight difference when IDF device is used afterwards (Figure 13). Cell viability is similar for all conditions. The IDF device will exclude the traditional filtration step after digestion and the accompanied artifacts. Therefore, the combination of Digestion device and IDF device was used for final evaluation of the platform.

Interval condition was used as described previously. It can be observed that collecting device effluent in 1,5- and 15-minutes time intervals will improve cell yield. Differences compared to liver tissue reflects the different mechanical properties of cell types in both tissues. First, the cell yield in first time interval, 1 minute is significantly low. It can be implied that heart ECM has higher rigidity, and it needs longer exposure to stress to loosen and release the cells (Figure 14). Secondly, cardiomyocyte cell yield in interval condition is 5 times higher than 15 minutes operation with MTD device only in same period (15 minutes). It is also notable that hepatocyte cell yield is 3 times higher than control condition in 60 minutes, as well. Therefore, our platform can significantly shorten the tissue dissociation time. The results explain that although the heart tissue has higher stiffness than liver, they

are still sensitive to long term exposure to stress. Therefore, elution of liberated cells will be favorable for higher total cell yield.

Higher yield will be achieved for all cell types including cardiomyocytes, endothelial cells, and leukocytes with Interval condition compared to the static condition for same period. However, cell yield for endothelial cells and leukocytes is lower than 60 minutes control condition. It can be a sign of the need for longer processing for liberation of these cell types.

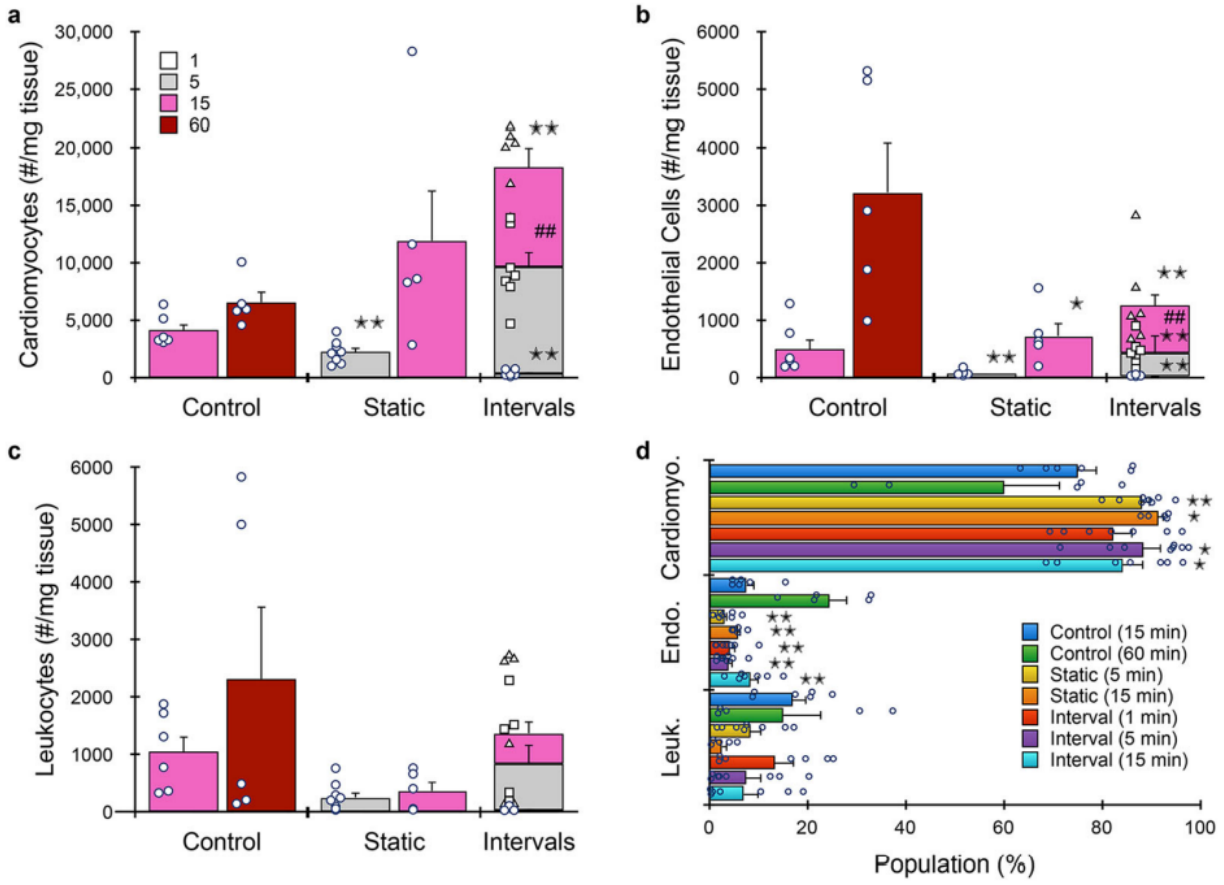

Figure 14- **Optimization of microfluidic platform for murine heart.** Hearts were resected, minced, processed with the microfluidic platform, and analyzed by flow cytometry. a) Cardiomyocytes b)

Endothelial cells, c) Leukocytes, d) Population distributions obtained for each processing condition. Microfluidic processing in 15 minutes produced ~3-fold higher Cardiomyocytes than the 60 min control. Interval condition produced optimal results again, increasing by ~50% and ~3-fold relative to the 15 min static and 60 min control conditions, respectively. Circles indicate values for experimental replicates. For stacked plots, experimental replicates are indicated by circles at 15 min, squares at 30 min, and triangles at 60 min. Two-sided T test was used for statistical testing. Stars indicate $p < 0.05$ and double stars indicate $p < 0.01$ relative to the 60 min control. Cross-hatches indicate $p < 0.05$ and double cross-hatches indicate $p < 0.01$ relative to the static condition at the same digestion time. p values for all comparisons are presented in the Source Data file.

Since Troponin T is an intracellular marker, we used a fixable viability dye, Zombie Violet, in place of 7-AAD. Viability results is in acceptable range of 80-90% and higher than the control conditions for all cell types. However, it is important to study cellular functionality for the recovered cells from digestion process.

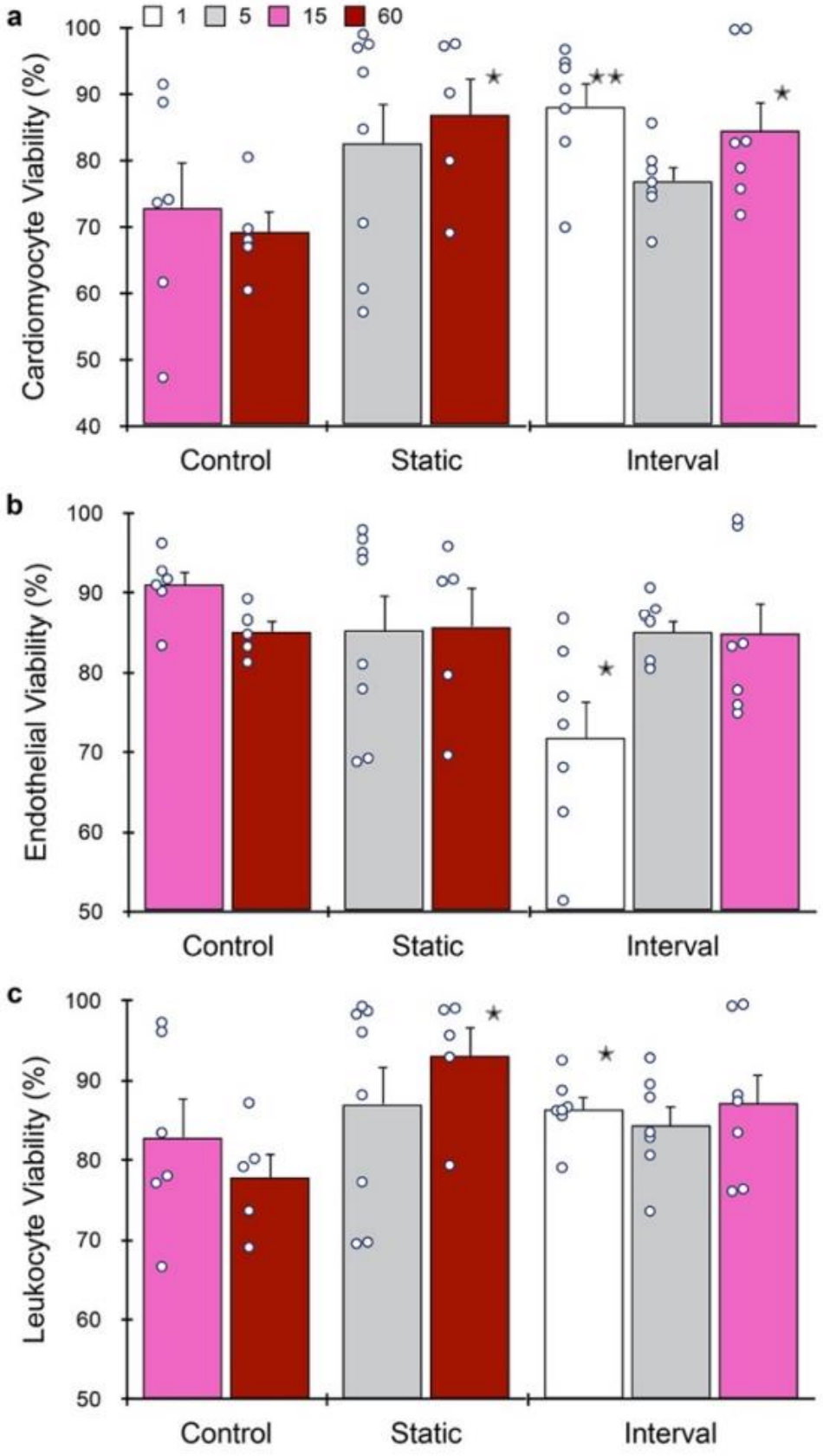
a
1
5
15
60
Cardiomyocyte Viability (%)
100
90
80
70
60
50
40
Control
Static
Interval
b
Endothelial Viability (%)
100
90
80
70
60
50
Control
Static
Interval
c
Leukocyte Viability (%)
100
90
80
70
60
50
Control
Static
Interval

Figure 15- **Cell viability from final microfluidic platform studies using murine heart**. (a) Cardiomyocyte viability for device processed samples matched or exceeded controls. (b) Endothelial cell and (c) leukocyte viability was generally >80% for device and control conditions. Data are presented as mean values +/- SEM from at least three independent experiments. Circles indicate values for experimental replicates. Two-sided T test was used for statistical testing. Stars indicate $p < 0.05$ and double stars indicate $p < 0.01$ relative to the 60 min control. p-values for all comparisons are presented in the Source Data file.

2.4. Conclusion

A microfluidic tissue processing platform was presented to automate the tissue dissociation workflow so that single cell suspensions are immediately ready for downstream analysis or alternative use. This platform is comprised of a digestion device with features to facilitate loading and processing of minced specimens, as well as a dissociation/ filter device that was integrated. The minced tissue digestion device accelerated tissue breakdown and produced significantly more single cells than traditional methods, while the integrated dissociation/ filter device increased yield further, while also increasing reproducibility and fully maintaining viability. Heart and liver tissue types was tested that exhibited a wide range of properties. Cell yield and viability was evaluated for different cell types through flow cytometry to ensure that total cell count is reflecting the functional cells with intact surface proteins. We also introduced a processing scheme, interval operation, which allowed us to extract single cells at different time points during microfluidic digestion. Interval condition dramatically increases the cell yield for both heart and liver. Different cell types react differently to interval operation since their sensitivity to shear stress is different. Hepatocyte yield with interval operation is 2.5 times higher than static condition and 10 times higher

than control condition in similar time frame. Cardiomyocyte yield with interval condition at 15 minutes is 2 times higher than static condition and 3 times higher than control condition in 60 minutes. It reflects the sensitivity of cardiomyocytes and hepatocytes to long time exposure to shear stresses while recirculating in the device. Heart failure is another leading cause of drug withdrawal from the market, combining with liver failure to account for ~70% of withdrawals[73]. Thus, there is robust interest in developing organ on chip technologies for preclinical drug screening[74, 75]. It highlights the significance of continuous separation of cells from the platform during the process though another module.

CHAPTER 3: Optimization of different dissociation mechanisms using the Integrated dissociation and filtration module

3.1. Introduction

Dissociation of aggregated particulates is a fundamental process in numerous scientific fields including polymer suspensions [76], microbeads/nanoparticles [77], and various cellular constructs in the life sciences [78]. Currently, the need for efficient disaggregation is particularly strong to help enable powerful single cell analysis technologies to be employed on tissue and organ samples [15, 79]. Traditional diagnostic methods provide information about biological traits that have been averaged over an entire population of heterogenous cells, which masks cell-to-cell variability and the presence of rare cell populations [26]. This necessitates the analysis of individual cells, which can then be evaluated globally to better understand normal function and diseased states [15]. Towards this goal, single cells must be liberated from tissues efficiently without changing viability or activation state [28]. Cell aggregate dissociation is also needed for regenerative medicine, as current methods can alter stem cell fate and viability [79, 80]. Therefore, continued development and refinement of rapid and efficient methods for processing tissues and cell aggregates into single cells is a major area of need in the biotechnology and medical arenas.

The traditional method for preparing single cells from tissue includes i) mincing to reduce tissue size, ii) digesting with enzymes to break down the extracellular matrix and/or cell-cell junctions, iii) mechanically dissociating to release cells, and iv) filtering to remove remaining aggregates. Long chemical exposure times may cause transcriptional and/or proteomic changes, and incomplete dissociation may enrich for specific cell types in the final suspension [81-83]. More importantly, high levels of mechanical stress needed to release cells from deep inside the aggregates can induce damage, and subsequently reduce cell yield and/or viability. Hence, there is a critical need to develop methods that will provide well-defined environmental factors including chemical exposure time and hydrodynamic shear stress levels to uniformly release cells from aggregates with minimum damage. Microfluidic systems can facilitate precise manipulation of cell aggregates to achieve high-throughput, cost-effective, and tunable methods [84-86]. However, only a few systems have been developed for dissociation of tissue and cellular aggregates [33-35, 43, 87]. Among these efforts, our team has developed three different microfluidic devices that can perform the entire dissociation process workflow including digestion, dissociation, and filtration [35, 36, 87]. We recently combined all three technologies into a platform and demonstrated improved release of single cells from several tissue types [38]. For this work, we integrated the branching channel dissociation and filter modules into a monolithic device, and since both modules can contribute to break down of cellular aggregates, we now refer to this as the Integrated Disaggregation and Filtration (IDF) device. Our initial study was focused primarily on optimization of the first device component, the digestion device, and so the IDF device was used only as a final polishing step. Notably, the IDF device was not used with tissue that was digested in a traditional manner, which could be as format of high interest to

some researchers due to operational simplicity. Finally, we believe that the IDF device could serve as an ideal test bed for a controlled study into the role of mechanical forces on the dissociation of tissue and cell aggregates. This is because the IDF device allows for variation of processing parameters, such as flow rate and device pass number, as well as the mode of dissociation via the microchannel array, the nylon mesh membranes, or both in concert. Optimization of mechanical dissociation would maximize cell yield, as well as potentially reduce proteolytic digestion time and compensate for differences between tissues in terms of extracellular matrix (ECM) density, cell-cell adhesion strength, and secondary structures such as vessels and ducts.

Here, we evaluate the IDF device with samples ranging from cell culture aggregates to minimally digested tissue in an effort to better understand and optimize mechanical dissociation. We first evaluate small, strongly cohesive aggregates produced from the MCF-7 cell line and show that single cell recovery is maximal at flow rates greater than 40 ml/min and that the filtration module exerts a greater effect than the branching channel array. In fact, multiple passes through the filters produces the highest yield. We then employ minced and digested murine kidney and observe that the primary dissociation mechanism shifts to the branching channel array, with a single filter pass now producing the best results. Notably, we find that the IDF device releases as many epithelial cells following minimal digestion (i.e., 20 min) as a full digestion (i.e., 60 min), if device pass number is increased to compensate. However, this result does not extend to endothelial cells, which appear to have a greater reliance upon enzymatic digestion. This work confirms that the IDF device provides distinct mechanisms for dissociation that depend on aggregate/tissue size, cell-ECM interactions,

and cell-cell adhesion. Importantly, the IDF device increases single cell recovery for all samples and cell subtypes, by at least 2-fold.

3.2. Materials and Methods

3.2.1. Device fabrication

The integrated disaggregation/filtration (IDF) device was fabricated by ALine, Inc. (Rancho Dominguez, CA), as previously described [38]. Briefly, fluidic channels, vias, and openings for fittings were laser cut on 250 μm thick polyethylene terephthalate (PET) layers. Nylon mesh membranes were purchased from Amazon Small Parts (15 and 50 μm pore sizes; Seattle, WA) as large sheets and were laser cut into 8.76 mm diameter circles. Then, the PET layers and nylon mesh membranes were sandwiched between two additional layers of PET, the top containing holes for placement of hose barbs. All layers are aligned and bonded with pressure sensitive adhesive using pressure lamination.

3.2.2. Cell culture and tissue models

MCF-7 cells were purchased from ATCC (Manassas, VA) and cultured at 37^0C and 5% CO2 in tissue flasks containing DMEM media containing 10% FBS, non-essential amino acids, 1 mM sodium pyruvate, 2 mM L-glutamine, 100 μg mL−1 streptomycin, 100 U mL−1 penicillin, and 44 U L−1 Novolin R insulin (Thermo Fisher, Waltham, MA). Prior to experiments, MCF-7 cell monolayers were briefly treated with trypsin-EDTA to release cells as aggregates and washed with PBS containing 1% BSA (PBS^+).

For tissue dissociation studies, kidneys were harvested from freshly sacrificed C57Bl/6J mice (Jackson Laboratory, Bar Harbor, ME) that were deemed waste from a research study approved by the University of California, Irvine, Institutional Animal Care and Use Committee (courtesy of Dr. Angela G. Fleischman). A scalpel was used to mince the tissue into ~1 mm^3 pieces. Then, approximately 10 mg of minced tissue was placed within a conical tube with 300 µl of 0.25% collagenase type I (C9263, Sigma Aldrich, US). After digesting at 37°C in an incubator under gentle agitation by a rotating mixer for 20 to 60 min, 700 µl of PBS^+ was added to deactivate the enzyme. Controls were dissociated using conventional methods comprised of repeated vertexing and pipetting to mechanically disrupt aggregates and filtration with a cell strainer (35 µm) to remove cell debris. All cell suspensions were treated with 100 Units of DNase I (Roche, Indianapolis, IN) for 10 min at 37°C, washed, and resuspended for further analysis.

3.2.3. Dissociation studies

Devices were prepared by affixing 1/32 in ID tubing (Nalgene, Rochester, NY) to the hose barbs at both the inlet and outlet. Prior to use, devices were primed with PBS+ and incubated for 15 minutes to prevent non-specific cell adhesion to the channel walls. Aggregate and tissue models were passed through the microchannel array and/or nylon mesh filter modules of the IDF device under different flow rates (20-60 ml/min) and/or device pass numbers (5-20 passes) by a syringe pump. Finally, devices were flushed with 2 mL PBS^+ to wash out remaining cells and both device effluents were combined.

3.2.4. MCF-7 cell count and viability

Cell suspensions from dissociated MCF-7 samples were analyzed for the number of single cells and aggregates using a hemocytometer. Viability was also assessed using Trypan blue stain. The single cell and aggregate counts for each dissociation condition were normalized to the counts prior to device processing.

3.2.5. Flow cytometry

Kidney cell suspensions were evaluated for epithelial cells, endothelial cells, leukocytes, and red blood cells by flow cytometry, as described [38]. Briefly, cells were stained concurrently with 5 μg/mL anti-mouse CD45-AF488 (clone 30-F11, BioLegend, San Diego, CA), 7 μg/mL EpCAM-PE (clone G8.8, BioLegend, San Diego, CA), and 5 μg/mL TER119-AF647 (clone TER-119, BioLegend, San Diego, CA) monoclonal antibodies for 30 minutes. Samples were then washed twice using PBS+ by centrifugation, stained with 3.33 μg/mL viability dye 7-AAD (BD Biosciences, San Jose, CA) on ice for at least 10 minutes, and analyzed on a Novocyte 3000 Flow Cytometer (ACEA Biosciences, San Diego, CA). Flow cytometry data was compensated using compensation beads (Invitrogen, Waltham, MA). Gates encompassing the positive and negative subpopulations within each compensation sample were inputted into FlowJo (FlowJo, Ashland, OR) to automatically calculate the compensation matrix. A sequential gating scheme was used to identify live and dead single epithelial cells from leukocytes, red blood cells, non-cellular debris, and cellular aggregates. Signal positivity was determined using appropriate Fluorescence Minus One (FMO) control. All cell counts were normalized to the mass of tissue that was dissociated.

3.3. Results and Discussion

3.3.1 IDF device features

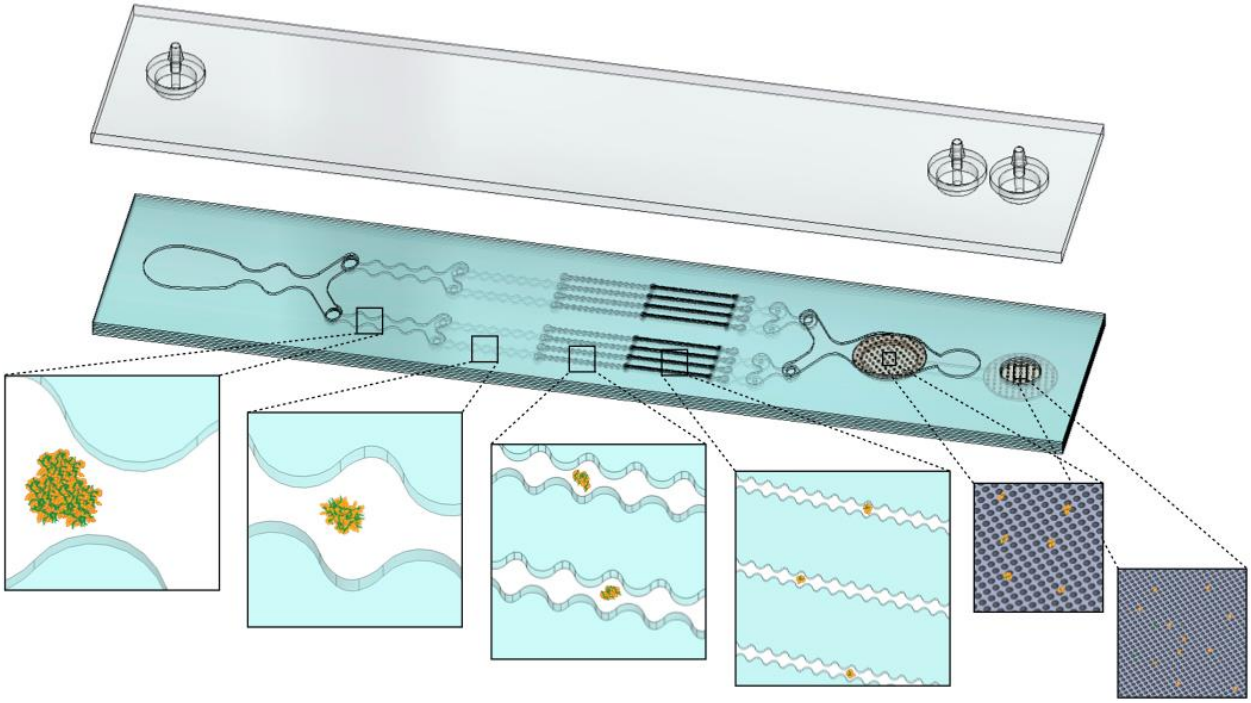

Figure 16- **Schematic representation of the IDF device.** Large aggregates containing high extracellular matrix (ECM) content, such as digested tissue, are exposed to stepwise increases in shear stress throughout the branching channel array as the width narrows from 1 mm to 125 μm. Cell aggregates are held together via through cell-cell (dark orange perimeter) and cell-ECM (green fibers) interactions. As ECM has been digested by collagenase, the channel array gradually reduces aggregate size via hydrodynamics shear forces. The smallest channels and nylon mesh membranes then break down the cell-cell interactions that hold together the smallest aggregates and clusters. Channels, cell aggregates, and membrane pore sizes are not shown to scale.

Figure 16 shows a schematic of the IDF device, as recently presented [38]. This device combines our branching channel array and dual-filtration modules, which provides two

distinct mechanisms for dissociation of cellular aggregates and/or digested tissue. The branching channels gradually and uniformly dissociate cellular aggregates via exposure to stepwise increases in shear stress as channels decrease in size from millimeters to hundreds of microns and cross-sectional width is modulated to generate fluidic jets [35, 87]. We anticipate that these shear stresses will release cells from the surface, without affecting those that are deeper within an aggregate. Filters have been integrated into microfluidic devices to provide high throughput cell manipulation for drug development studies and to reduce clogging [88, 89]. Our filtration device utilizes two nylon mesh membranes for removal of residual large aggregates, as well as increasing cell yield via dissociation [36]. We expect that the dissociation mechanism is related to direct physical interaction with the nylon threads or an alternative hydrodynamic effect. In either case, we anticipate that dissociation occurs for aggregates and clusters that are on the size scale as the pores, which were 50 and 15 μm sizes for this device. The IDF was fabricated using a commercial lamination process, with channel features laser micro-machined into hard plastic layers that were aligned and bonded using pressure sensitive adhesive using pressure lamination. The goal of this study is to perform a detailed examination of the different dissociation mechanisms offered by the branching channel array and filtration modules, as a function of different operational conditions and cell aggregate types. Efficiency of these mechanisms in dissociation of aggregates based on intercellular interactions and adhesion forces for different cell types in tissue will be explored.

3.3.2. Optimization of the branching channel array using MCF-7 cell aggregates

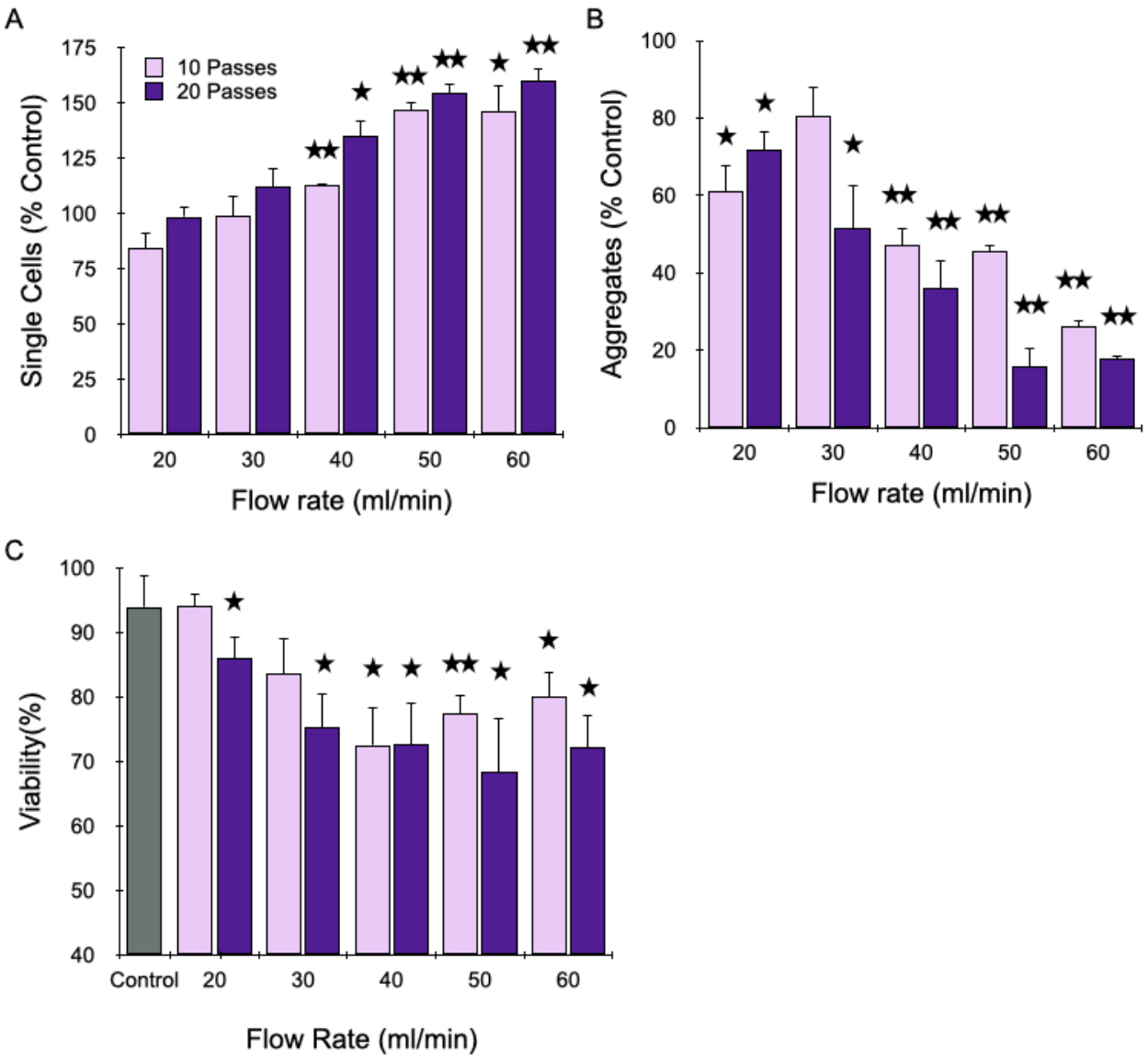

Figure 17- **Optimization of the branching channel array using cell aggregates.** MCF-7 cells were passed through the channels at different flow rates for either 10 or 20 passes. Results are shown for (A) single cell yield, (B) aggregate yield, and (C) viability, which are all normalized to the control that did not pass through the channels. Strong effects were observed for each metric above 40 ml/min, but higher pass number did not influence results. Data are presented as mean values +/- SEM from

at least three independent experiments. Two-sided T test was used for statistical testing. Stars indicate $p < 0.05$ and double stars indicate $p < 0.01$ relative to the unprocessed control.

We began by investigating only the branching channel array, which has been characterized in previous work using cell and tissue models, but under a limited set of operating conditions. Specifically, samples were either applied using a syringe pump at 10.5 ml/min flow rate and actuated back and forth through the device for up to 10 passes [35, 87] or using a peristaltic pump to recirculate up to 10 min at as high as 20 ml/min flow rate [38]. We have chosen to return to the syringe pump format, which can provide higher precision and control. We did employ the IDF device for these studies, but sample exited from the first outlet so as not to pass through the filters. We used the MCF-7 breast cancer cell line because it provides a simple model containing smaller cell aggregates and clusters with a minimal ECM [90, 91]. This will provide key insights into dissociation mechanisms within the smaller channel sections, which would result from disrupting cell-cell adhesions, that will help shape subsequent studies with larger tissue aggregates containing different cell types, higher ECM interactions, and overall greater complexity. MCF-7 cell suspensions were passed though the branching channel array using a syringe pump at flow rates ranging from 20 to 60 ml/min for either 10 or 20 passes, which is a far broader range than previously investigated. Single cell recovery was determined using a hemocytometer and is presented in Figure 17A after normalization by the single cell count before device treatment. Single cells increased steadily with flow rate up to ~150% at 60 ml/min before stabilizing, and all results were statistically significant relative to the control at 40 and 60 ml/min flow rates. Increasing device pass number did increase single cell number at all flow rates, but differences were marginal. Cell aggregates were also quantified using the hemocytometer, defined as two cells or more, and

normalized to the control value (Fig. 2B). As expected, aggregates decreased dramatically with flow rate, and in this case with pass number as well. Although not represented in the data, we also observed that most of the aggregates that remained after device processing were composed of only 2 or 3 three cells, whereas the control had substantially larger aggregates of more than 10 cells . These findings demonstrate that the microchannel array reduced both aggregate number and size, which corroborates the single cell number increases in Figure 17A for most conditions. However, we do note that the 20 and 30 ml/min conditions exhibited a decrease in aggregates that was statistically significant without generating more single cells. This may have been due to a secondary effect such as holdup within the branching channel array. Alternatively, cell reaggregation may have played a role. We generally assume reaggregation is unlikely since the buffer lacks divalent cations necessary for most cell-cell adhesion molecules, but a contributing factor could be DNA released from damaged cells that can cause cells to adhere together [92]. We also note that reaggregation can be promoted under certain hydrodynamic conditions [93]. The channel constrictions and expansions provide elongational and shear flows similar to previous studies of colloidal aggregates [94]. Therefore, it can be concluded that reaggregation is playing a role in lower flow rates which is reflected in higher aggregate percentage in low flow rates. Cell viability was determined using Trypan blue stain, and results are shown in Figure 17C. We observed a decrease in viability with both flow rate and pass number, from the control value of ~90% to as low as 70%. This shows that some damage can be associated with more aggressive dissociation conditions.

3.3.3. Assessment of MCF-7 aggregate dissociation using the nylon mesh filters.

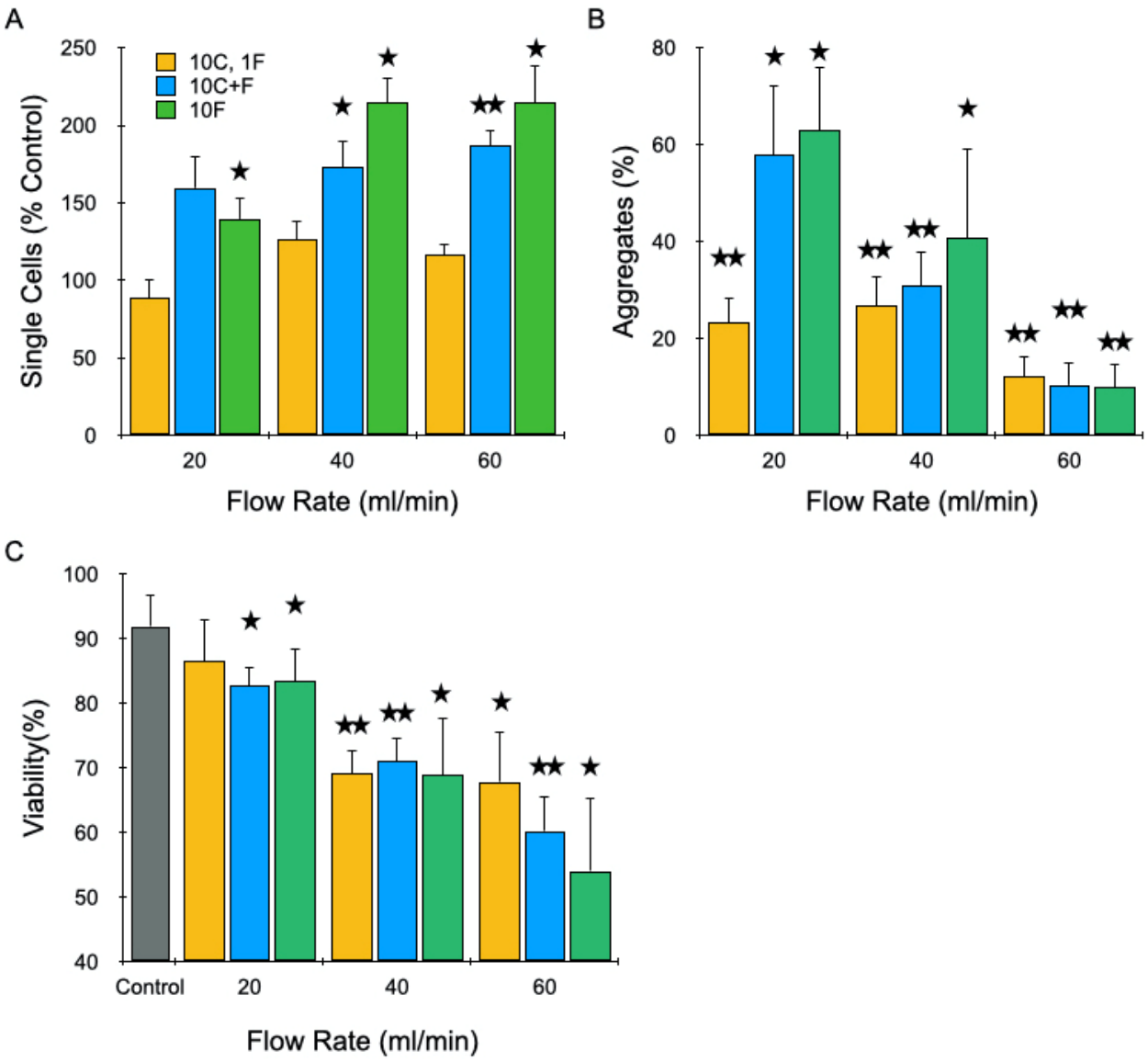

Figure 18- **Evaluation of different dissociation formats using cell aggregates.** MCF-7 cells were passed through the channel module 10 times and filter module once (10C,1F), both channel and filter modules 10 times (10C+F), or the filter module 10 times (10F) at 40 ml/min. Results are shown for (A) single cell yield, (B) aggregate yield, and (C) viability, which are all normalized to the unprocessed control. Optimal results were observed at 40 ml/min using multiple filter module passes. Data are presented as mean values +/- SEM from at least three independent experiments. Two-sided T test was used for statistical testing. Stars indicate $p < 0.05$ and double stars indicate $p < 0.01$ relative to

the unprocessed control. Stars indicate $p < 0.05$ and double stars indicate $p < 0.01$ relative to the unprocessed control.

Next, we evaluated the effect of filtration on dissociation of MCF-7 aggregates under different operational configurations, including with and without the branching channel array. Based on results from the previous section, we employed flow rates of 20, 40, and 60 ml/min. Moreover, we chose to limit pass number to 10, since 20 did not alter results substantially. Finally, we selected three different device configurations: 1) 10 passes through the channel array followed by 1 pass through the filters (10C,1F), 2) 10 passes simultaneously through both the channel array and filters (10C+F), and 3) 10 passes through the filters alone (10F). Results obtained for single cells, aggregates, and viability are presented in Figure 18. Upon comparison of Figure 17A and Figure 18A, we found that a single filtration offered no benefit to the branching channel array. In fact, the increase in single cell recovery that was observed at higher flow rates was now lost, which may have been due to greater sample holdup within the full IDF device. Passing sample through both devices in series enhanced performance, resulting in statistically significant increases in single cell recovery at 40 and 60 ml/min, with the latter approaching 2-fold. Interestingly, single cell recovery was highest using the filtration module as a standalone treatment, exceeding 2-fold increases at both 40 and 60 ml/min. The presence of aggregates was primarily dependent on flow rate and not the device configuration (Figure 18B). However, aggregate values were lower than when the branching channel array was used along (Figure 18B), particularly at the higher flow rates. We note that enhanced removal of aggregates by the filters may have been due to either dissociation or filtration effects. Viability also predominantly correlated with flow rate (Figure 18C), although viability was lowest using multiple filtrations passes at 60

ml/min. Taken together, the surprisingly strong performance of filtration alone was likely heavily influenced by the simple MCF-7 model, with most aggregates starting at <100 μm and held together primarily by strong cell-cell adhesions. The filtration module clearly performed better on this sample type, which can be traced to the physical barrier and optimal sizing of the sequential 50 and 15 μm mesh filters. The smallest feature size of the branching channel array is much larger at 125 μm, although shear stresses generated by the fluidic jets act on a smaller scale. Consequently, the channel dissociation mechanism does not add substantially to the filter dissociation mechanism with this cell model, and thus primarily detracted from cell recovery via losses from device hold-up and/or damage. In sum, filtration is critical for dissociation of smaller aggregates and the 40 ml/min flow rate provides the optimal balance between promoting dissociation and limiting damage.

3.3.4. Evaluation of disaggregation and filtration using digested kidney tissue

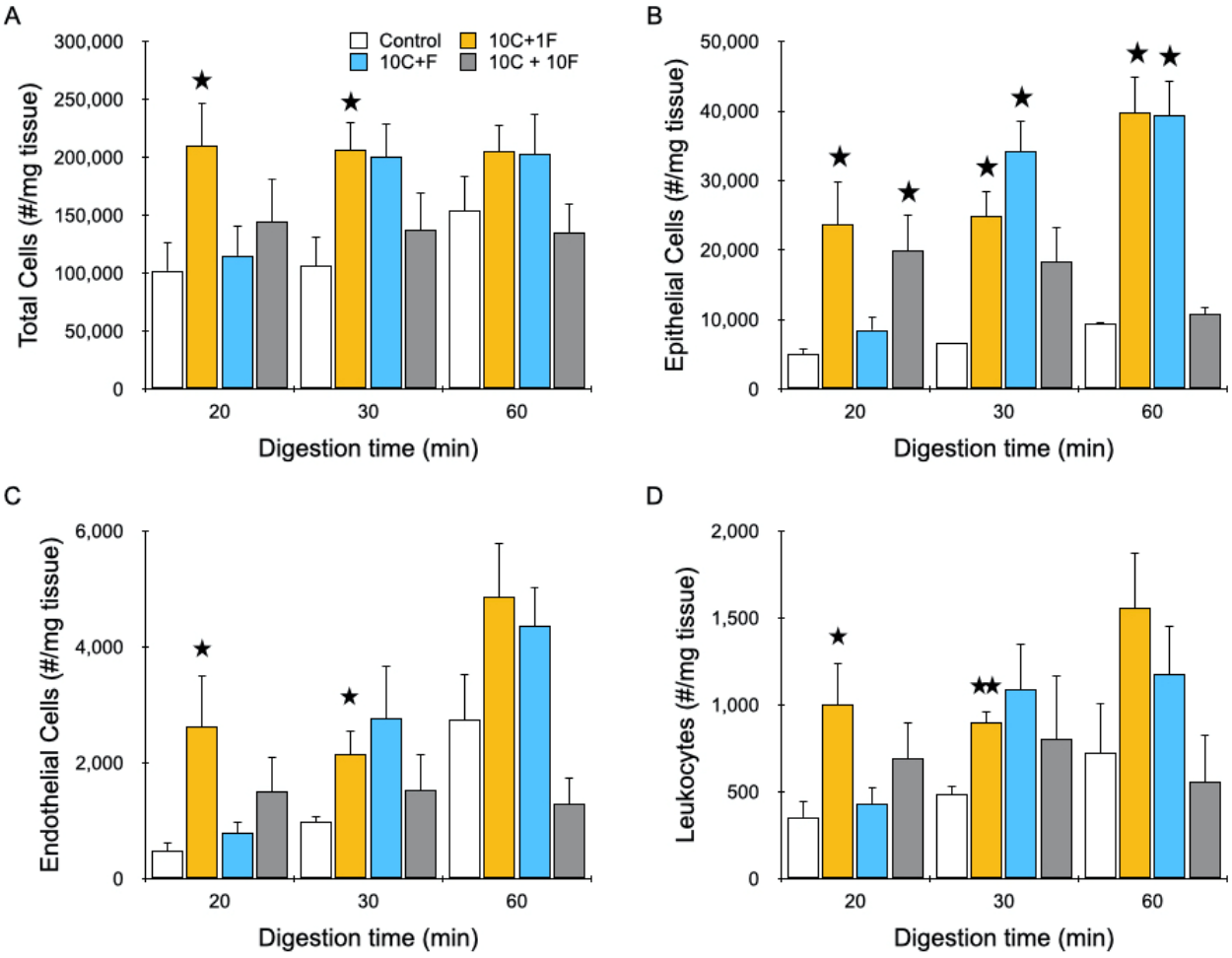

Figure 19- **Evaluation of dissociation formats using murine kidney**. Kidneys were harvested, minced, and digested for the indicated time periods. Samples were then passed through the channel module 10 times and filter module once (10C,1F), simultaneously through both modules 10 times (10C+F), or sequentially through both modules 10 times (10C+10F) at 40 ml/min and resulting cell suspensions were analyzed using flow cytometry. Controls were pipetted/vortexed and passed through a cell strainer. Results are shown for viable and single (A) total cells, (B) EpCAM+ epithelial cells, (C) endothelial cells, and (D) leukocytes. Optimal results were attained using the single filter pass at each digestion time. Data are presented as mean values +/- SEM from at least three

independent experiments. Two-sided T test was used for statistical testing. Stars indicate $p < 0.05$ and double stars indicate $p < 0.01$ relative to the control at the same digestion time.

Our next goal was to test the performance of the branching channel array and filters for dissociation of murine kidney tissue that was digested for different periods of time. Specifically, we chose to digest minced kidney with collagenase for 20, 30, or 60 min to produce aggregates of varying size and ECM content. Collagenase cleaves collagen, the major structural element of ECM that provides tensile strength and anchors cells [95, 96]. Therefore, collagenase digestion weakens cell-ECM interactions, facilitating isolation of single cells via mechanical disaggregation, but while maintaining the surface membrane and proteins intact [97]. Cell suspensions from digested tissue were loaded into the IDF device for processing at 40 ml/min flow rate under one of three configurations: 1) 10 passes through the channel array followed by 1 pass through filters (10C,1F), 2) 10 passes simultaneously through both the channel array and filters (10C+F), and 3) 10 passes sequentially through the channel array and filters (10C,10F). We chose not to test the filter device alone since digested tissue was likely to require the branching channel array to first reduce larger fragments down in size before encountering the filters, which would otherwise be retained on the mesh membranes as expected for classical filtration. Flow cytometry was then used to identify and enumerate epithelial cells, endothelial cells, and leukocytes based on surface marker expression. Cell membrane proteins are vital for proper cell function and survival by mediating interactions with environmental cues and other cells [98], but can be affected by proteolytic digestion [99], and therefore expression is an important functional metric. We also employed the viability stain 7-AAD. Live single cell counts are presented in Figure 19 for total cells and the three cell subtypes detected. For total cells (Figure 19A), we

found that cell yield was highest for the condition with only a single filtration device pass (10C,1F). This result was surprising given the relatively poor performance seen for the MCF-7 model, but it was consistent across all digestion time points. For the 20- and 30-min digestion times, approximately 2-fold more single cells were recovered using the IDF device under the single filtration format relative to the respective controls (~200,000 verses ~100,000 per mg), and these differences were statistically significant. For the 60 min digestion time, single cells remained static, but the control increased to 150,000/mg, and the difference was not statistically significant. The simultaneous processing condition (10C+F) was similar to the control at the 20 min time point, but produced similar cell yields as the single filtration case at both 30 and 60 min digestion times. The third and final condition, with separate and sequential 10 passes treatment through each module (10C,10F), produced the lowest yield for each digestion time, which were all comparable to the corresponding controls. We conclude that these samples were over-processed, causing cell damage and lower overall yields. Epithelial cell results were very similar to total cells, but with substantially greater differences between the device conditions and controls (Fig. 4B), likely due to the strong cell-cell adhesions holding epithelial cells together with each other. Specifically, differences were in the range of 4- to 5-fold and were statistically significant for both the single filtration (10C,1F) and dual processing (10 C+F) formats at the longer digestion times. However, only the single filtration (10C, 1F) format was statistically significant at the 20 min digestion time. We found that endothelial cell (Fig. 4C) and leukocyte (Figure 19D) yields closely followed total cells. Viability data for each cell type is presented in Figure 20, and show that epithelial and endothelial cells maintain viability (>95%) even with IDF device processing. Leukocyte viability was lower at ~80%, but again

was not affected by the IDF device. Taken together, these results suggest that shear forces from the branching channel array plays a critical role in dissociation of minced and digested kidney tissue regardless of the degree of digestion, particularly for strongly cohesive epithelial cells. Although not directly tested, we presume that the single pass through the filter device was beneficial, and at minimum ensured that a follow-up cell straining step was not necessary. Based on our data, passage through the filter component more than one time, either simultaneously or sequentially, would not be recommended for any cell type due to limited benefit, or even detrimental effects, to cell yield and/or viability.

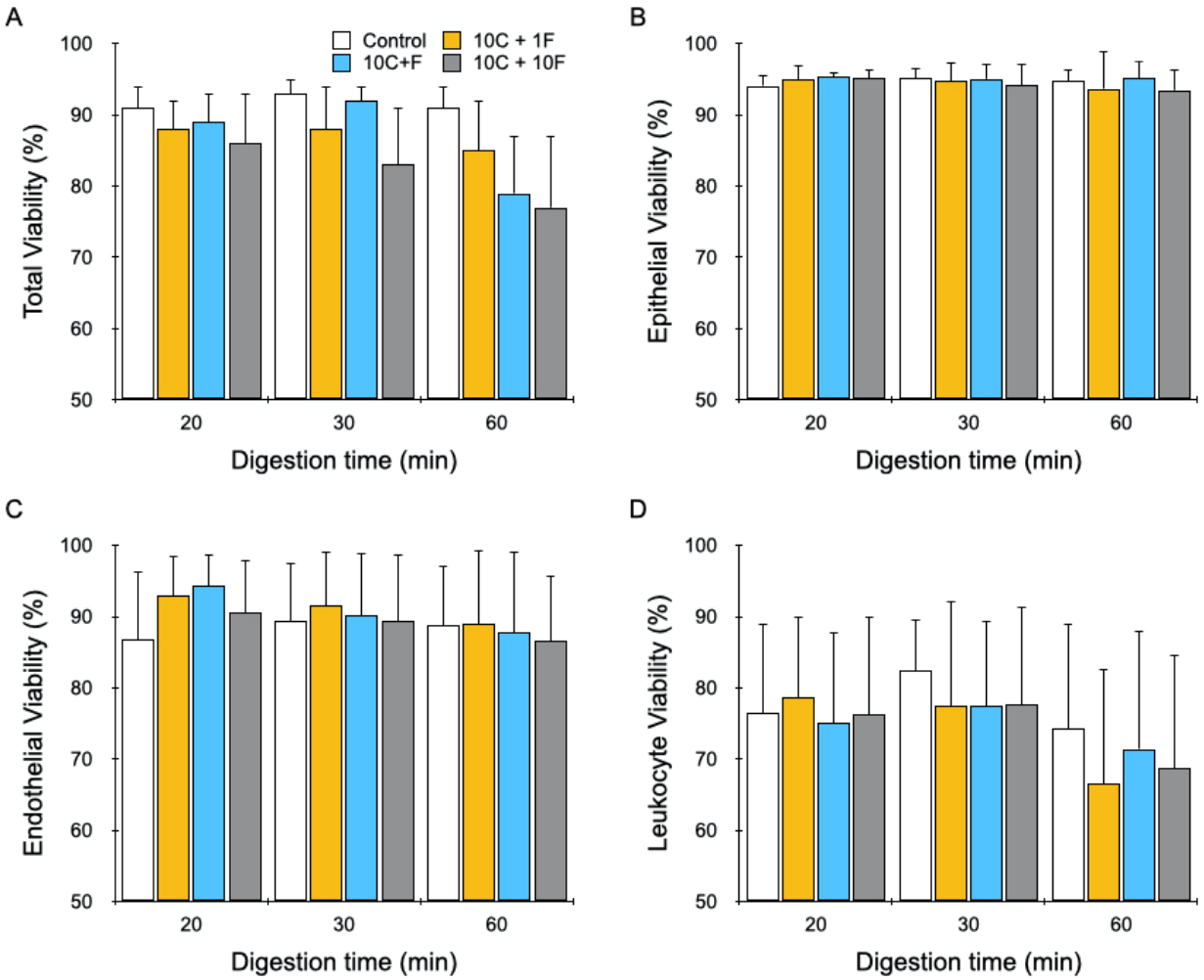

Figure 20- **Cell viability from evaluation of dissociation formats using murine kidney** A) total cells B) epithelial C) endothelial D) leukocyte viability. Kidneys were harvested, minced, and digested for the indicated time periods. Samples were then passed through the channel module 10 times and filter module once (10C,1F), simultaneously through both modules 10 times (10C+F), or sequentially through both modules 10 times (10C+10F) at 40 ml/min and resulting cell suspensions were analyzed using flow cytometry. Controls were pipetted/vortexed and passed through a cell strainer.

3.3.5. Optimization of kidney dissociation using the IDF device

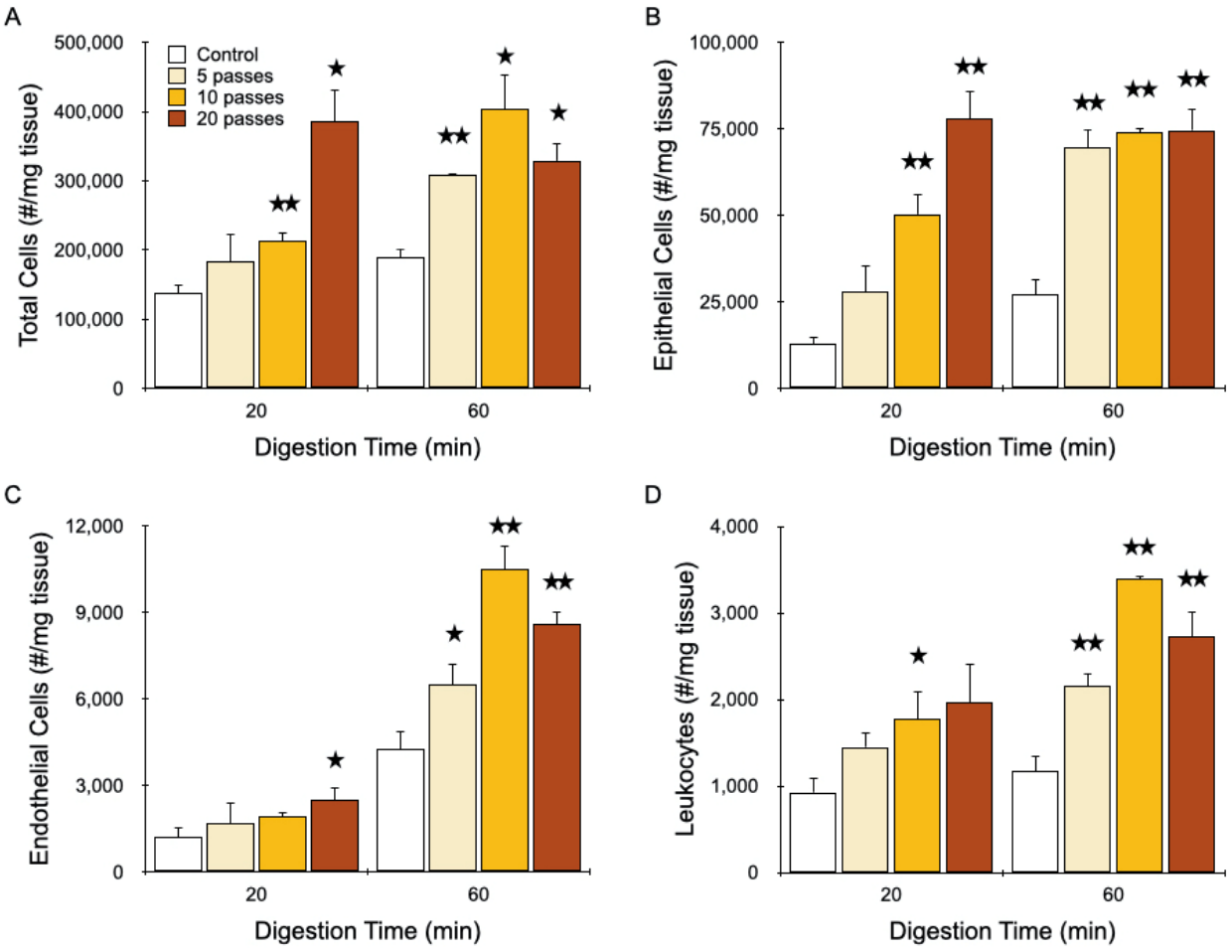

Figure 21- **Final optimization of murine kidney**. Kidneys were harvested, minced, and digested for the indicated time periods. Samples were then passed through the channel module for the indicated

number of times and filter module once (10C,1F) and resulting cell suspensions were analyzed using flow cytometry. Controls were pipetted/vortexed and passed through a cell strainer. Results are shown for viable and single (A) total cells, (B) EpCAM+ epithelial cells, (C) endothelial cells, and (D) leukocytes. Similar epithelial yields were obtained after 20 min digestion time using 20 passes and 60 min digestion time using 10 passes. However, maximal endothelial and leukocyte yields required 60 min digestion time and 10 passes. Data are presented as mean values +/- SEM from at least three independent experiments. Two-sided T test was used for statistical testing. Stars indicate $p < 0.05$ and double stars indicate $p < 0.01$ relative to the control at the same digestion time.

Finally, we sought to determine the most efficient operating conditions for the IDF device. Based on the previous study, this would involve the branching channel array followed by a single pass through the filters. We again used different digestion times and a flow rate of 40 ml/min, but now varied branching channel array pass number from 5 to 20. We contend that this will provide the most controlled approach to modulate mechanical treatment level and subsequently identify optimal conditions for different tissue inputs and cell type outputs. Results for total cell recovery are presented in Figure 21A. After only 20 min of digestion, 5 and 10 passes through the channel array generated only modest increases in cell yield relative to the control, although the latter was statistically significant. However, increasing pass number to 20 enhanced cell recovery to nearly 3-fold that of the control. After a full 60 min digest, 5 passes produced a difference of 50% that was statistically significant. Further treatment initially increased cell yield to 2-fold, before dropping back to ~50% at 20 passes. Notably, cell recovery was the same for the 20 min digest using 20 passes as the 60 min digest with 10 passes, which would result in a substantial reduction in processing time without sacrificing performance. Findings were similar for epithelial cells

(Figure 21B), but now with a more stepwise response observed for pass number after a 20 min digest and no response at all after a 60 min digest. Importantly, equivalence of cell yield was preserved between the 20 min digest/20 pass and 60 min digest/10 pass conditions. We also note that the maximum epithelial cell recoveries of ~80,000/mg tissue are substantially greater than the ~40,000 to 60,000/mg tissue range from our previous works [35, 36, 38], highlighting the power of the IDF device when deployed in an optimal manner. Results for endothelial cells (Figure 21C) and leukocytes (Figure 21D) were comparable to total cells, however in both cases, additional mechanical processing could not compensate for shorter digestion time. The difference was particularly pronounced for endothelial cells, with ~4-fold less cells obtained from the 20 min digest relative to the 60 min digest, even after 20 passes. Thus, the potential digestion time savings that the IDF device can offer to epithelial cells did not apply to all cell types. Viability data for each cell type is presented in Figure 22, and show that epithelial cell viability is above 80% in all cases. However, it drops for endothelial cells and leukocytes, suggesting that there is room for optimization of the process to keep viability high.

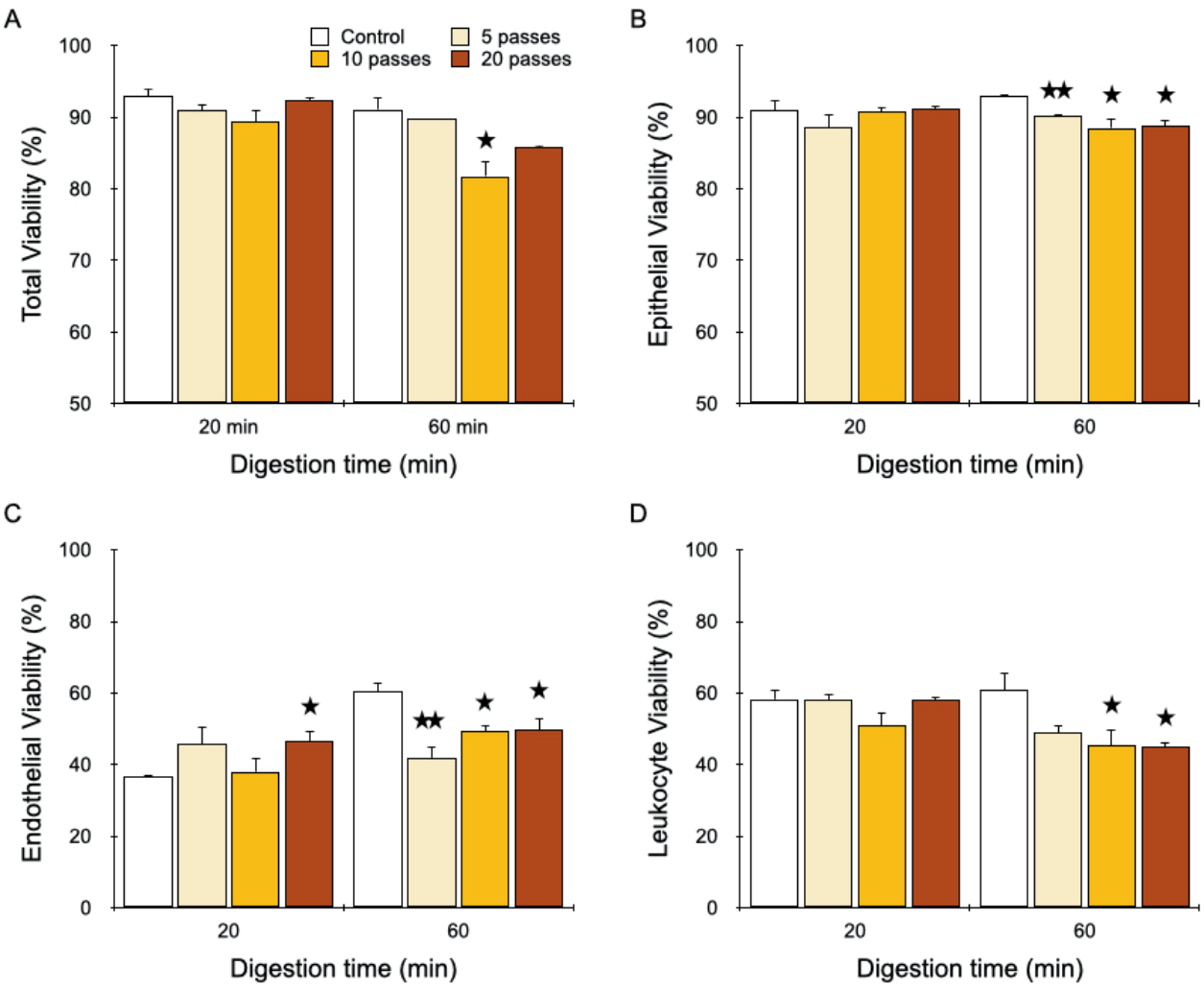

Figure 22- **Cell viability for final optimization of murine kidney** A) total cells B) epithelial C) endothelial D) leukocyte viability at different number of passes and digestion times. Kidneys were harvested, minced, and digested for the indicated time periods. Samples were then passed through the channel module for the indicated number of times and filter module once (10C,1F) and resulting cell suspensions were analyzed using flow cytometry. Controls were pipetted/vortexed and passed through a cell strainer. Results are shown for viable and single (A) total cells, (B) EpCAM+ epithelial cells, (C) endothelial cells, and (D) leukocytes. Similar epithelial yields were obtained after 20 min digestion time using 20 passes and 60 min digestion time using 10 passes. However, maximal endothelial and leukocyte yields required 60 min digestion time and 10 passes. Data are presented as mean values +/- SEM from at least three independent experiments. Two-sided T test was used for

statistical testing. Stars indicate $p < 0.05$ and double stars indicate $p < 0.01$ relative to the control at the same digestion time.

Tissues are composed of cells that are anchored to the ECM and/or neighboring cells via different types of adhesive interactions, including various integrins and cadherins, which includes complex structures such as focal adhesions, tight junctions, gap junctions, and adherens junctions [100, 101]. Bearing that in mind, isolation of single cells from tissue can only be ensued by overcoming all cell-cell and cell-ECM adhesions through chemical and/or mechanical means. Epithelial cells are typically arranged in sheets of cells that are connected to neighbors through cadherins as well as to the ECM through integrins. The adhesive force of epithelial cell-ECM interactions has been measured to be ~250 nN, while epithelial cell-cell interactions were similar at ~100 nN [102]. Moreover, it has been shown that tissue digestion can result in heterogeneous distribution of ECM, which can then reposition to stabilize the weaker cell-cell adhesions [103]. Hence, removing the cell-ECM interaction can provide an additive effect by means of making it easier to release epithelial cells from each other [104-106]. We believe that these effects are clearly represented in our data. After 60 min digestion, collagen has largely been eliminated from the ECM, leaving only weakened cell-cell interactions that could be overcome by minimal mechanical processing with 5 passes through the branching channel array and 1 pass through the filter. Additional channel passes did not affect single cell yield, which may simply mean that cells were neither released nor damaged, although it is possible that these processes were in balance. This finding is most likely related to the fact that cell aggregates were smaller in nature after extensive digestion. Based on our results with MCF-7 cells, we would have expected that multiple passes through the filter device would have aided dissociation of smaller

aggregates/clusters, but this was clearly not the case (Fig. 4B). This may have been due epithelial cells from kidney either being more sensitive to filter-induced damage or possessing weaker cell-cell adhesions that could sufficiently be overcome by the single filter pass. We acknowledge that this result may change for different tissues and/or cell types, such as tumors, which will be studied in future work. For the 20 min digestion time, substantial ECM still remained, and cell aggregates were presumably larger. This provided an opportunity for mechanical dissociation by the branching channel array to exert a key effect, releasing more single cells in a dose-dependent manner, culminating in the surprising result that 20 passes could provide a single cell yield that rivaled the full 60 min digestion. Shortening digestion time without compromising cell yield is of critical importance to limit the time that enzymes are in contact with cells, as well as stress response pathways that can interfere with transcriptomic analysis [107-109], as we have recently shown using the full microfluidic platform including the digestion device [38].

Endothelial cells and leukocytes displayed similar results, but with distinct differences to epithelial cells, as well as each other. These differences can likely be linked to anatomic origin within tissues, namely within blood vessels, which are densely located throughout the kidney to facilitate the primary physiological role of blood filtration and waste removal. Importantly, blood vessels are a secondary structure within the tissue, requiring deeper access of enzymes and shear forces before chemical and/or mechanical dissociation can ensue. However, most leukocytes simply reside within the blood, which can be released as soon as that deeper access is attained. For these reasons, maximal leukocyte and endothelial recoveries after 20 min digestion could only reach ~70% and ~25%, respectively, of the 60 min digestion values. For endothelial cells, several molecules mediate

cell-ECM interactions including proteoglycans and proteins, of which integrins are the best studied [110, 111]. Interestingly, endothelial cells display an inherent shear stress sensitivity, including ECM remodeling [112], stimulation of integrin-mediated cell-cell and cell-ECM adhesions [113], and relocation of adherins junction proteins [114, 115]. Although unclear at this time, a chemo-mechanical response may have played a role in the relatively poor performance of mechanical processing at short digestion times, when vessels were more intact. As stated, most CD45-positive leukocytes are present in free suspension within blood as monocytes, neutrophils, and lymphocytes. However, some can still be found throughout the tissue as resident tissue macrophages, T lymphocytes, or natural killer cells [116, 117], which would be held primarily by cell-ECM interactions [41, 118-120]. It should be also considered that leukocytes can interact with endothelial cells through binding between junctional adhesion molecules at endothelial cell borders and surface receptors on leukocytes [121], which could result in some correlation of cell yield pattern for leukocytes and endothelial cells.

Epithelial cells, endothelial cells, and leukocytes represented approximately one-quarter of the total cell count. The balance could include non-EpCAM expressing cells from the proximal tubules, distal convoluted tubules, loop of Henle, collecting duct, and mesangial cells, which comprise the bulk of cell subtypes detected using single cell RNA-sequencing by us and others [38, 122-124]. Additional structural cells such as podocytes, fibroblasts, and pericytes may have also contributed [107, 125]. Generally, these other cells displayed release dynamics that were most similar to EpCAM+ epithelial cells.

3.4. Conclusions

Herein, we have performed a detailed optimization study of cell aggregate and tissue dissociation using our branching channel array and dual-filter modules that comprise our integrated disaggregation and filtration device (IDF). We tested substantially higher flow rates than in previous work and found that 40 ml/min was optimal for all samples. The dominant mechanism of dissociation varied, however, with smaller (<100 μm) and highly cohesive MCF-7 cell aggregates requiring multiple passes through the filters to achieve maximal single cell yield. Conversely, minced and digested murine kidney relied upon the branching channel array, and multiple filter passes was detrimental. This result was due to the larger size of the tissue aggregates and, as we hypothesize, a greater dependence on cell-ECM interactions. The most exciting finding was that the IDF device can release as many epithelial cells after a substantially shorter digestion (i.e. 20 vs 60 min) by simply passing through the device more times. Reducing processing time in this manner could strongly impact long-term cell viability under culture settings and reduce stress responses that can interfere with transcriptomic-based cell classification, which will be studied in future work. Shortening processing time will also reduce the cell treatment in metabolically active which will lessen the risk of transcriptomic or proteomic changes. This result did not extend to endothelial cells, however, due to greater reliance on digestion, which could result in cell subtype biasing. Overall, the optimal processing condition for all cell subtypes was to digest for 60 min, pass 10 times through the branching channel array at 40 ml/min, and then pass once through the filters at 40 ml/min. This work with the IDF device has enhanced our understanding of different dissociation mechanisms and cell/tissue aggregate properties.

Moreover, it was shown that IDF device can shorten the digestion time significantly while giving higher single cell yield. It is worth mentioning that tissue processing at physiological temperature(37^0C) for enzyme activity, will cause stress response since cell transcriptional machinery is active and hence, gene expression can be changed[27]. Therefore, minimizing digestion time and temperature is recommended to minimize these unwanted effects[126]. Shortening digestion time and temperature is an important advantage of IDF device to achieve unbiased single cell population for downstream analysis.

In the future, we will continue to expand this knowledge by performing similar tests in conjunction with the digestion device, evaluating different tissues and enzyme solutions, and analyzing results using single cell RNA sequencing.

CHAPTER 4: Optimization of the integrated dissociation platform in pulsatile flow

4.1. Introduction

Cellular heterogeneity is known as a major challenge in different field of biology including stem cell biology, immunology, and cancer research[127]. Single cell analysis can tackle this challenge and unveils the link between molecular events in single cells and tissue behaviors[128, 129]. This field has extensively progressed with high-throughput single cell analysis methods such as single cell RNA sequencing, mass cytometry and flow cytometry[130-132]. These methods are redefining our understanding of biological systems with identification of new cell types, their states, and their development in the vast landscape of events[133]. For example, specific stem cell population is responsible for regeneration in response to injury.

Although single cell analysis can unveil new aspects of biological systems, there are major resources of error that casts doubt on the reliability of results. Process of single cell preparation is the first step toward single cell analysis which can introduce artifacts and batch to batch variations. It is significantly important when it comes to isolation of specific rare cell types in tissue. Tissue dissociation has several intertwined aspects that has blocked us from significant biological events. However, these different aspects have been thoroughly studied in other systems which are analogous to tissue dissociation. For example, cell size and shape can affect the dissociation process in analogy with nanoparticle aggregates[134].

ECM resembles the entangled amorphous network in polymers which can affect its mechanical properties through disaggregation and competitive processes[135]. The fact that cells are connected to each other within the ECM resembles the interaction of monomers in a polymer chain in bead spring model[136]. While the cell act like beads, ECM has a function similar to springs. Studies in materials field inspires us to consider the effect of flow type in dissociation of tissue. On the other hand, cell response to chemical and mechanical cues add to the complexity of disaggregation process which has not been noticed in literature to the best of our knowledge. For example, studies show that endothelial cells respond to flow type through alterations in elongation and alignment[137]. However, it has not been studied if dissociation of endothelial cells will also be affected by flow type. Microfluidics offers a robust platform for studying different effective parameters of tissue dissociation including the effect of flow type on tissue dissociation process. Microfluidic devices have recently attracted attention for dissociation of cell aggregate and tissue. [32, 33, 43, 138].Our group as a leader in this field has introduced several microfluidic devices as replacement of different steps of tissue dissociation which can work as a platform to make this process automated, labor free and precise [35, 36, 38, 87]. Here, we focus on study of flow type in tissue dissociation process on dissociation device as the major module of our platform. Syringe pump was used in our previous study for understanding the dissociation mechanisms playing role in IDF device. Syringe pump provides a stable flow rate which helps in reproducibility of biological studies. Also, flow rate stability is critical for stable shear stress exposed to cells. In addition, the flow rate setup in our platform provides laminar flow in our device which ensures us about steady tangential component of shear forces generated at the cell surface to break down the cell-cell and cell-ECM interactions. However, it would

be favorable to use pulsatile flow for our platform since it can be beneficial for specific cell types based on their inherent environmental characteristics. Also, pulsatile flow is easier for automation and commercialization. The first device in our platform, the Digestion device works with pulsatile flow to provide recirculation of enzyme over the tissue. Here, we focus on studying the effect of pulsatile flow provided by peristaltic pump on the performance of the IDF device. This can determine if we can use pulsatile flow for the whole platform. A peristaltic pump, also commonly known as a roller pump, is a type of positive displacement pump. It works through rotary motion, of rotor attached to rollers which compress a flexible tube as they rotate by. The part of the tube under compression is closed, forcing the fluid to move through the tube. Additionally, as the tube opens to its natural state after the rollers pass, more fluid is drawn into the tube. This process happens in biological systems such as the gastrointestinal tract. Therefore, peristaltic pump provides a pulsatile flow which has analogy in physiology. In each pulse, there is a period of time for development of flow to laminar flow. It means that cells will be exposed to normal stresses (pressure) periodically. These normal stresses can cause instability while it can also be helpful in breaking the intercellular interactions. With that in mind, it is desirable to study the effect of pulsatile flow on dissociation of tissue with IDF device.

4.2. Materials and Methods

4.2.1. Device Fabrication

The integrated dissociation/filter (IDF) device was fabricated by ALine, Inc. (Rancho Dominguez, CA) through laser cutting and pressure lamination as described in our previous work. Briefly, fluidic channels, vias and openings were laser cut over Polyethylene

terephthalate (PET) layers. Nylon mesh membranes were purchased from Amazon Small Parts (15, and 50 μm pore sizes; Seattle, WA) as large sheets and were laser cut to size. Then, PET layers and nylon mesh membranes were sandwiched between two layers containing holes at the top for placement of hose barbs. Multiple layers are then aligned, and adhesive bonded with pressure lamination.

The Digestion device was designed to process ~1mm^3 pieces of tissue into cellular suspensions that can be integrated with downstream Integrated Dissociation and Filtration (IDF) device including branching channel array and filter modules. The Digestion device is composed of 3 primary components. The first component is a ~5 mm x 5 mm tissue chamber, which retains the pieces of minced tissue while proteolytic enzyme solution is pumped through the chamber. These chamber dimensions were designed to be easily filled by loading tissue through the ~2.5 mm diameter input port above it. The chamber height is 1.5 mm, slightly larger than the pieces of tissue to prevent clogging. The second part is a cover sticker to seal the tissue chamber. The third and final component is a series of upstream and downstream fluidic channels. The upstream channels were designed to focus the enzymatic solution into high velocity fluidic jets directed at the pieces of tissue, agitating the pieces. The downstream channels function as a sieve to prevent large pieces of tissue from leaving the chamber, while single cells and small aggregates can exit the chamber for collection or further microfluidic processing. Channel widths entering and leaving the tissue chamber were chosen to be 250 μm. Channel height is 300 μm like the other devices. Channels were separated by 1 mm to allow reliable fabrication by laser cutting and pressure lamination, and four channels could comfortably be accommodated across the sides of the tissue chamber. The channel length is 4 mm to avoid clogging. The device was fabricated using

pressure lamination method which includes laser cutting features in polymeric sheets and attach them together with pressure-sensitive adhesive (PSA) under pressure.

4.2.2. Cell culture and tissue model

MCF-7 cells purchased from ATCC (Manassas, VA) were cultured at 37 ^{0}C and 5% CO2 in tissue flasks containing DMEM media containing 10% FBS, non-essential amino acids, 1 mM sodium pyruvate, 2 mM L-glutamine, 100 µg mL−1 streptomycin, 100 U mL−1 penicillin, and 44 U L−1 Novolin R insulin (Thermo Fisher, Waltham, MA). Prior to experiments, MCF-7 cell monolayers were harvested using trypsin-EDTA for 3 minutes to liberate cells while retaining significant cellular aggregates and then, resuspended in PBS containing 1% BSA (PBS^{+}).

For tissue dissociation studies, kidneys were harvested from freshly sacrificed C57Bl/6J mice (Jackson Laboratory, Bar Harbor, ME) that were deemed waste from a research study approved by approved by the University of California, Irvine, Institutional Animal Care and Use Committee (courtesy of Dr. Angela G. Fleischman). A scalpel was used to mince the tissue to ~1mm^3 pieces. Then, approximately 10 mg of minced tissue was placed within a conical tube with 300µL of 0.25% collagenase type I (C9263, Sigma Aldrich, US). Samples were digested at 37 °C in an incubator under gentle agitation by a rotating mixer for 20 or 60 min. Subsequently, 700 µl of PBS^{+} was added to deactivate the digestive enzyme. Finally, it was run through different configuration of dissociation and filtration modules in the IDF device. The results were compared to the conventional method which comprises of repeated vertexing and pipetting to mechanically disrupt aggregates and then, filtration to remove cell debris. Cell suspensions were then treated with 100 Units of DNase I (Roche,

Indianapolis, IN) for 10 min at 37 °C. Finally, cells were washed and resuspended for further analysis.

4.2.3. Dissociation studies

Devices were prepared by affixing 1/32 ID tubing (Nalgene, Rochester, NY) to the hose barbs at both the inlet and outlet. Prior to use, devices were primed with PBS+ and incubated for 15 minutes to prevent cell adhesion to the channel walls. Samples (MCF-7 cell aggregate or digested tissue suspension) were loaded into a syringe and administered into the IDF device by a syringe pump or peristaltic pump. In syringe pump setup, samples were passed through the IDF device between syringes connect to the inlet and outlet with the desired configuration, flow rate and number of passes. In peristaltic pump setup, samples were injected to the closed loop of the IDF device connected to peristaltic pump through a three-way stopcock valve and run with different configurations, flow rate and times. Finally, devices were flushed with PBS^{+} to wash out remaining cells and the sample was collected.

For the Digestion device process, Digestion device was prepared by affixing 0.05" ID tubing to the device inlet and outlet hose barbs. Then, the device was washed with PBS+ to reduce cell binding to channel walls. Freshly dissected tissue was minced into 1 mm^3 pieces and then loaded into the chamber. Then, a cover sticker was adhered to the top of the chamber for sealing. The channels were primed with collagenase type I. In the next step, the enzyme filled tubing was connected to make a close circuit between the device and peristaltic pump. Then, circulation of enzyme was done inside an incubator at 37 ^{0}C at specified flow rate and time. After that, the cell suspension was collected in a conical tube. Then, the effluent was processed further through the IDF device with syringe pump or peristaltic pump.

4.2.4. Cell counting

Dissociation efficiency for MCF-7 cell was determined based on single cell recovery and yield. Single cell count for each condition was normalized to the single cell count prior to device processing. Single cell and aggregates were counted using Trypan blue vital staining and cell counting using a Bürker chamber.

4.2.5. Flow cytometry

Kidney cell suspensions were stained concurrently with 5 μg/mL anti-mouse CD45-AF488 (clone 30-F11, BioLegend, San Diego, CA), 7 μg/mL EpCAM-PE (clone G8.8, BioLegend, San Diego, CA), and 5 μg/mL TER119-AF647 (clone TER-119, BioLegend, San Diego, CA) monoclonal antibodies for 30 minutes. Samples were then washed twice using PBS+ by centrifugation, stained with 3.33 μg/mL viability dye 7-AAD (BD Biosciences, San Jose, CA) on ice for at least 10 minutes, and analyzed on a Novocyte 3000 Flow Cytometer (ACEA Biosciences, San Diego, CA). Flow cytometry data was compensated using single stained cell samples or compensation beads (Invitrogen, Waltham, MA). Gates encompassing the positive and negative subpopulations within each compensation sample were inputted into FlowJo (FlowJo, Ashland, OR) to automatically calculate the compensation matrix. A sequential gating scheme was used to identify live and dead single epithelial cells from leukocytes, red blood cells, non-cellular debris, and cellular aggregates. Signal positivity was determined using appropriate Fluorescence Minus One (FMO) controls.

4.3. Results and discussion

4.3.1. MCF7 cell aggregate dissociation in IDF device with pulsatile flow

At first, MCF7 cell line was used to study the best configuration of branching channels array and filter modules. 10 and 20 ml/min flow rates were chosen since it matches the dynamics used for the tissue processing platform in our previous studies. Circulation through the device was done for 0.5 and 2 minutes to study short-term and long-term effect of the modules on dissociation of aggregates. The results show that recirculation for 0.5 minute at 20 ml/min shows the highest single cell yield. In this condition, the best cell yield is achieved when the filter module is used alone. It has been observed that filter module alone can give the highest cell yield in our studies with syringe pump as well. However, it is worth mentioning that using the filter module will cause more fluctuations in the single cell yield in higher flow rate (20 ml/min). Also, deeper look shows that increasing the flow rate and recirculation time reduces the stability of results and the error bars get bigger. It can be justified with the fact that at higher flow rate, instability period in each pulse will increase which will cause larger error bars. In the most extreme condition, 20 ml/min with 2 minutes recirculation time, number of aggregates drops significantly. However, the cell yield doesn't increase as expected. Also, viability is affected detrimentally. It shows that cells will break down to debris at high flow rate and recirculation time. It warns that increasing the flow rate and recirculation time cannot be an option for improving dissociation of aggregates. It is the most important takeaway from this study. Although we are interested in higher flow rate for a faster processing, it should be done in short amount of time. Therefore, flow rate of 20 ml/min with short circulation time would be the choice for the next studies. On the other hand, among different configurations, filter module alone shows the highest single cell yield, which is favorable, but it costs higher instability. Therefore, the best configuration is using

the branching channel array module for the circulation time and passing the effluent though the filter module for one time.

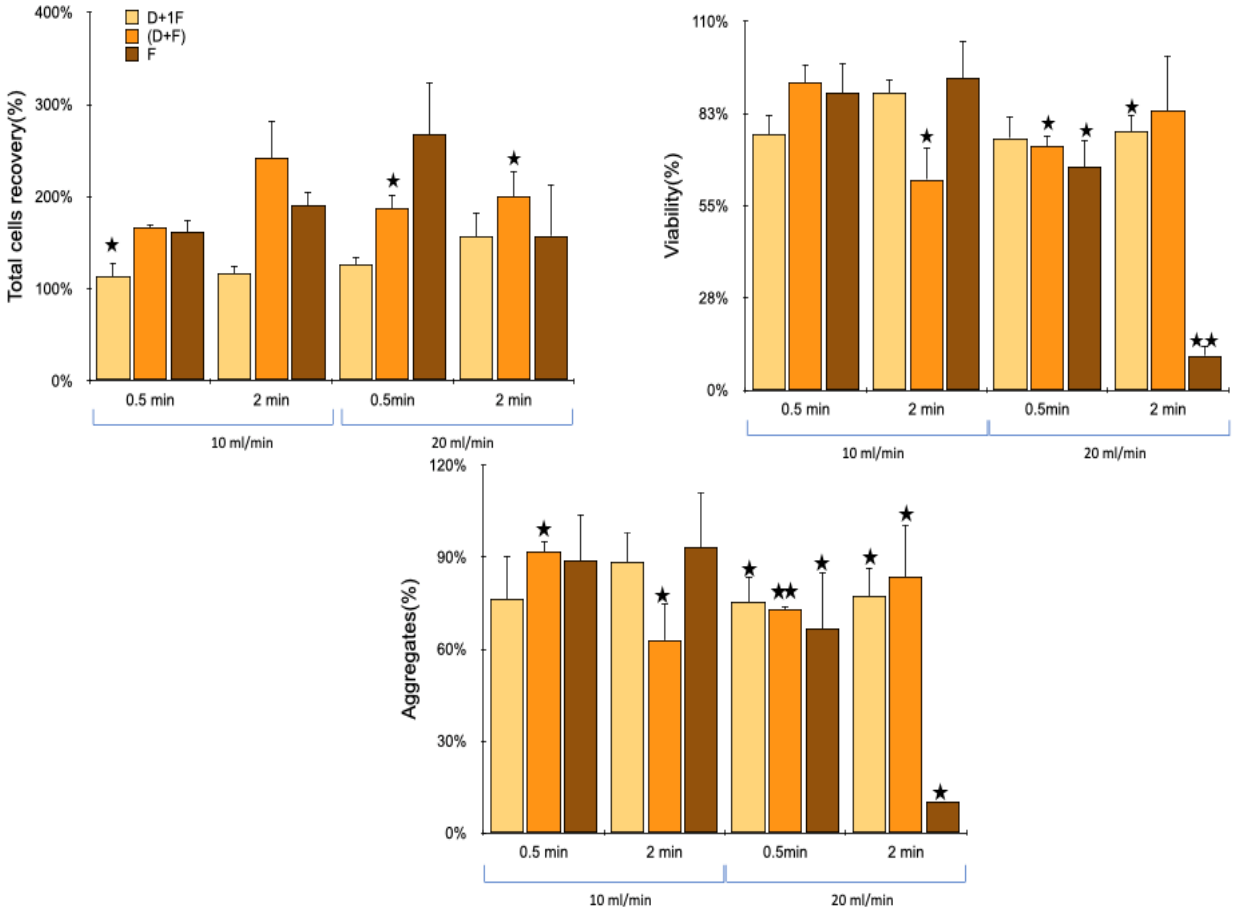

Figure 23- **Evaluation of different dissociation formats using cell aggregates.** MCF-7 cells were passed through the channels at 10 and 20 ml/min flow rates for either 0.5 or 2 minutes with different formats of branching channel array and filter modules including: recirculation over branching channel array for the specified period of time followed by one pass through filter, D+1F, recirculation over both branching channel array and filter modules, (D+F), and recirculation over filter module ,F. Results are shown for (A) single cell yield, (B) viability, and (C) aggregate yield which are all normalized to the control that did not pass through the channels. Recirculation happens through pulsatile flow provided by peristaltic pump. Data are presented as mean values +/- SEM from at least

three independent experiments. Two-sided T test was used for statistical testing. Stars indicate $p < 0.05$ and double stars indicate $p < 0.01$ relative to the control,100%.

In the next step, we looked into the effect of flow rate and recirculation time on optimal configuration of branching channel array and filter modules. MCF cell aggregates were recirculated in branching channel array module at Flow rates of 10,20 and 30 ml/min for 1,2 and 4 minutes followed by one pass through the filter module. Increasing the flow rate reduces the aggregates significantly. It slightly reduces the viability as well. It is notable that at 10 ml/min and 1 min circulation time, aggregate percentage increases as well as single cell recovery (160%). It shows that at low flow rate and recirculation time, large aggregates break down to smaller clusters and release single cells as well (flow rate=10 ml/min, 1 min recirculation time). In order to have a better evaluation of aggregate dissociation, aggregates must be categorized based on their size and population. Overall, lower flow rates are safer in studies with peristaltic pump with IDF device.

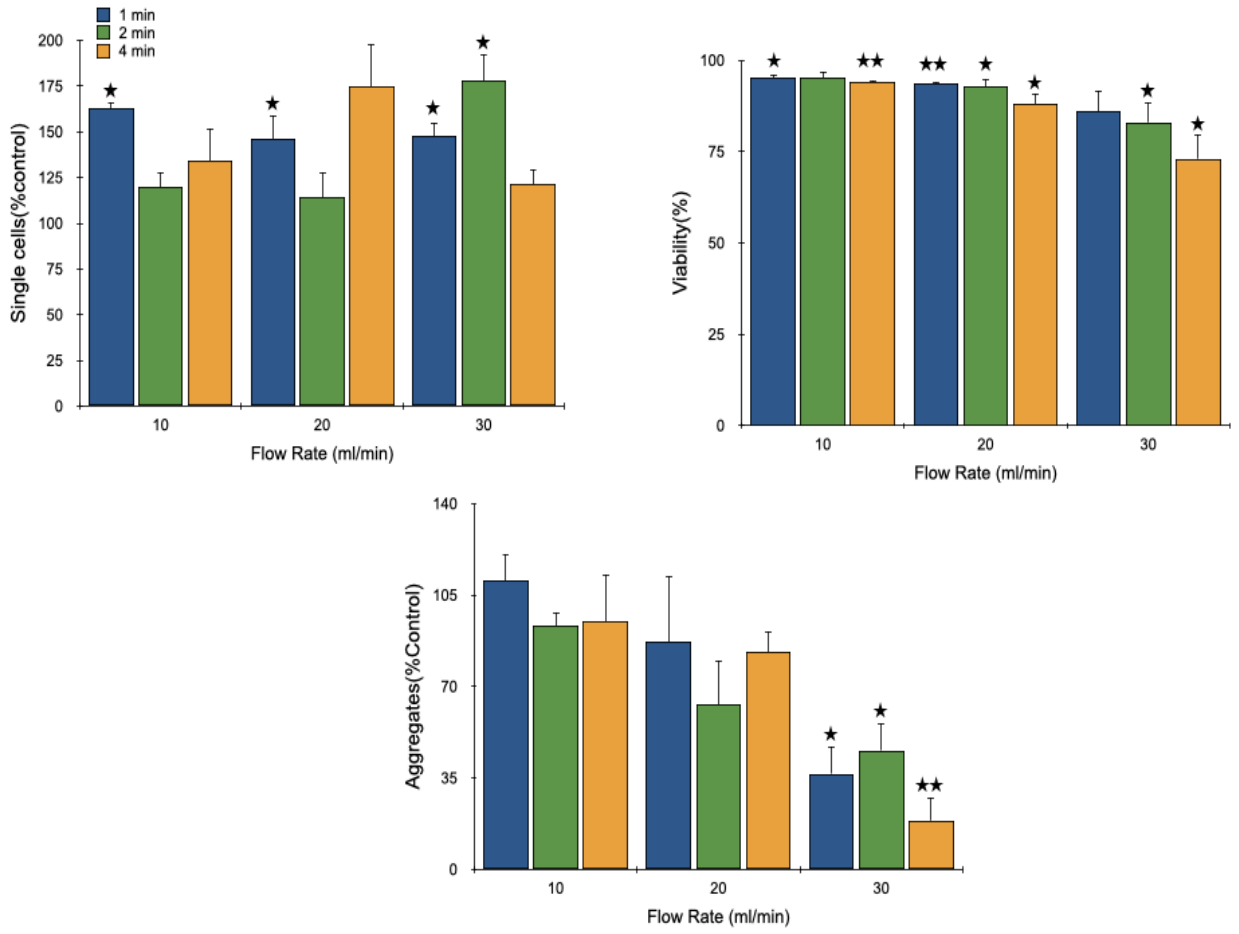

Figure 24- **Optimization of the branching channel array processing using cell aggregates**. MCF-7 cells were recirculated through the channel module with peristaltic pump for 1,2, and 4 minutes at flow rates of 10,20 and 30 ml/min. Next, the effluent went through the filter module once. Results are shown for (A) single cell yield, (B) viability, and (C) aggregate yield, which are all normalized to the unprocessed control. Data are presented as mean values +/- SEM from at least three independent experiments. Two-sided T test was used for statistical testing. Stars indicate $p < 0.05$ and double stars indicate $p < 0.01$ relative to the control,100%.

4.3.2. Optimization of recirculation time in IDF with pulsatile flow

After preliminary studies with MCF7 cell line to understand the effect of flow rate and recirculation time in different configurations of branching channel array and filter modules with the pulsatile flow, tissue dissociation was studied. Kidney was used as the model tissue because of its mechanical properties.

The effect of recirculation time with pulsatile flow was studied on dissociation of kidney at 20 ml/min flow rate. First, the kidney tissue was digested with traditional method for 20 and 60 minutes. Then, the effluent was recirculated through the IDF device with peristaltic pump for different periods of time from 0.5 to 4 minutes. The results show that cell yield is optimum in 1 minute recirculation. Tissue digested for 60 minutes shows more sensitivity to recirculation time than 20 minutes digested tissue. This trend can be seen for different cell types including epithelial cells, white blood cells and endothelial cells. Increasing the recirculation time to 1 minute, improves the cell yield however if recirculation goes for a longer time, cell yield will reduce which can be a proof of damage to the cells. It is similar to what was observed for MCF7 cell line.

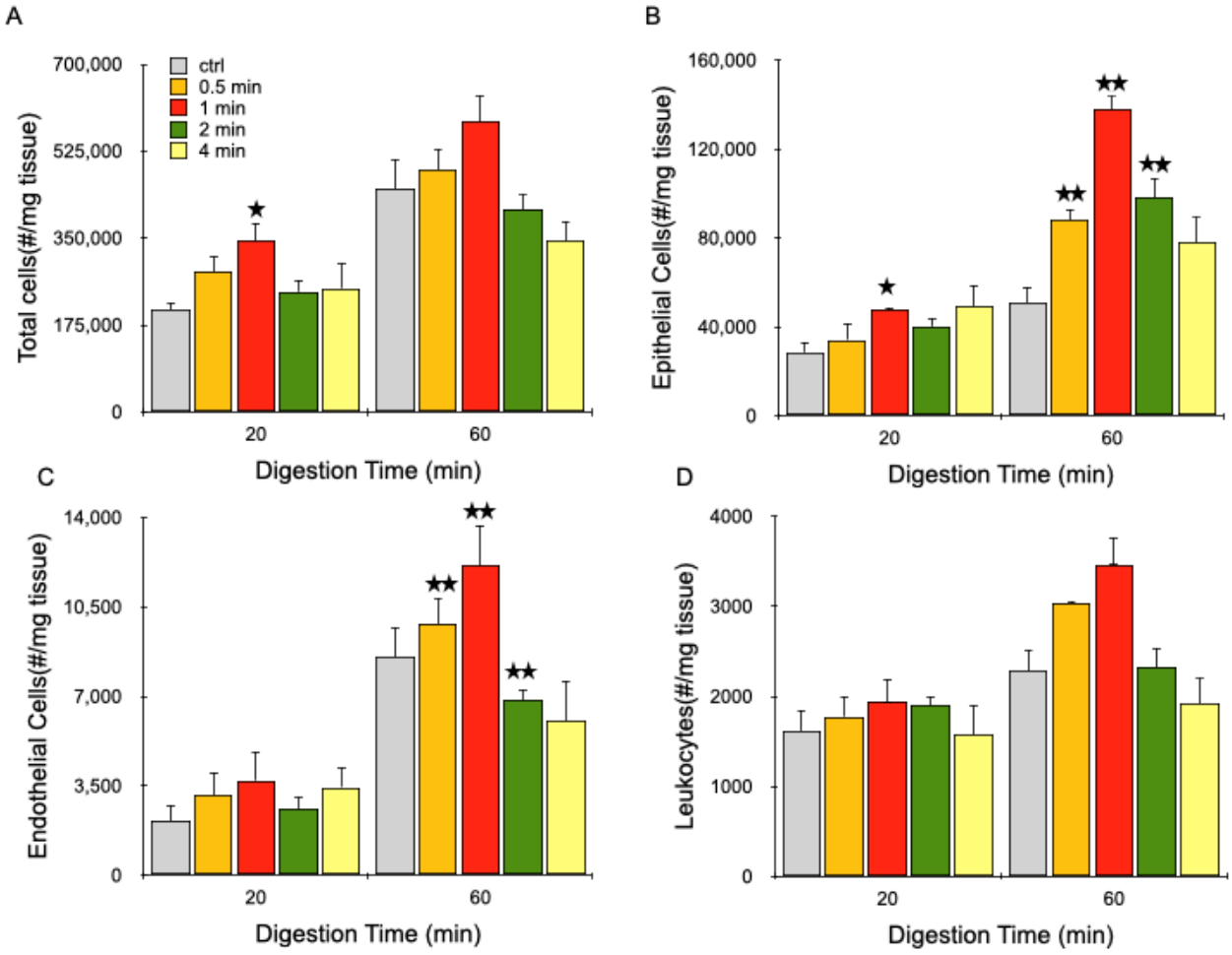

Figure 25- **Optimization of recirculation time with Branching channel array.** Kidneys were harvested, minced, and digested for the indicated time periods (20 or 60 minutes). Samples were then recirculated through the channel module for the indicated time followed by one pass through the filter module. Results are shown for viable and single (A) total cells, (B) EpCAM+ epithelial cells, (C) endothelial cells, and (D) leukocytes. Data are presented as mean values +/- SEM from at least three independent experiments. Two-sided T test was used for statistical testing. Stars indicate $p < 0.05$ and double stars indicate $p < 0.01$ relative to the control at the same digestion time.

After 20 min digestion, the cell yield is generally low across different recirculation times. In this case, increasing the recirculation time doesn't significantly change the cell yield.

It is worth noting that in short digestion time, cellular interactions with ECM are still the strongest barrier against single cell release. As it was mentioned before, cells will go under normal stresses with each pulse in the pulsatile flow. Pulsatile flow doesn't give enough time for flow development and therefore cells are barely experiencing shear flow in fully develop laminar region. Therefore, pulsatile flow cannot be efficient enough to break down the ECM and overcome the cell-ECM adhesion. However, after long digestion time when the cell-ECM interactions have been loosened enough, pulsatile flow can provide enough shear stress to break down the left intercellular interactions. Therefore, cell yield will increase with time to 1 min. Although exposure to shear stress can break the cellular interactions and loosened cell-ECM interactions, it can also damage the cells. Therefore, these two sides need to be balanced which happened at 1 min. The viability results show that device processing didn't significantly reduce the cell viability for epithelial cells. Endothelial cells and leukocytes show lower viability, but device processing doesn't reduce the viability compared to the control condition.

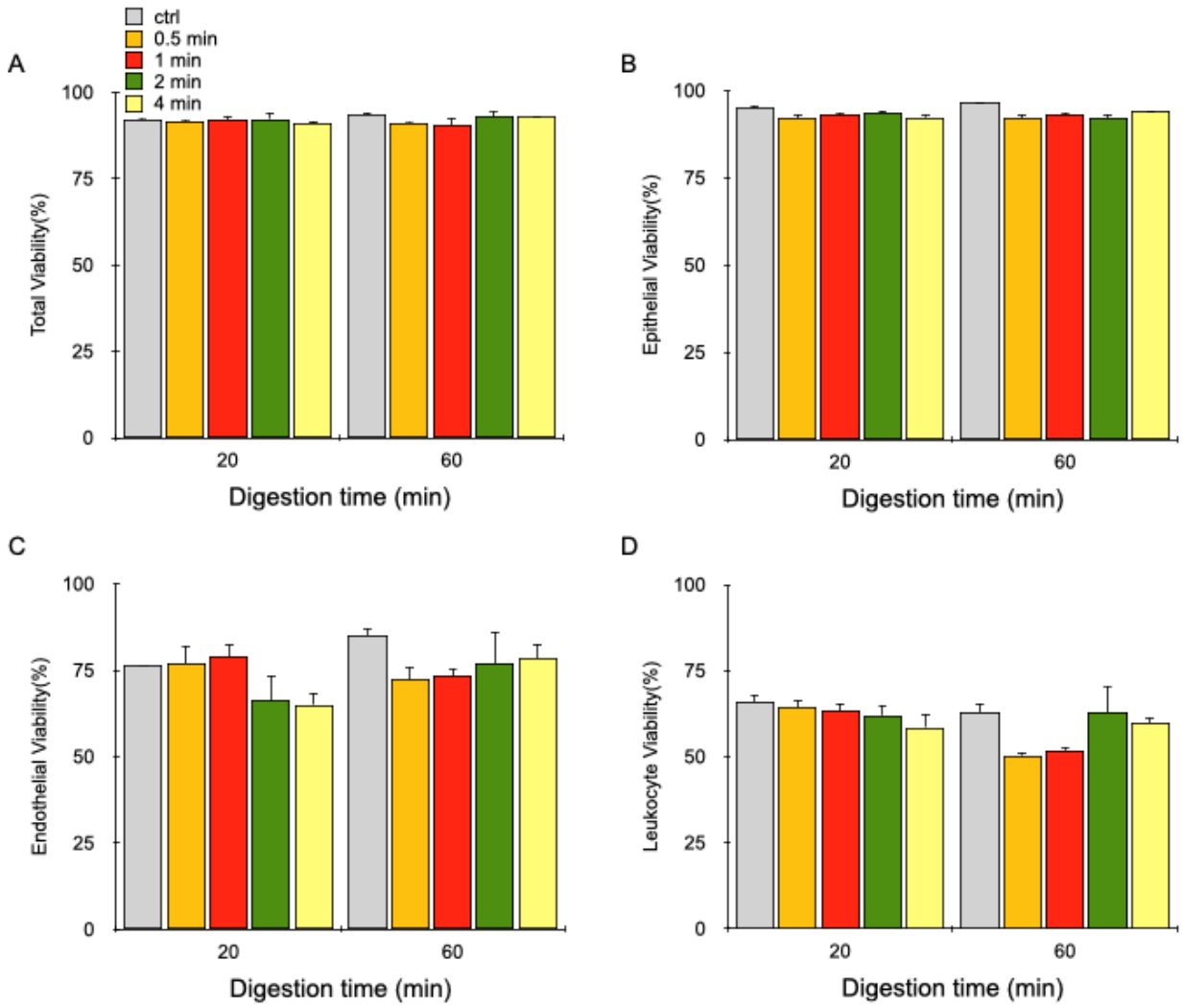

Figure 26- **Cell viability for optimization of recirculation time using murine kidney** A) total cells B) epithelial C) endothelial D) leukocyte viability at different recirculation times and digestion times. Kidneys were harvested, minced, and digested for the indicated time periods. Samples were then recirculated through the channel module for the indicated time followed by passing through filter module once and resulting cell suspensions were analyzed using flow cytometry. Controls were pipetted/vortexed and passed through a cell strainer. Data are presented as mean values +/- SEM from at least three independent experiments. Two-sided T test was used for statistical testing.

4.3.3. Comparison of steady shear flow and pulsatile flow with IDF

In our previous study, we found that IDF device can boost cell yield significantly for a shortly digested tissue in a steady flow provided by syringe pump. In the next step, the syringe pump was compared to the peristaltic pump. Different flow rates and recirculation times were used with peristaltic pump to compare the results.

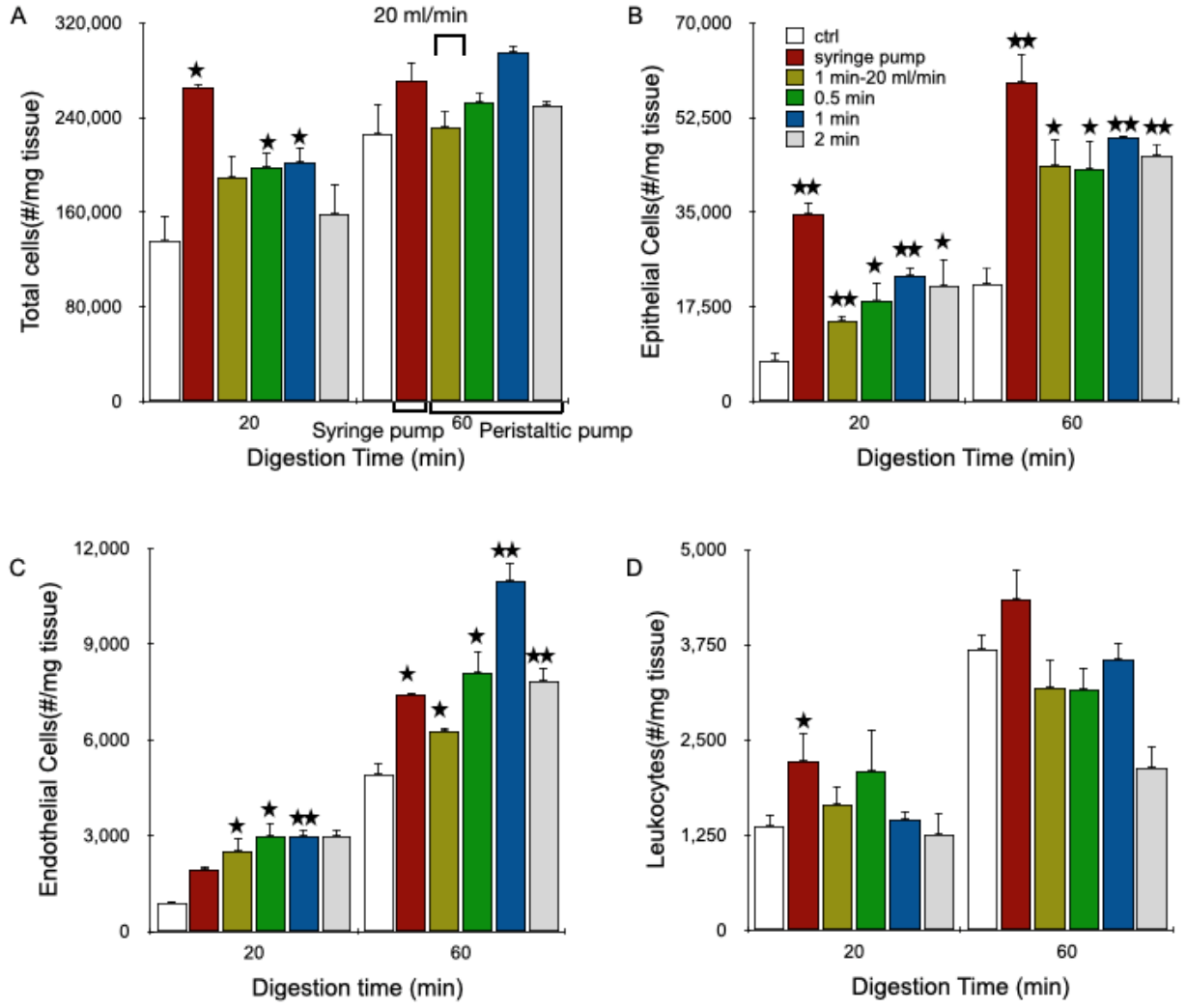

Figure 27- **Comparison of steady and pulsatile flow effect on IDF performance.** Kidneys were harvested, minced, and digested for the indicated time periods. Samples were then processed through the channel module followed by one pass through the filter module. For the condition named "Syringe pump", samples were passed through the device with syringe pump (20 times for 20-minute

digested sample and 10 times for 60 minute digested sample). This condition was chosen based on optimum condition found in our previous paper. For other conditions, samples were recirculated through the channel module for the specified period of time. Flow rate is 40 ml/min for all conditions unless it is mentioned differently. Resulting cell suspensions were analyzed using flow cytometry. Controls were pipetted/vortexed and passed through a cell strainer. Results are shown for viable and single (A) total cells, (B) EpCAM+ epithelial cells, (C) endothelial cells, and (D) leukocytes. Optimal results were attained using the single filter pass at each digestion time. Data are presented as mean values +/- SEM from at least three independent experiments. Two-sided T test was used for statistical testing. Stars indicate $p < 0.05$ and double stars indicate $p < 0.01$ relative to the control at the same digestion time.

Different flow rate and recirculation times were used for peristaltic pump. 1 minute recirculation time was chosen at 20 ml/min flow rate based on the previous results (Figure 25). In order to investigate the effect of higher flow rate, processing at 40 ml/min for 0.5,1 and 2 minutes were used. First, device performance on 20 min digested tissue will be explored. Epithelial cell yield is 2-3 times higher with syringe pump compared to the peristaltic pump. It proves our hypothesis that stable shear stresses exposed to tissue aggregates in syringe pump is providing higher cell yield while the instability and portion of normal stresses in peristaltic pump is not capable of breaking Cell-ECM interactions and hence the cell yield is low. Changing the recirculation time doesn't cause any statistically significant change in cell yield. On the other hand, endothelial cells and white blood cells yield didn't show any privilege of syringe pump over the peristaltic pump. It can be suggested that cell-ECM interactions are responsive to shear stresses and hence, epithelial cell yield improves with syringe pump because of the steady exposure to shear stresses. Endothelial

cells and leukocytes interactions with ECM is not showing sensitivity to flow type provided by syringe pump or peristaltic pump. This hypothesis should be explored more deeply by more studies on mechanical properties of cell- ECM interactions. Although heterogeneity of tissue doesn't allow to study each one individually, organ-on-chip technologies can provide this opportunity.

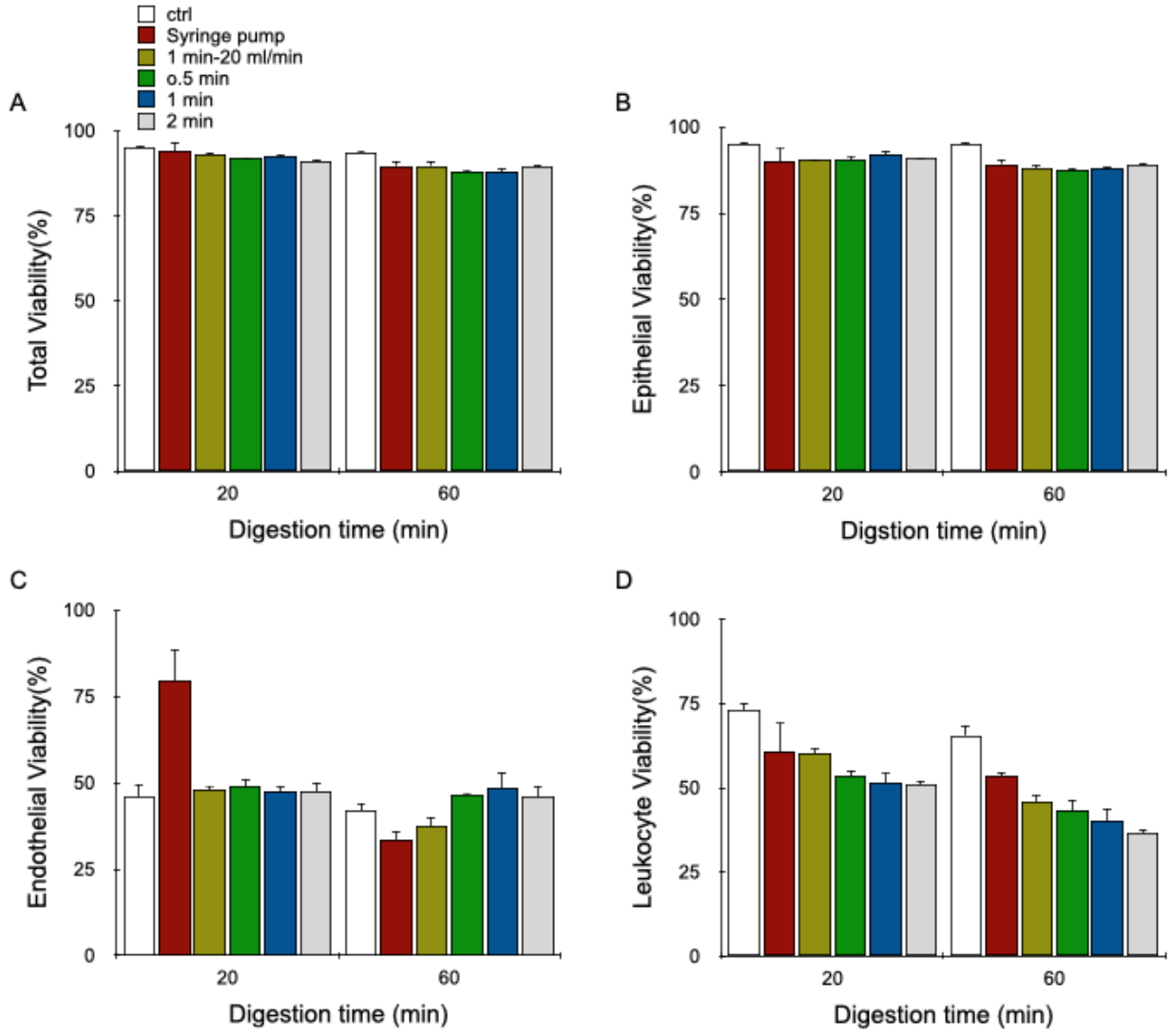

Figure 28- **Cell viability for comparison of pulsatile and steady shear flow** A) total cells B) epithelial C) endothelial D) leukocyte viability at different conditions and digestion times. Kidneys

were harvested, minced, and digested for the indicated time periods. Samples were then processed through the channel module followed by one pass through the filter module. For the condition named "Syringe pump", samples were passed through the device with syringe pump (20 times for 20-minute digested sample and 10 times for 60-minute digested sample). This condition was chosen based on optimum condition found in our previous paper. For other conditions, samples were recirculated through the channel module for the specified period of time. Flow rate is 40 ml/min for all conditions unless it is mentioned differently. Resulting cell suspensions were analyzed using flow cytometry. Controls were pipetted/vortexed and passed through a cell strainer. Data are presented as mean values +/- SEM from at least three independent experiments. Two-sided T test was used for statistical testing. Stars indicate $p < 0.05$ and double stars indicate $p < 0.01$ relative to the control at the same digestion time.

Device performance on dissociation of 60-minute digested tissue elucidates another aspect of adhesion forces of cells involved in tissue structure. Epithelial cell yield is higher in steady flow with syringe pump compared to pulsatile flow with peristaltic pump. It is similar to what was observed in 20 min digested tissue processing. After 60 minutes digestion, ECM interactions have been loosened and therefore, cell-cell interactions are the main barrier against single cell isolation. The results show that breaking epithelial cells interactions is better achieved with steady shear flow. It suggests that where the goal is isolation of epithelial cells and their enrichment, syringe pump should be chosen.

Interestingly, Endothelial cells yield improves with pulsatile flow. Cell yield at 20 ml/min with pulsatile flow (60000 cells/mg) is lower than the optimum condition of steady flow with syringe pump (75000 cells/mg). However, increasing flow rate to 40 ml/min

improves the cell yield to 8000 cells/mg in 0.5 minute and 11500 cells/mg in one minute. Endothelial cells show better cell yield with peristaltic pump which can be correlated with their physiological characteristics related to their exposure to pulsatile flow in blood vessels. Studies have shown that steady laminar shear stress can upregulate endothelial genes while turbulent shear stress doesn't. There is also evidence that laminar shear flow can down regulate expression of vascular cell adhesion molecules while upregulates the expression of intercellular adhesion molecules. It has been shown that this shear modulation of ECs through Mechano-transduction is transient when the shear exposure time is shorter than 1 hour[115, 139]. Therefore, any changes in gene or expression will eventually return to normal when the flow field is waned. However, exposure time to high level of stresses (shear and normal stress) at 40 ml/min will damage the cells surface. The results reflect that exposure to stress longer than 1 minute will cause cell damage to the extent that cell yield will reduce.

Leukocytes as stated before can be found in blood vessels and residing in tissue. Another fact proven in literature is that pulsatile flow can attract leukocytes to the surface of endothelial cells and hence, their isolation in response to flow will follow the same trend as endothelial cells[140]. Therefore, portion of leukocytes interacting with endothelial cells in blood vessels are responsive to pulsatile flow similar to endothelial cells and hence, the best leukocyte yield is observed in 1 minute at 40 ml/min similar to endothelial cells. However, the majority of leukocytes, freely suspended in blood or residing in tissue can lead to higher cell yield in steady shear flow provided by syringe pump. It is also worth mentioning that viability is more than 90% for epithelial cells for all conditions. Endothelial cells and leukocytes show lower viability in general. Viability reduction is significant for 60

min digested tissue. Further studies are required for process optimization to improve cell viability.

4.3.4. Optimization of tissue dissociation with Digestion device followed by IDF

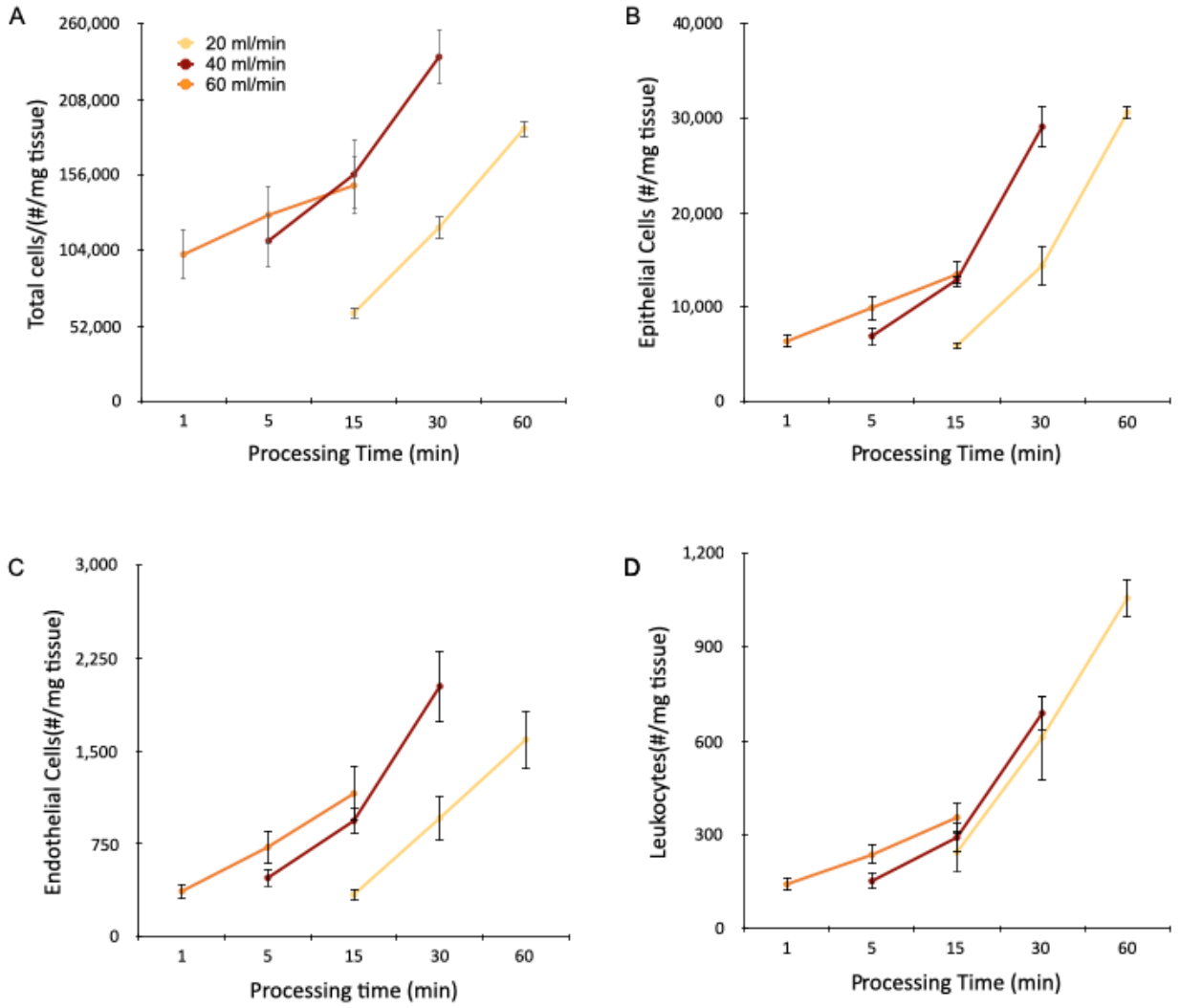

Figure 29- **Studying the effect of flow rate on cell yield for the tissue dissociation platform** Kidneys were harvested, minced, and processed through the Digestion device with peristaltic pump. Then, samples were passed through the channel module for 10 times with syringe pump. Processing

with peristaltic pump was done for different time intervals at different flow rates. 1,5,15-minute intervals for 60 ml/min flow rate. 5,15,30-minute intervals for 40 ml/min and 15,30,60-minute intervals at 20 ml/min. Results are shown for viable and single (A) total cells, (B) EpCAM+ epithelial cells, (C) endothelial cells, and (D) leukocytes. Optimal results were attained using the single filter pass at each digestion time. Data are presented as mean values +/- SEM from at least three independent experiments.

Our studies on effect of pulsatile flow on cell yield and viability with IDF device showed that best cell yield will be achieved with 10 passes through the syringe pump in a steady shear flow. Therefore, this condition was chosen for the next series of experiments where we studied the integration of IDF device with our previously developed Digestion device. Interval operation was chosen for processing tissue with the Digestion device as it was proven to be the optimal condition for improving cell yield. Our previous study showed that long term recirculation of cells through the device will damage the cells and hence interval condition can improve the cell yield by extracting liberated cells and preventing damage caused by over exposure to shear stresses. Higher speed can shorten the shear stress exposure while it is also favorable from the clinical standpoint of view. It is worth mentioning that tissue was completely gone at 60 and 30 for 20,40 ml/min flow rates, respectively. However, small piece of tissue was left after 15 minutes at 60 ml/min. Since the residual tissue was negligible, tissue processing was stopped at 15 minutes. The results showed that total cell yield is the highest at 40 ml/min. Epithelial Cell yield at 40 ml/min is close to the yield at 20 ml/min but it is achieved in 30 minutes processing while it takes 60 minutes at 20 ml/min. Endothelial cell yield at 40 ml/min is slightly higher than 20 ml/min in half

processing time. However, leukocytes yield is the highest at 20 ml/min which shows that high level of shear stress can damage leukocytes (Figure 29).

Cell yield at 60 ml/min is significantly lower than 20 and 40 ml/min for all cell types. It shows that high flow rate will expose cells to high shear stresses that can break down the cells and reduce the cell yield. Based on these results, we can estimate the maximum shear stress that can be applied in tissue dissociation without breaking the liberated cells.

It is also worth noting that leukocytes liberation rate after 15 minutes is similar at 40 and 60 ml/min rates. However, the liberation is lower before 15 minutes. In general, it can be concluded that cell liberation rate is lower before 15 minutes for different cell types and it slightly increases after 15 minutes. It can be an indication of different mechanisms during the course of tissue processing. At first, cell-ECM interactions are stronger and hence cell release is slower. However, cell-ECM interactions weaken by time and cell-cell interactions are broken more easily which increases the cell liberation rate.

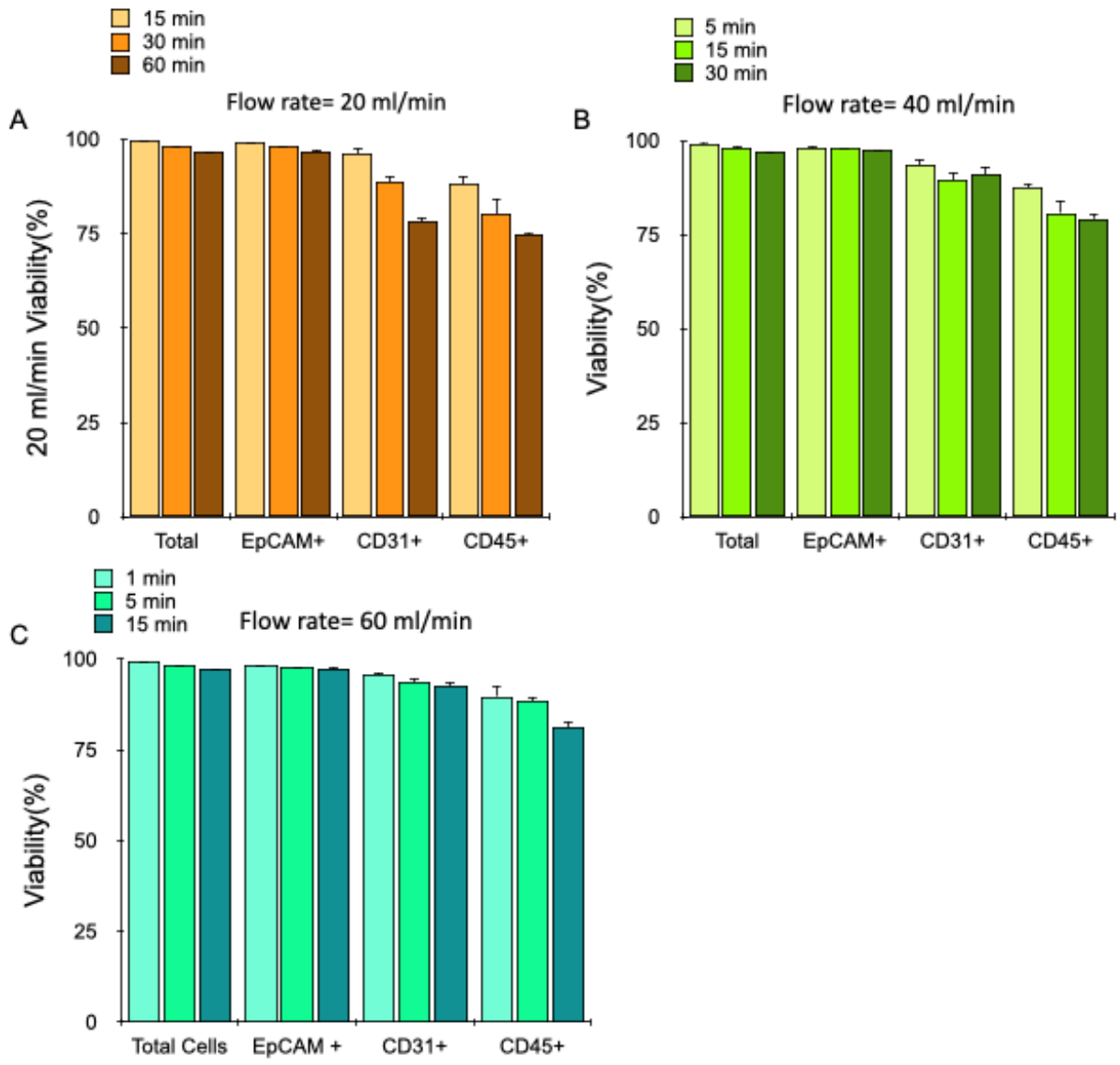

Figure 30- **Cell viability for flow rate optimization study** A) 20 ml/min B) 40 ml/min C) 60 ml/min at different time intervals mentioned in legend. Kidneys were harvested, minced, processed with the microfluidic platform, and analyzed by flow cytometry. Samples were run through the Digestion device for specified time with interval operation method. Then, the effluent was processed through IDF device at 40 ml/min for 10 times with syringe pump. Data are presented as mean values +/- SEM

from at least three independent experiments. Two-sided T test was used for statistical testing. Stars indicate $p < 0.05$ and double stars indicate $p < 0.01$ relative to the control at the same digestion time.

Immune cells usually freely move with and between tissues because of their inherent functions. Therefore, they are less sensitive to stress level because of being removed from a 3D tissue in contrast with structural cell types, as epithelial and endothelial cells, which heavily depend on physical interactions with adjacent cells. Additionally, they are generally easier to release since most of them don't reside in the tissues[126]. However, it was mentioned before that some portion of leukocytes can move in tissue and in connection with endothelial cells. These features largely influence the liberation rate of leukocytes.

Viability results are shown in Figure 30. Cell viability reduces slightly at longer processing times. This reduction is more significantly in endothelial cells and leukocytes. Further studies are required for improvement of cell viability.

4.4. Conclusion

Optimization of cell aggregate and tissue dissociation using our branching channel array and dual-filter modules that comprise our integrated disaggregation and filtration device (IDF) in pulsatile flow was studied. MCF7 aggregate dissociation provided a simple model to understand the dissociation mechanisms functioning in IDF device. Different flow rates and recirculation times with different configurations of channel array and filter module were studied. It showed the risk of flow instability at high flow rate (20 ml/min) and the necessity of shorter recirculation times at high flow rates. Also, this study elucidated the dominant function of filter module in dissociation of cell aggregates through breaking the

cell-cell interactions. Conversely, minced and digested murine kidney relied upon the branching channel array, and multiple filter passes was detrimental. As it was seen in steady flow provided by syringe pump, it can be due to the larger size of the tissue aggregates and, as we hypothesize, a greater role of cell-ECM interactions. Studying the efficiency of the IDF device after a substantially shorter digestion (i.e., 20 vs 60 min) improved our understanding of differences in cell-ECM interactions for different cell types. Although it is expected to see cell yield increase with longer recirculation time, 20-minute digested tissue didn't show significant change of cell yield with increasing the recirculation time which can reflect the weakness of pulsatile flow to overcome the adhesion forces involved in cell interaction with ECM. Pulsatile flow exposes tissue to normal stresses because of disturbed non-developed flow which is not strong enough to overcome the cell-ECM interactions in shortly digested tissue. However, after 60 minutes digestion, cell adhesion to ECM has been loosened enough to let the pulsatile flow stresses overcome the cell-cell interactions and release the cells. The optimum cell yield for different cell types was observed at 1 minute. Longer exposure to flow field can damage the cells and reduce the cell yield. The effect of pulsatile flow with peristaltic pump was compared with steady flow provided by syringe pump, as well. Interestingly, endothelial cells show more sensitivity to pulsatile flow which can be attributed to their mechano-transduction. This work with the IDF device has advanced our understanding of different dissociation mechanisms and cell/tissue aggregate properties in different flow types. Deeper knowledge of these effective parameters and their link with cellular interactions can pave the way to development of a universal microfluidic platform for single cell preparation. IDF device provides a stage to study dissociation of cell and tissue aggregates with different mechanisms through branching channel array and filter module.

In addition, integration of IDF device with our previously developed Digestion device was investigated. Studying the effect of flow rate showed the optimum flow rate is 40 ml/min. High speed and High throughput of this platform facilitates its translation to industrial applications. Our future studies will expand our knowledge of tissue dissociation by evaluating different tissues and enzyme solutions and analyzing results using single cell RNA sequencing.

CHAPTER 5: Separation of cells from enzyme with bulk acoustic waves

5.1. Introduction

Dominant biological traits in a population are usually explained by average analysis methods. In these methods, cell-to-cell variability and the presence of rare cell populations is masked causing challenges for building disease models and drug development[5, 10, 15, 131]. Single cell technologies provide a powerful tool to unravel the complexity of tissue and redefine our understanding of biological events[21]. It has provided a powerful tool to transform our knowledge of cells from macroscopical characteristics like morphology, anatomical location, and origin to molecular expressions such as proteins, DNAs and RNAs. High sensitivity of these technologies particularly scRNA seq magnifies the significance of minimizing batch effects and technical variations in the process[8, 107, 124, 126]. Single cell preparation is the major source of unwanted variations due to uncontrolled exposure of tissue to chemical and mechanical treatments which can change protein and gene expression and overshadow the true biological events. Microfluidic devices provide an effective sensitive and quantitative technique which fits the requirements of single cell analysis. Microfluidics has provided attractive solutions for many issues in biological studies with the advantages of automation, portability, lower cost, and possibility of integration of different functions.

Our team has developed a microfluidic platform comprising of different modules for tissue dissociation. Performance of different modules, digestion device, dissociation device, filtration device, integrated dissociation and filtration device was studied with cell aggregates and different types of tissue. These studies have improved our understanding of different dissociation mechanisms in each module and their significance in isolation of different cell types in a wide range of tissues including liver, heart, and kidney. It has helped us to optimize the platform processing conditions which can empower us to move toward a universal platform for tissue dissociation with the advantages including shorter processing time, higher cell yield and viability and reduced genomic and phenotypic changes.

One of the findings in our previous studies was the cell damage in the digestion device because of long circulation time for isolated cells. Our current digestion device takes advantage of enzyme recirculation to isolate cells from tissue because single pass operation would not be economically feasible from the standpoint of proteolytic enzymes cost (i.e., collagenase). However, cells that are liberated from the tissue are also recirculated, which could lead to damage or even destruction. This long-term exposure of isolated cells to enzyme is a concern in traditional method as well. Moreover, cells will be collected from the enzyme after the digestion process, through centrifugation which may negatively affect the functionality and integrity of cells. It can cause artifacts in sc-RNA Sequencing data and other downstream analysis. To mitigate this risk, we need a technology to isolate the cells from the enzyme in a continuous way. Various attempts have been made for isolating the cells based on microfluidic platforms which introduce external forces like electrophoresis, inertial focusing and acoustophoresis[141]. The throughput of these platforms is often too low to be considered as a candidate for substituting the traditional method. Recently, application of

acoustofluidics for cell manipulation has advanced rapidly since it doesn't affect cell viability in a negative way. Acoustofluidic devices face barriers regarding fabrication and throughput in translation to industrial applications. However, bulk acoustic wave has the capability to boost acoustofluidics to high throughput applications[142].

Another important criterion is a simple design that can be fabricated in a fast and cheap method to facilitate its translation to the industrial application[141]. Right now, common BAW devices are built on silicon, metal or glass which limits rapid prototyping[51]. These materials may cause cell adherence to their surface. Moreover, the cost of materials and their fabrication complexity will make them unsuitable for commercialization[45, 143].

Therefore, we focused on development of a new high throughput polymeric device that continuously transfers cells from the processing device effluent into a parallel buffer stream. This High-throughput Acoustic Elution Device (AED) will be part of the final dissociation platform. Our device will be polymeric which makes it disposable. Also, the fabrication process will be multilayer pressure lamination that is simple, cost-effective, and fast.

AED elute cells continuously from recirculating enzyme in a single broad, shallow channel geometry (Figure 31). The buffer and cells suspension in enzyme are fed from their corresponding inlet. Cells are exposed to acoustic field in the middle of the channel where both fluid streams are in contact. Acoustic radiation force pushes the cells to the buffer stream toward the pressure node designed at the top of the channel. Cells in the buffer are collected from Cells outlet while the Enzyme can be led back into the digestion device from the enzyme outlet to assist with further tissue break down. This configuration makes it

possible to continuously remove cells from the system, preventing damage and shear-induced phenotypic changes, while recycling the enzyme for further tissue digestion. Another benefit is that the recovered cells are free of ambient RNA and debris since the acoustic field is just able to move particles with diameter greater than 5 μm. Debris size is usually smaller than 1 μm which make them suitable to be trapped in acoustic streaming.

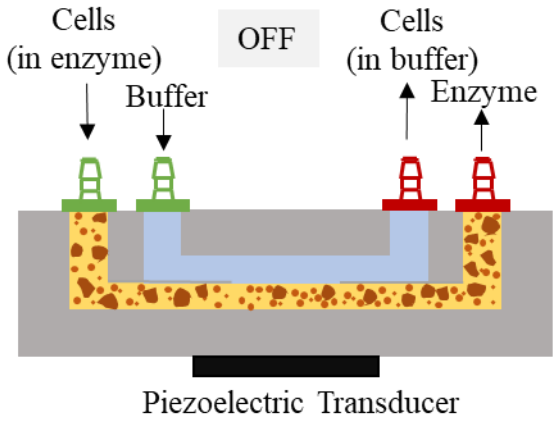

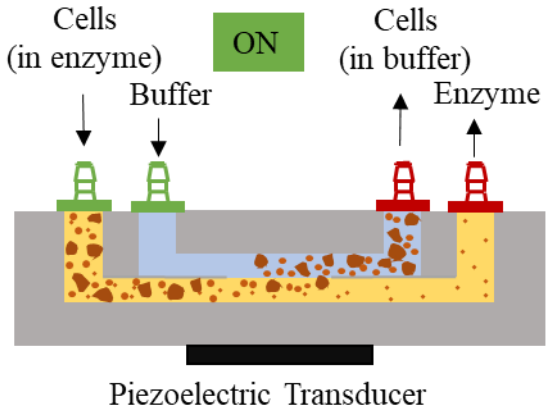

Figure 31- **Schematic presentation of the Acousto-Elution Device (AED)**. when the acoustic field is A) Off and B) On. Single cells, aggregates and debris trajectory are shown.

AED is a disposable device that facilitates continuous separation and enzyme purification with high throughput. It can be a substitute for current methods for centrifugation and filtration with translation potential.

5.2. Materials and methods

5.2.1. Theory and design

The design is based on bulk acoustic wave (BAW) resonance which is provided with a total fluid layer height equal to one-quarter wavelength and reflector layer thickness equal to one-half wavelength of the sound wave[144]. Designing the device with corresponding dimensions builds a resonance in the device that will result in pressure nodes located at the reflector boundary. Cells suspension will enter from the Cells (1st) inlet into the bottom part of the channel, near the transducer. At the same time, buffer enters from the Buffer (2nd) inlet into the top part of the channel. When the acoustic field is on, cells in the bottom part of the channel are pushed towards the reflector, the top part of the channel into the buffer stream by a positive acoustic force. Buffer exits the system through the Cells outlet (1st outlet) while the purified enzyme exits the Enzyme outlet (2nd outlet) to be recirculated through the Digestion device. Figure 31 represents a schematic view of the device in on/off situation of the acoustic field. Cells will move toward the pressure node under the acoustic radiation force generated with standing wave. The amount of acoustic radiation force can be calculated as:

$$F_{ac} = 4\pi a^3 k_0 E_0 \left[\frac{\rho_c + \frac{2}{3}(\rho_c - \rho_f)}{2\rho_c + \rho_f} - \frac{1}{3}\frac{\text{k}_c}{\text{k}_f}\right] \sin\left(2\text{k}_f z\right) \quad (2)$$

Where $k_0 = \frac{2\pi}{\lambda o}$, λo is the sounds wavelength, a is the cell diameter, E_0 the acoustic energy density, k the compressibility, ρ density and subscripts c and f denote the cell and fluid, respectively. This equation is using the approximation of inviscid fluid which is correct when $\delta \gg a$. δ is th boundary layer thickness given by, $\delta = \sqrt{\frac{2v}{\omega}}$, where v is fluid kinematic viscosity (momentum diffusivity) and ω is the acoustic field angular frequency. Since δ is around 0.5 μm, when cell diameter is more than 5 μm, the effect of viscosity can be neglected[145]. The acoustic force balances with drag force and particle velocity $u=F_{ac}/(6\pi\eta a)$ and so the velocity has a radius-squared dependence of particle size and hence, larger particles will move faster. The flight time over a fixed distance is proportional to the inverse of squared particle diameter ($1/r^2$).

For MCF7 cell line, which is used as a model cell line for preliminary study with radius of 25 μm, Contrast factor will be 0.25(Table 2). Assuming $p_0 = 250\ kP$ from a similar work[44], we can estimate acoustic Energy, $E_{ac} = \frac{{p_a}^2}{4\rho_m {c_m}^2} = 6.97\frac{J}{m^3}$. Therefore, the acoustic force is $3.5 \times 10^{-11} N$ which can overcome $F_g = (\rho_c - \rho_m)V_c g$ equal to $4.29 \times 10^{-12} N$.

Table 2- Acoustic parameters used for calculation of acoustic force

Parameter	Symbol	Value	Unit
Density, water	ρ_m	1000	kg/m^3
Density, cells	ρ_c	1068	kg/m^3
Density, PS	ρ_{PS}	1050	kg/m^3
Compressibility, water	β_m	5.2×10^{-10}	Pa^{-1}
Compressibility, MCF7[139]	β_c	4.2×10^{-10}	Pa^{-1}
Compressibility, PS	β_{PS}	2.2×10^{-10}	Pa^{-1}
Speed of sound, water	C_m	1497	m/s
Speed of sounds, PMMA	C_{PMMA}	2680	m/s

Although theoretical calculations won't perfectly match the 3D device with polymeric materials, estimation of acoustic force shows that flight time for cells/beads (time required for cells/beads to move from the bottom enzyme stream to top buffer stream) is short enough (less than second) to isolate the cells from the enzyme at high flow rates of 10 to 20 ml/min.

5.2.2. Simulation

To understand the acoustic pressure and cell displacement in the AED device, numerical simulation was conducted using a finite-element-based software package, COMSOL Multiphysics version 4.3a to solve the acoustic field on a vertical cross section of the device within the transducer-functioning area by using a frequency domain model solver at the resonance frequency of the transducer. The laminar flow and particle tracing for fluid flow modules were used to predict the cell displacement in the lateral cross section inside the channel under the acoustic radiation force and the stokes drag force. For simplification, the device was assumed to be a three-layer geometry (bottom slide, channel layer, and top slide) placed on a piezo transducer.

5.2.3. Device Fabrication

AED was fabricated though different methods to find the balance between ease of fabrication and acoustic power to transfer cells to the parallel stream. At first, device fabrication was similar to Gu et al[44]. Channel depth was engraved in top and bottom acrylic sheets (4615T73, McMaster-Carr) using laser cutter (VLS4.60, Universal Laser systems). The divider layer in between was made of a thin PET sheet (8567K62, McMaster-Carr) etched with laser in the middle to provide two fluids meeting window. All the layers were attached with double-sided PSA (ARcare 92712, Adhesive Research) under pressure. Barbs (BDMR210-9, Nordson Medical) with 1.6 mm inner diameter made of clear polycarbonate were attached to the inlet and outlet holes by a cyanoacrylate adhesive. 0.05” tubing was affixed to the barbs.

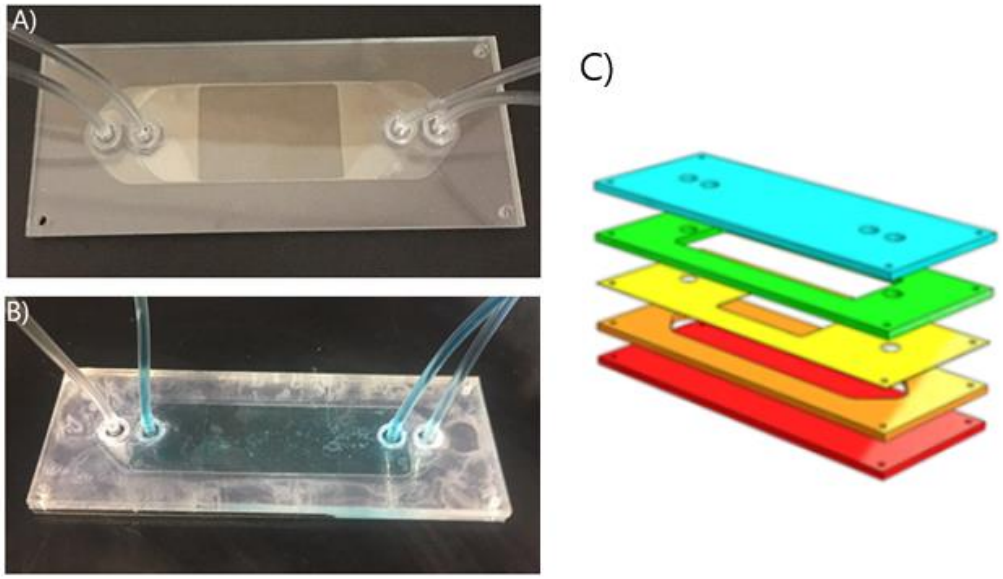

Figure 32- **AED device fabrication with multilayer lamination**. A) Photo of fabricated device with multilayer pressure lamination. B) demonstration of flow inside the fabricated device to visualize fluid mixing. Clear and blue dyed PBS/1%BSA were injected to the Cell and Buffer inlet and the collected fluid in each outlet was analyzed by UV spectrophotometry to find the fluid mixing.

Laser power and speed was adjusted to achieve the reliable engraving depth. Profilometer (Tencor, AlphaStep 200) was used to determine the engraving depth through the length of acrylic sheets.

As an alternative, multilayer pressure lamination method was applied (**Error! R eference source not found.**). Five plastic layers were laser etched completely through and stacked together as shown in **Error! Reference source not found.** . The red layer is the c arrier, and the blue layer is reflector, both made of PMMA. The middle 3 layers are made of PET and form the fluid channel. The yellow layer is the divider that divides channel into two sections for the cells and buffer stream. It provides a 30 mm long window for two fluids to meet where the cells will relocate from the cell to the buffer stream.

Three layers of PET with 0.12 mm thickness and four layers of PSA with 0.07 mm thickness between each two layers build up the quarter wavelength height of channel, 0.63 mm. The reflector layer was designed to be half of the wavelength to build the resonator, 2.27 mm. The carrier layer was 1 mm thick to secure the minimum energy loss. The fabrication method was simpler and more precise and both fluids have evenly distributed through the channel width (Figure 32).

Two other fabrication methods with PDMS and glass were also studied. Half wavelength channel design was tried similar to what was presented by Adams et al[45]. The structure was designed such that the standing wave had a half wave in the bottom slide, a half wave in the microchannel and a quarter wave in the top slide. Top and bottom layers were glass slide while the middle layer was PDMS. PDMS middle layer was molded in a 3D printed mold. Channel width of 10 mm Then, 3 layers were clamped together for heat treatment and then, plasma treatment for adhesion.

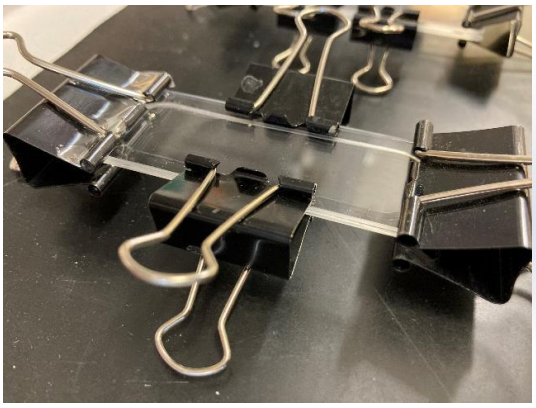

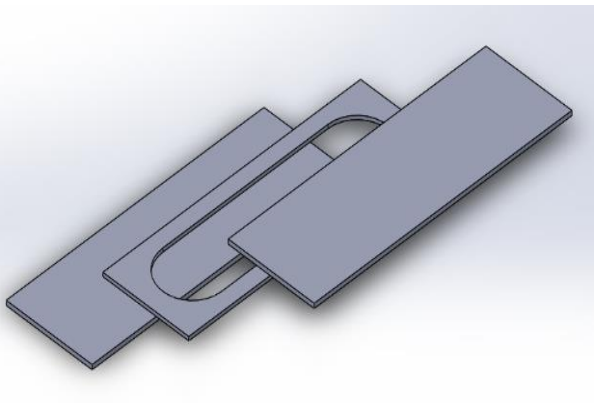

Figure 33- **Glass/PDMS/Glass device prototype**. The structure was designed such that the standing wave had a half wave in the bottom slide, a half wave in the microchannel and a quarter wave in the top slide. $h_{bottom\ glass} = 1000\ \mu m$, $h_{ch} = 830\ \mu m$, $h_{top\ glass} = 1000\ \mu m$, $w_{ch} = 8.5\ mm$

In addition, another device was designed to have a quarter wavelength with PDMS on top of glass slide of 1 mm. PDMS layer was molded and attached to the glass slide through plasma treatment. In this method, PDMS layer sags and blocks the chamber.

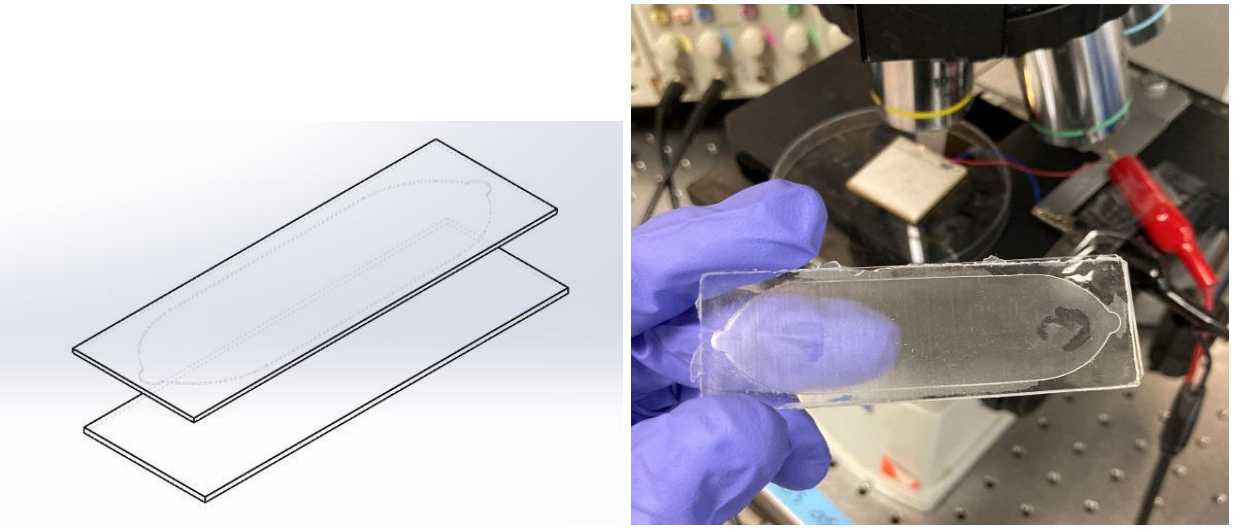

Figure 34- **Glass/PDMS device prototype**. with ¼ wavelength design. The structure was designed such that the standing wave had a half wave in the bottom slide, a quarter wave in the microchannel and a quarter wave in the top slide. $h_{PDMS} = 514\ \mu m$, $h_{ch} = 374\ \mu m$, $h_{glass} = 1000\ \mu m$, $w_{ch} = 10\ mm$

5.2.4. System setup

The device was primed with PBS/BSA buffer. PBS/BSA and cell suspension in PBS were injected to the Buffer inlet and cells inlet, respectively through a peristaltic or syringe pump. Suspension of MCF7 cell line in PBS/BSA with 10^6 cells/ml density or 10^5cells/ml poly

styrene microbeads(20μm) were used. The device was placed on piezoelectric transducer with a coupling gel to allow transmittance of energy to the device. For acoustic actuation, a function generator (Agilent Technologies, 33220A) with a voltage amplifier (Krohn-Hite, 7500) was used to provide the desired amplitude (Vpp) of the square waveform. An impedance spectroscope (Zurich Instrument, HF21S) was used to find the accurate resonant frequency after being bonded to the device.

5.2.5. Measurement of particle flight time

Figure 35- Setup for watching the particle movement.

Suspension of microbeads was injected to the device. Device was mounted on top of transducer. Device stood still to let the beads settle. Frequency sweep was done at different voltages while monitoring the signal with oscilloscope. After finding the frequency at which beads moved upward, flight time was measured by monitoring the time it took for particles to move from the bottom of the channel to the top of the channel through measuring focus time on microscope.

5.2.6. Cell count and viability

Efficiency of the device was determined by measurement of cell count and viability with LunaStem which stain cells live and dead cells with AO/PI marker. Briefly, 1.5 µl of AO/PI stain is mixed with 18 µl of the sample by pipetting up and down. Next, 10 µl of the mixed sample is loaded into the inlet of counting slide which will be inserted into the instrument. After 10 s, live and dead cells image and count are displayed on the screen.

5.3. Results

5.3.1. Optimization of the fabrication method

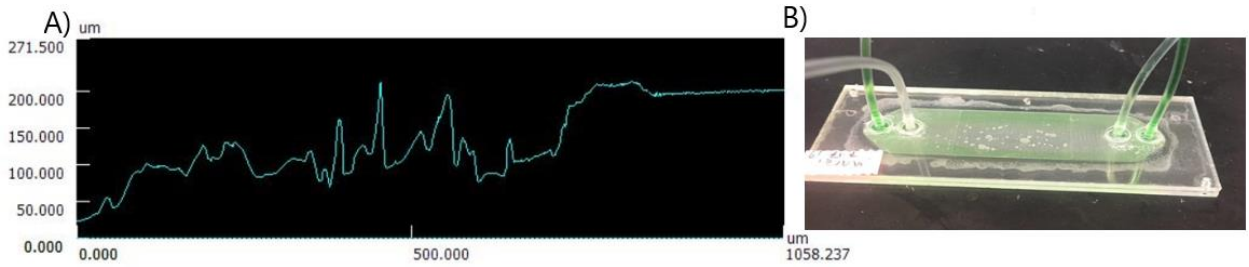

Figure 36- **AED device fabrication results with laser engraving**. A) Profilometry results for a specific point on channel edge show a broad range of engraving depth with a lot of fluctuations. B) dyed and clear PBS/1%BSA were injected to the device through the Cells and Buffer inlet. Sample fluid is directed to the edges which shows higher depth in the edges compared to the center.

There are different methods available for fabrication of microfluidic devices among which rapid, cheap, and simple methods are preferred. Also, there are challenges like thermal stress buildup problem in micromachining and low interlayer adhesion in multilayer soft lithography[146].

AED was fabricated though different methods to find the balance between ease of fabrication and acoustic power to transfer cells to the parallel stream.

The data with laser cutter was not reproducible. Also, desired precision with less than 10% tolerance was not achieved (Figure 36 A). Moreover, laser cutting causes a rough, uneven surface that can increase the potential of cell adhesion and flow disturbance. Another profiler (Bruker, Dektak 3 Stylus) was used to measure the channel depth profile through the width. The results showed that the engraving depth is higher in the edges which causes the fluid to be directed to the channel edges (Figure 36 B). Therefore, the working area for acoustic field will be significantly reduced and its efficiency will drop. It is also likely that any lack of flatness or parallelism between the two faces will also appear to increase the system damping(for layered resonators)[52].

As an alternative, multilayer pressure lamination method was applied (**Error! R eference source not found.**). Multilayer pressure lamination is more robust than soft lithography and it has the benefit of supporting high flow rates and pressures. Since it is made of polymeric layers, it is cheap and disposable. The use of double-sided pressure sensitive adhesive (PSA) for this fabrication process makes it more compatible for different applications since they can be patterned using simple cutting tools and offers high adhesion strength. The fabrication method was simpler and more precise and both fluids have evenly distributed through the channel width.

In order to improve the acoustic force, two other fabrication methods with PDMS and glass were also studied. Half wavelength channel design was tried similar to what was presented by Adams et al[45]. The structure was designed such that the standing wave had a half wave in the bottom slide, a half wave in the microchannel and a quarter wave in the top slide. Top and bottom layers were glass slide while the middle layer was PDMS. PDMS

middle layer was molded in a 3D printed mold. This fabrication method encounters difficulties in insertion of inlet and outlet connectors, adhesion of layers and channel height precision. Channel height tolerance can cause a detrimental reduction of acoustic radiation force as shown in Figure 37. Also, non uniform acoustic pressure feld might have induced disordered motion of the fluid which would have mixed the buffer and enzyme fluids streams.

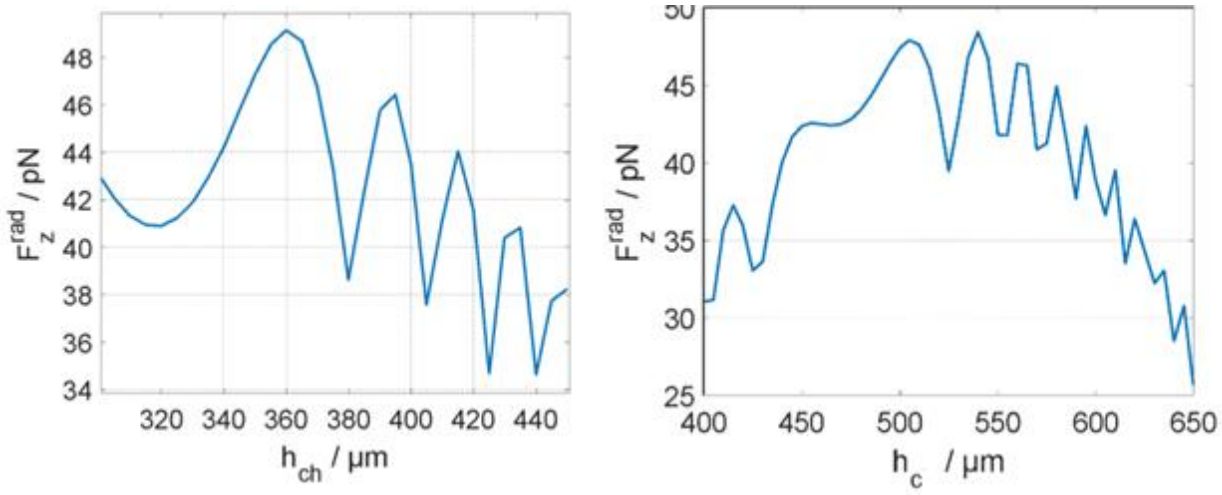

Figure 37- **Acoustic radiation force dependence on channel height and reflector height.** Radiation force changes significantly with reflector and channel height for quarter wavelength channel and half wavelength reflector. h_c(reflector height)= 500 µm , h_{ch}(channel height)= 370 µm, carrier layer=1 mm, resonance frequency=1 MHz

In Glass/PDMS design, PDMS layer sags and blocks the chamber. The PDMS on top will sag into the channel and it can touch the channel bottom. PDMS deflection can be estimated through the following equation:

$$d_{max} = \frac{5\rho g w^4}{32 h^2 E} \quad (3)$$

Where d_{max} is the maximum deflection of PDMS, w is the channel width, h is the PDMS thickness and E is the PDMS elastic modulus. The results of plotting maximum deflection versus PDMS thickness is shown in Figure 38.

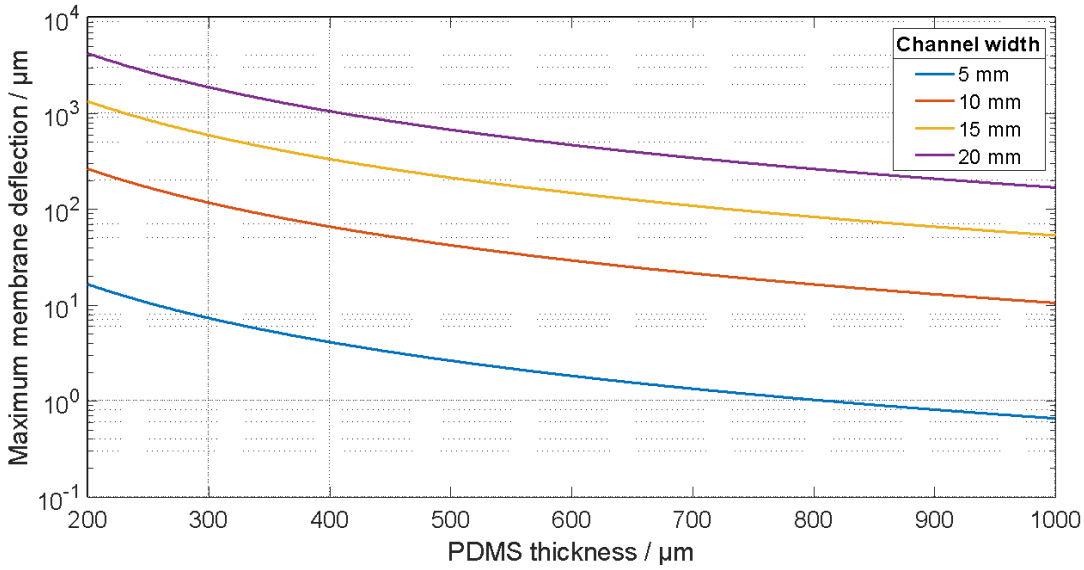

Figure 38- Membrane deflection versus PDMS thickness for different channel widths.

Among different devices, multilayer lamination offers more precise dimensions, faster fabrication and easy connection of the inlets and outlets and it gives the best channel height accuracy which is crucial for BAW resonance.

5.3.2. Flow rate adjustment for minimum fluid mixing

Since two fluid streams will be in contact within a 30 mm long window, there is a chance of mixing between two fluid layers which will alleviate the enzyme efficiency. The channel dimensions and flow rate make Reynolds number lower than 50 which means a fully

laminar flow in the channel. Although the channel flow is in laminar regime, it is not considered viscous flow (Re<<1), So, a degree of mixing is inevitable. Therefore, sample and buffer flow rates were optimized to have the minimum mixing. For preliminary study, blue dyed and clear PBS/1%BSA were injected into the Cells and Buffer inlets, respectively. Mixing was evaluated based on percentage of blue color in each outlet effluent. Percentage of color was measured based on calibration curve of UV absorption in 630 nm wavelength vs composition with spectrophotometer (Thermo Scientific, NanoDrop 2000). It was found that highest purity in sample flow will be achieved when the buffer flow rate is half the sample flow rate (Table 3).

The other effective parameter is the hydrodynamic resistance. Since buffer flow has a shorter fluid pathway compared to the sample flow, hydrodynamic resistance for buffer is lower. The outlet tubing of two fluids were adjusted to achieve same resistance. Since same buffer has been used for both sample and buffer flows, viscosity of both streams will be same, and resistance can be adjusted by the length of outlet tubing. It was found that when the length of Cells outlet tubing (L_b) is 1.3 times the length of Enzyme outlet tubing (L_b), equal resistance can be achieved for both buffer and sample stream.

Table 3- Effect of sample and buffer flow rate on fluids mixing

Sample flow rate ml/min	Buffer flow rate ml/min	Cells outlet (%)	Enzyme outlet (%)
10	10	19.45%	78.48%
	20	20.95%	32.15%
	5	50.34%	93.92%
5	5	34.15%	85.70%
	10	12.98%	33.65%
	2.5	53.33%	90.93%
2.5	2.5	39.88%	78.98%
	5	22.19%	62.54%
	1.25	61.79%	80.22%

5.3.3. Resonant frequency adjustment

For acoustic actuation, a function generator (Agilent Technologies, 33220A) with a voltage amplifier (Krohn-Hite, 7500) was used to provide the desired amplitude (Vpp) of the square waveform. The acoustic wave is sensitive to external perturbation based on the following equation:

$$\Delta f = \frac{2\Delta m f_r^2}{A\sqrt{\rho\mu}} \quad (4)$$

Where μ is the mass/area ratio, ρ is the material density, A is the surface area and f_r is the resonant frequency. Therefore, the device weight can reduce the resonance frequency[147].

An impedance spectroscope (Zurich Instrument, HF21S) was used to find the accurate resonant frequency. Resonance happens where the acoustic impedance, the

product of density, and acoustic velocity, is the highest, and hence, the highest acoustic energy will be achieved. The fundamental resonant frequency was detected at 591 kHz. When the device filled with the sample fluid was loaded on the transducer, the resonant frequency was shifted to 585 kHz.

Since the fluid-polymer interface doesn't behave as an ideal reflector, the optimum operating frequency will be determined by observation of focusing with frequency scanning. Therefore, the Deflection of green fluorescent beads(Phosphorex, 2106G) suspension in the device was monitored while scanning a frequency range around the fundamental resonant frequency.

5.3.4. Effect of pump type

Table 4- Evaluation of syringe and peristaltic pump for minimum mixing

sample flow rate	Buffer flow rate	Syringe pump		Peristaltic pump	
		1st outlet	2nd outlet	1st outlet	2nd outlet
ml/min	ml/min	(%)	(%)	(%)	(%)
5	2.5	0.34	0.92	0.52	0.89
	5	0.14	0.89	0.24	0.84
	10	0.03	0.71	0.10	0.65
10	5	0.38	0.91	0.45	0.87
	10	0.28	0.85	0.26	0.82
	20	0.04	0.69	0.11	0.64
2.5	1.25	0.42	0.97	0.43	0.84
	2.5	0.12	0.83	0.29	0.78
	5	0.06	0.68	0.13	0.64

We tried two different pumps, syringe pump and peristaltic pump. Peristaltic pump has the advantage of pumping at higher flow rates and recirculation ability, but it is not stable. Syringe pump can provide steady flow, but recirculation is not possible, and it is not

compatible with our other devices. It was found that the pump type does not affect the mixing significantly (Table 4). Therefore, both pump types can be used for this application.

5.3.5. Displacement time for different device designs

According to impedance spectrometry, resonance frequency of the transducer was found at 933 KHz. Frequency sweep was done in 900-1200 KHz. For this study, lower amplification was used. Displacement of particles for two PDMS devices with half and quarter wavelength channel were monitored. Average displacement time for Quarter wavelength design was 5 s which happened at 1090KHz and 12 Vpp. It corresponds to Acoustic energy density of 9.5 J/m^3. This design has a major fabrication issue.

The Glass/PDMS/Glass design with half wavelength channel was also studied. Particle displacement happened at f = 840 kHz with Actuation: 12 Vpp, 8 W. The average displacement time was ~ 8s and Acoustic energy density: 6.5 J/m^3 .

Finally, the multilayer laminated device was tested. Particles displacement happened at 1.007 MHz and 1.4 Vpp. The average displacement time was 2 s and acoustic energy density of 13.5 J/m^3.

5.3.6. Device performance

First, the device was primed with PBS/BSA buffer. Efficiency of the device was determined by measurement of cell count and viability with LunaStem. Suspension of MCF7 cell line in PBS/BSA with 10^6 cell/ml density was injected to the Cells inlet. At the same time, PBS/BSA was injected to the Buffer inlet. Optimum flow rates of previous section were used.

The device was placed on piezoelectric transducer with a coupling gel to allow transmittance of energy to the device. The results show that when the acoustic field is off, majority of cells will go straight to the Enzyme outlet. When the acoustic field is turned on, the cells are pushed to the top part of channel and hence, the cells count will be higher in Cells outlet.

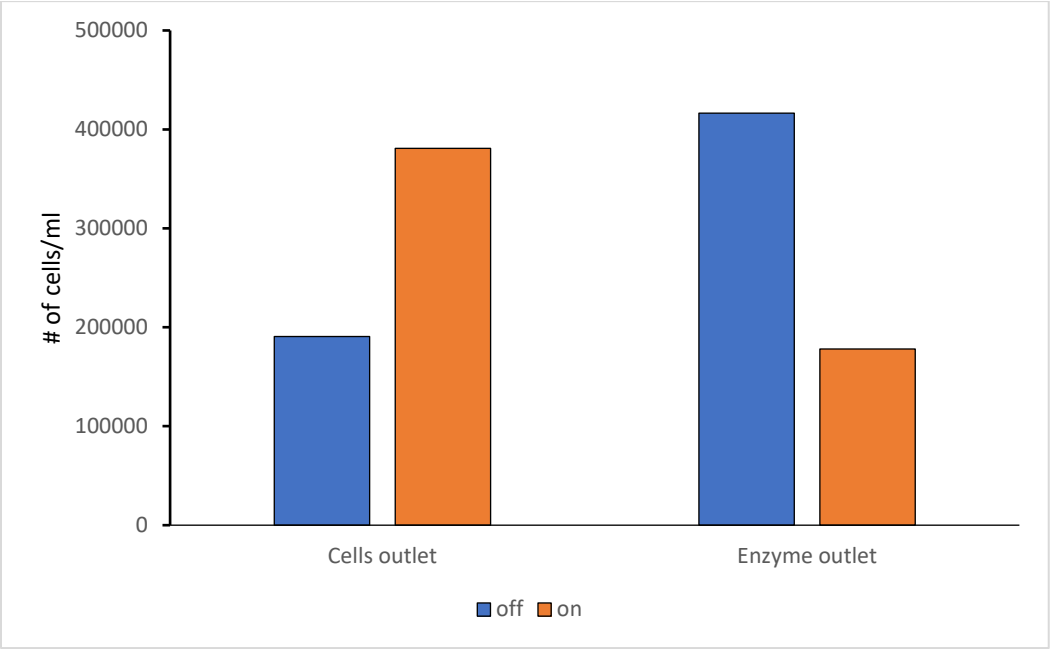

Figure 39- **Results of multilayer laminated device ran with MCF7 cell line.** Suspension of MCF7 cell line in PBS/BSA with 106 cell/ml density was injected to the Cells inlet. Frequency=590.2 KHz voltage=65 Vpp Buffer flow rate=5 ml/min sample flow rate=10 ml/min.

Although the current setup shows a positive total force (acoustic radiation force – gravitational force) in the middle of the channel, it has low efficiency because of negative force near the walls and at the top of the channel. Therefore, optimization of device design with simulation can help in fabrication of a device with higher separation efficiency.

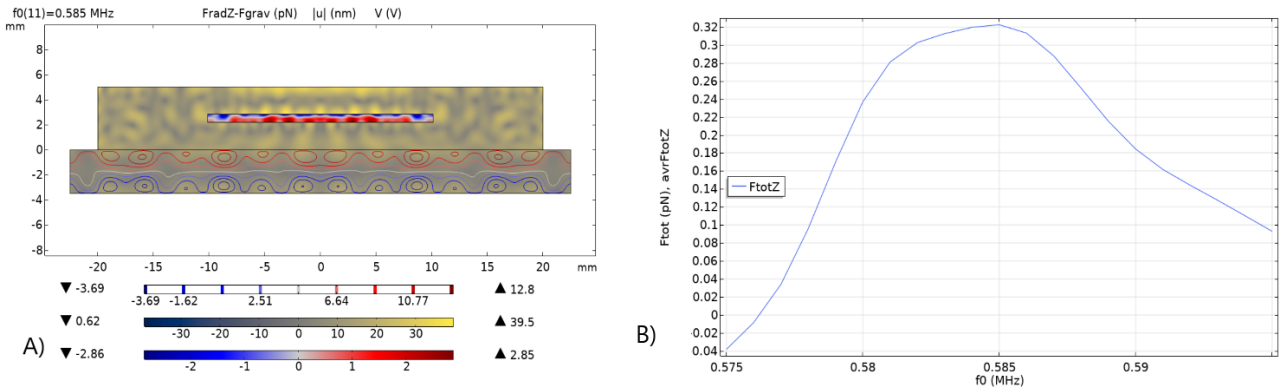

Figure 40- **Simulation results for the current device and Optimized version**. A) Heat map of FradZ-Fgrav (acoustic radiation force - gravitational force) (in pN) in channel, equipotential curves in piezoelectric transducer (in V) and the displacement field (in nm) in the transducer and device body (PMMA) for current device. Parameters: Frequency=0.585 MHz, Channel height=0.64 mm, Bottom layer thickness=2.2 mm, Top layer thickness=2.2 mm, Channel width=20 mm. B) Total force (Ftot) curve versus frequency(f0)

5.4. Conclusion

Tissue dissociation process is currently a manual time-consuming laborious procedure which can introduce artifacts to the results of single cell analysis. Our group has developed a microfluidic platform to offer a fast, cheap, automated, and precise method for single cell preparation. In our studies, it was found that collecting extracted cells in different intervals will increase the cell yield since it reduces the cell exposure time to shear stresses. This finding inspired us to develop a microfluidic device with high throughput to continuously elute liberated cells. Acoustic field can provide cell transfer from one buffer to another in a microfluidic device with high throughput which is desirable in our platform.

Here, we proposed a polymeric acoustofluidic device which can be integrated with previous modules in our platform. This device is manufactured by multilayer lamination which makes it suitable for translation to industrial applications. Our device shows 70% efficiency in transferring cells from one buffer to another. Improving the elution efficiency will be done through adjustment of acoustic field, device design and fluids viscosity. This technology offers a powerful tool for label-free elution of cells and enzyme recycling. It is worth noting that operational parameters of sound waves in our devices are comparable to the power and intensity used in ultrasonic imaging, which is regarded as a safe method even for fetal imaging. Typical cell separation process is done offline which is troublesome for complete automation of microfluidic platforms, but this device will offer inline continuous cell elution from the platform. In a nutshell, our acoustic device has several advantages including biocompatibility, low cost, ease of preparation and operation.

CHAPTER 6: summary and future directions

Tissues are highly complex ecosystems composed of heterogenous cell population that vary in gene expression and function. In order to capture this significant heterogeneity, high throughput single cell analysis methods like flow cytometry and sc RNA sequencing must be employed. However, the analysis methods require that tissues first be dissociated into cellular suspensions. Conventional tissue dissociation protocols are inefficient relying on manual time-consuming process which can cause major artifacts in single cell analysis. In addition, the laborious and uncontrolled manual processing will be a major regulatory barrier hindering the clinical application of single cells in areas of regenerative medicine. Advances in microfluidic technologies has the potential to execute the tissue dissociation process with an automated fast, precise, and high-throughput method. Our group has developed a microfluidic platform for dissociation of tissue to single cells. In my thesis, I have worked on optimization of this platform for heart and liver tissue which gave us a better understanding of processing conditions on device efficiency. It shows how our platform affects cell viability, and recovery. It was shown that this platform significantly shortens the processing time and improves the cell yield. Each tissue has its unique cell types with its specific mechanical and biological properties. It is crucially important to develop a digestion process that will not compromise specific cell type because of their sensitivity to an enzyme treatment or shear stress. Since tissue stiffness is a crucial factor determining the cell-cell and cell-ECM interactions, heat and liver tissues were studied which covers a range of tissue stiffness. Four different cell types, representatives of the major tissue functions were chosen to evaluate the device efficiency on cell yield and viability based on counting cells with flow

cytometry based on their protein expression on surface or nucleus. Results showed significant improvement of cell yield for static condition compared to control. More importantly, cell yield was soared notably for interval operation compared to static condition. The major outcome of this step was shortening digestion time while increasing cell yield to 10 times higher for hepatocytes and 4 times higher for cardiomyocytes. Another takeaway was the fact that overexposure to shear stresses after cell liberation will damage the cells and reduce the cell yield.

Next, I focused on the second module in our platform, integrated dissociation, and filtration (IDF) device to understand the dissociation mechanisms involved and their role in cell yield improvement for different cell types. It helps us to design processing conditions for the optimum cell yield. This study showed that we can reduce tissue processing time significantly by application of IDF device. Also, I studied the effect of flow type, pulsatile flow versus continuous shear flow on cell yield. Interestingly, endothelial cells show higher cell yield in pulsatile flow while epithelial cells yield is higher with steady shear flow provided by syringe pump. This study included other effective parameters like flow rate, as well. Flow rate studies showed that flow rate can be increased to 40 ml/min to cut the tissue dissociation time in half without any compromise in cell yield and viability. Finally, I designed an acoustofluidic device which uses acoustic waves in order to move cells from enzyme to a parallel buffer stream, continuously. This device can be integrated to our previous devices and reduce the cell exposure to shear stresses and hence, improve the cell yield. Acoustic elution device (AED) has the privilege of working with high throughput due to the wide channels which makes it compatible with other modules in our tissue dissociation platform. It is a disposable polymeric device fabricated with multilayer

lamination, which is important for commercialization. This device offers continuous purification of the enzyme and its recovery which is valuable for saving time, cost, and labor in research labs. In future, we will add a nylon mesh filter, like those used in the Filter Device, to the divider layer to retain cell aggregates within the sample stream. The aggregates would then be recycled back to the Digestion Device for further dissociation.

This platform can translate to a universal platform for preparation of single cell analysis. It can be an essential part of labs working on single-cell analysis for the development of personalized medicine, regenerative medicine, and pharmacokinetic study of drugs. Additional downstream microfluidic operations such as cell sorting, or capture can be integrated into the final platform for further development of technology.

REFERENCES

1. Dinh, H.Q., et al., *Integrated single-cell transcriptome analysis reveals heterogeneity of esophageal squamous cell carcinoma microenvironment.* Nature Communications, 2021. **12**(1): p. 7335.
2. Lee, R.D., et al., *Single-cell analysis identifies dynamic gene expression networks that govern B cell development and transformation.* Nature Communications, 2021. **12**(1): p. 6843.
3. Mascré, G., et al., *Distinct contribution of stem and progenitor cells to epidermal maintenance.* Nature, 2012. **489**(7415): p. 257-262.
4. Mardis, E.R., *The emergence of cancer genomics in diagnosis and precision medicine.* Nature Cancer, 2021. **2**(12): p. 1263-1264.
5. Fernandez, D.M. and C. Giannarelli, *Immune cell profiling in atherosclerosis: role in research and precision medicine.* Nature Reviews Cardiology, 2022. **19**(1): p. 43-58.
6. Soret, P., et al., *A new molecular classification to drive precision treatment strategies in primary Sjögren's syndrome.* Nature Communications, 2021. **12**(1): p. 3523.
7. Kürten, C.H.L., et al., *Investigating immune and non-immune cell interactions in head and neck tumors by single-cell RNA sequencing.* Nature Communications, 2021. **12**(1): p. 7338.
8. Kang, J.B., et al., *Efficient and precise single-cell reference atlas mapping with Symphony.* Nature Communications, 2021. **12**(1): p. 5890.
9. Luecken, M.D., et al., *Benchmarking atlas-level data integration in single-cell genomics.* Nature Methods, 2021.
10. Uhlén, M., et al., *Tissue-based map of the human proteome.* Science, 2015. **347**(6220): p. 1260419.
11. Holmes, G., et al., *Single-cell analysis identifies a key role for Hhip in murine coronal suture development.* Nature Communications, 2021. **12**(1): p. 7132.
12. Rouco, R., et al., *Cell-specific alterations in Pitx1 regulatory landscape activation caused by the loss of a single enhancer.* Nature Communications, 2021. **12**(1): p. 7235.
13. Oltersdorf, T., et al., *An inhibitor of Bcl-2 family proteins induces regression of solid tumours.* Nature, 2005. **435**(7042): p. 677-681.
14. Hosic, S., S.K. Murthy, and A.N. Koppes, *Microfluidic Sample Preparation for Single Cell Analysis.* Analytical Chemistry, 2016. **88**(1): p. 354-380.
15. Heath, J.R., A. Ribas, and P.S. Mischel, *Single-cell analysis tools for drug discovery and development.* Nature Reviews Drug Discovery, 2016. **15**(3): p. 204-216.
16. Gibellini, L., et al., *Single-Cell Approaches to Profile the Response to Immune Checkpoint Inhibitors.* Frontiers in Immunology, 2020. **11**(490).
17. Spitzer, Matthew H. and Garry P. Nolan, *Mass Cytometry: Single Cells, Many Features.* Cell, 2016. **165**(4): p. 780-791.
18. Adan, A., et al., *Flow cytometry: basic principles and applications.* Critical Reviews in Biotechnology, 2017. **37**(2): p. 163-176.
19. Bashour, F.A., T. McConnell, and W.F. Miller, *Circulatory and respiratory changes in patients with Laennec's cirrhosis of the liver.* American Heart Journal, 1967. **74**(4): p. 569-577.
20. Moignard, V., et al., *Decoding the regulatory network of early blood development from single-cell gene expression measurements.* Nature biotechnology, 2015. **33**(3): p. 269-276.
21. Papalexi, E. and R. Satija, *Single-cell RNA sequencing to explore immune cell heterogeneity.* Nature Reviews Immunology, 2018. **18**(1): p. 35-45.

22. Li, D., et al., *Isolation and culture of adult mouse cardiomyocytes for cell signaling and in vitro cardiac hypertrophy.* Journal of visualized experiments : JoVE, 2014(87): p. 51357.
23. Pinto, A.R., et al., *Isolation and analysis of single cells from the mouse heart.* Journal of Immunological Methods, 2013. **393**(1): p. 74-80.
24. Liu, W., et al., *Sample preparation method for isolation of single-cell types from mouse liver for proteomic studies.* PROTEOMICS, 2011. **11**(17): p. 3556-3564.
25. Welch, E.C., H. Yu, and A. Tripathi, *Optimization of a Clinically Relevant Chemical-Mechanical Tissue Dissociation Workflow for Single-Cell Analysis.* Cellular and Molecular Bioengineering, 2021. **14**(3): p. 241-258.
26. Tung, P.-Y., et al., *Batch effects and the effective design of single-cell gene expression studies.* Scientific Reports, 2017. **7**(1): p. 39921.
27. Denisenko, E., et al., *Systematic assessment of tissue dissociation and storage biases in single-cell and single-nucleus RNA-seq workflows.* Genome Biology, 2020. **21**(1): p. 130.
28. Nguyen, Q.H., et al., *Experimental Considerations for Single-Cell RNA Sequencing Approaches.* Frontiers in Cell and Developmental Biology, 2018. **6**(108).
29. Posch, A., *2D PAGE: Sample Preparation and Fractionation*. Methods in Molecular Biology. 2008: Humana Press. 340.
30. McBeth, C., et al., *Automated Tissue Dissociation for Rapid Extraction of Viable Cells.* Procedia CIRP, 2017. **65**: p. 88-92.
31. Liu, Y. and A.K. Singh, *Microfluidic Platforms for Single-Cell Protein Analysis.* Journal of Laboratory Automation, 2013. **18**(6): p. 446-454.
32. Hattersley, S.M., et al., *Development of a microfluidic device for the maintenance and interrogation of viable tissue biopsies.* Lab on a Chip, 2008. **8**(11): p. 1842-1846.
33. Wallman, L., et al., *Biogrid—a microfluidic device for large-scale enzyme-free dissociation of stem cell aggregates.* Lab on a Chip, 2011. **11**(19): p. 3241-3248.
34. Lin, C.-H., et al., *Single-Cell Enzyme-Free Dissociation of Neurospheres Using a Microfluidic Chip.* Analytical Chemistry, 2013. **85**(24): p. 11920-11928.
35. Qiu, X., et al., *Microfluidic channel optimization to improve hydrodynamic dissociation of cell aggregates and tissue.* Scientific reports, 2018. **8**(1): p. 2774-2774.
36. Qiu, X., et al., *Microfluidic filter device with nylon mesh membranes efficiently dissociates cell aggregates and digested tissue into single cells.* Lab on a Chip, 2018. **18**(18): p. 2776-2786.
37. Qiu, X., et al., *Microfluidic device for rapid digestion of tissues into cellular suspensions.* Lab on a Chip, 2017. **17**(19): p. 3300-3309.
38. Lombardo, J.A., et al., *Microfluidic platform accelerates tissue processing into single cells for molecular analysis and primary culture models.* Nature Communications, 2021. **12**(1): p. 2858.
39. Baldan, V., et al., *Efficient and reproducible generation of tumour-infiltrating lymphocytes for renal cell carcinoma.* British journal of cancer, 2015. **112**(9): p. 1510-1518.
40. Kang, Y.-T., et al., *Label-free Rapid Viable Enrichment of Circulating Tumor Cell by Photosensitive Polymer-based Microfilter Device.* Theranostics, 2017. **7**(13): p. 3179-3191.
41. Ahmed, O., et al. *Tissue dissociation miniaturized platform for uterine stem cell isolation and culture*. in *2014 Cairo International Biomedical Engineering Conference (CIBEC)*. 2014.
42. Jiang, L., et al. *Dissociation of brain tissue into viable single neurons in a microfluidic device*. in *2015 9th IEEE International Conference on Nano/Molecular Medicine & Engineering (NANOMED)*. 2015.
43. Al-Mofty, S., et al., *A microfluidic platform for dissociating clinical scale tissue samples into single cells.* Biomedical Microdevices, 2021. **23**(1): p. 10.
44. Gu, Y., et al., *Plastic-based acoustofluidic devices for high-throughput, biocompatible platelet separation.* Lab on a Chip, 2019. **19**(3): p. 394-402.

45. Adams, J.D., et al., *High-throughput, temperature-controlled microchannel acoustophoresis device made with rapid prototyping.* Journal of Micromechanics and Microengineering, 2012. **22**(7): p. 075017.
46. Bruus, H., *Acoustofluidics 2: Perturbation theory and ultrasound resonance modes.* Lab on a Chip, 2012. **12**(1): p. 20-28.
47. Lenshof, A., C. Magnusson, and T. Laurell, *Acoustofluidics 8: Applications of acoustophoresis in continuous flow microsystems.* Lab on a Chip, 2012. **12**(7): p. 1210-1223.
48. Antfolk, M. and T. Laurell, *Acoustofluidic Blood Component Sample Preparation and Processing in Medical Applications*, in *Applications of Microfluidic Systems in Biology and Medicine*, M. Tokeshi, Editor. 2019, Springer Singapore: Singapore. p. 1-25.
49. Ding, X., et al., *Cell separation using tilted-angle standing surface acoustic waves.* Proceedings of the National Academy of Sciences of the United States of America, 2014. **111**(36): p. 12992-12997.
50. Leibacher, I., P. Reichert, and J. Dual, *Microfluidic droplet handling by bulk acoustic wave (BAW) acoustophoresis.* Lab on a Chip, 2015. **15**(13): p. 2896-2905.
51. Lenshof, A., et al., *Acoustofluidics 5: Building microfluidic acoustic resonators.* Lab on a Chip, 2012. **12**(4): p. 684-695.
52. Hill, M., Y. Shen, and J.J. Hawkes, *Modelling of layered resonators for ultrasonic separation.* Ultrasonics, 2002. **40**(1): p. 385-392.
53. Hill, M., *The selection of layer thicknesses to control acoustic radiation force profiles in layered resonators.* The Journal of the Acoustical Society of America, 2003. **114**(5): p. 2654-2661.
54. Moiseyenko, R.P. and H. Bruus, *Whole-System Ultrasound Resonances as the Basis for Acoustophoresis in All-Polymer Microfluidic Devices.* Physical Review Applied, 2019. **11**(1): p. 014014.
55. Silva, R., et al., *Rapid prototyping and parametric optimization of plastic acoustofluidic devices for blood–bacteria separation.* Biomedical Microdevices, 2017. **19**(3): p. 70.
56. Lissandrello, C., et al., *Purification of Lymphocytes by Acoustic Separation in Plastic Microchannels.* SLAS TECHNOLOGY: Translating Life Sciences Innovation, 2018. **23**(4): p. 352-363.
57. Mueller, A., et al., *Continuous acoustic separation in a thermoplastic microchannel.* Journal of Micromechanics and Microengineering, 2013. **23**.
58. Luecken, M.D. and F.J. Theis, *Current best practices in single-cell RNA-seq analysis: a tutorial.* Molecular systems biology, 2019. **15**(6): p. e8746-e8746.
59. Du, Y., N. Li, and M. Long, *Chapter 6 - Liver sinusoid on a chip*, in *Methods in Cell Biology*, J. Doh, D. Fletcher, and M. Piel, Editors. 2018, Academic Press. p. 105-134.
60. Lee, W.-Y., et al., *An intravascular immune response to Borrelia burgdorferi involves Kupffer cells and iNKT cells.* Nature Immunology, 2010. **11**(4): p. 295-302.
61. Wilkening, S., F. Stahl, and A. Bader, *COMPARISON OF PRIMARY HUMAN HEPATOCYTES AND HEPATOMA CELL LINE HEPG2 WITH REGARD TO THEIR BIOTRANSFORMATION PROPERTIES.* Drug Metabolism and Disposition, 2003. **31**(8): p. 1035-1042.
62. Georges, P.C., et al., *Increased stiffness of the rat liver precedes matrix deposition: implications for fibrosis.* American Journal of Physiology-Gastrointestinal and Liver Physiology, 2007. **293**(6): p. G1147-G1154.
63. Desai, S.S., et al., *Physiological ranges of matrix rigidity modulate primary mouse hepatocyte function in part through hepatocyte nuclear factor 4 alpha.* Hepatology, 2016. **64**(1): p. 261-275.
64. Manbachi, A., et al., *Microcirculation within grooved substrates regulates cell positioning and cell docking inside microfluidic channels.* Lab on a Chip, 2008. **8**(5): p. 747-754.

65. Powers, M.J., et al., *A microfabricated array bioreactor for perfused 3D liver culture.* Biotechnology and Bioengineering, 2002. **78**(3): p. 257-269.
66. Kim, L., et al., *A practical guide to microfluidic perfusion culture of adherent mammalian cells.* Lab on a Chip, 2007. **7**(6): p. 681-694.
67. Li, Y.-S.J., J.H. Haga, and S. Chien, *Molecular basis of the effects of shear stress on vascular endothelial cells.* Journal of Biomechanics, 2005. **38**(10): p. 1949-1971.
68. Gaver, D.P. and S.M. Kute, *A Theoretical Model Study of the Influence of Fluid Stresses on a Cell Adhering to a Microchannel Wall.* Biophysical Journal, 1998. **75**(2): p. 721-733.
69. Zhou, P. and W.T. Pu, *Recounting Cardiac Cellular Composition.* Circulation research, 2016. **118**(3): p. 368-370.
70. Ackers-Johnson, M., W.L.W. Tan, and R.S.-Y. Foo, *Following hearts, one cell at a time: recent applications of single-cell RNA sequencing to the understanding of heart disease.* Nature Communications, 2018. **9**(1): p. 4434.
71. Forough, R., C. Scarcello, and M. Perkins, *Cardiac biomarkers: a focus on cardiac regeneration.* The journal of Tehran Heart Center, 2011. **6**(4): p. 179-186.
72. Hörning, M., et al., *Rigidity Matching between Cells and the Extracellular Matrix Leads to the Stabilization of Cardiac Conduction.* Biophysical Journal, 2012. **102**(3): p. 379-387.
73. Brown, G.E. and S.R. Khetani, *Microfabrication of liver and heart tissues for drug development.* Philosophical Transactions of the Royal Society B: Biological Sciences, 2018. **373**(1750): p. 20170225.
74. Abulaiti, M., et al., *Establishment of a heart-on-a-chip microdevice based on human iPS cells for the evaluation of human heart tissue function.* Scientific Reports, 2020. **10**(1): p. 19201.
75. Nguyen, T.V., et al., *Establishment of a Hepatocyte-Kupffer Cell Coculture Model for Assessment of Proinflammatory Cytokine Effects on Metabolizing Enzymes and Drug Transporters.* Drug Metabolism and Disposition, 2015. **43**(5): p. 774-785.
76. Petka, W.A., et al., *Reversible Hydrogels from Self-Assembling Artificial Proteins.* Science, 1998. **281**(5375): p. 389-392.
77. Mafuné, F., et al., *Dissociation and Aggregation of Gold Nanoparticles under Laser Irradiation.* The Journal of Physical Chemistry B, 2001. **105**(38): p. 9050-9056.
78. Lindvall, O. and Z. Kokaia, *Stem cells for the treatment of neurological disorders.* Nature, 2006. **441**(7097): p. 1094-1096.
79. Watanabe, K., et al., *A ROCK inhibitor permits survival of dissociated human embryonic stem cells.* Nature Biotechnology, 2007. **25**(6): p. 681-686.
80. Didar, T.F., et al., *Separation of rare oligodendrocyte progenitor cells from brain using a high-throughput multilayer thermoplastic-based microfluidic device.* Biomaterials, 2013. **34**(22): p. 5588-5593.
81. Mattei, D., et al., *Enzymatic Dissociation Induces Transcriptional and Proteotype Bias in Brain Cell Populations.* International Journal of Molecular Sciences, 2020. **21**(21): p. 7944.
82. Ayata, P., et al., *Epigenetic regulation of brain region-specific microglia clearance activity.* Nature Neuroscience, 2018. **21**(8): p. 1049-1060.
83. Mahat, Dig B., et al., *Mammalian Heat Shock Response and Mechanisms Underlying Its Genome-wide Transcriptional Regulation.* Molecular Cell, 2016. **62**(1): p. 63-78.
84. Huang, L.R., et al., *Continuous Particle Separation Through Deterministic Lateral Displacement.* Science, 2004. **304**(5673): p. 987-990.
85. Yeo, L.Y., et al., *Microfluidic Devices for Bioapplications.* Small, 2011. **7**(1): p. 12-48.
86. Gubala, V., et al., *Point of Care Diagnostics: Status and Future.* Analytical Chemistry, 2012. **84**(2): p. 487-515.

87. Qiu, X., et al., *Microfluidic device for mechanical dissociation of cancer cell aggregates into single cells.* Lab on a Chip, 2015. **15**(1): p. 339-350.
88. Booth, R. and H. Kim, *Characterization of a microfluidic in vitro model of the blood-brain barrier (μBBB).* Lab on a Chip, 2012. **12**(10): p. 1784-1792.
89. Schirhagl, R., et al., *Microfluidic purification and analysis of hematopoietic stem cells from bone marrow.* Lab on a Chip, 2011. **11**(18): p. 3130-3135.
90. Carlo, D.D., L.Y. Wu, and L.P. Lee, *Dynamic single cell culture array.* Lab on a Chip, 2006. **6**(11): p. 1445-1449.
91. Khademhosseini, A., et al., *Microscale technologies for tissue engineering and biology.* Proceedings of the National Academy of Sciences of the United States of America, 2006. **103**(8): p. 2480-2487.
92. Renner, W.A., et al., *Cell–cell adhesion and aggregation: Influence on the growth behavior of CHO cells.* Biotechnology and Bioengineering, 1993. **41**(2): p. 188-193.
93. Moreira, J., et al., *Formation and disruption of animal cell aggregates in stirred vessels: Mechanisms and kinetic studies.* Chemical Engineering Science, 1995. **50**(17): p. 2747-2764.
94. Harshe, Y.M., M. Lattuada, and M. Soos, *Experimental and Modeling Study of Breakage and Restructuring of Open and Dense Colloidal Aggregates.* Langmuir, 2011. **27**(10): p. 5739-5752.
95. Rozario, T. and D.W. DeSimone, *The extracellular matrix in development and morphogenesis: A dynamic view.* Developmental Biology, 2010. **341**(1): p. 126-140.
96. Zamprogno, P., et al., *Second-generation lung-on-a-chip with an array of stretchable alveoli made with a biological membrane.* Communications Biology, 2021. **4**(1): p. 168.
97. Reichard, A. and K. Asosingh, *Best Practices for Preparing a Single Cell Suspension from Solid Tissues for Flow Cytometry.* Cytometry Part A, 2019. **95**(2): p. 219-226.
98. Liao, M., et al., *Structure of the TRPV1 ion channel determined by electron cryo-microscopy.* Nature, 2013. **504**(7478): p. 107-112.
99. Ohuchi, E., et al., *Membrane Type 1 Matrix Metalloproteinase Digests Interstitial Collagens and Other Extracellular Matrix Macromolecules*.* Journal of Biological Chemistry, 1997. **272**(4): p. 2446-2451.
100. Yang, J. and R.A. Weinberg, *Epithelial-Mesenchymal Transition: At the Crossroads of Development and Tumor Metastasis.* Developmental Cell, 2008. **14**(6): p. 818-829.
101. Gonzalez, D.M. and D. Medici, *Signaling mechanisms of the epithelial-mesenchymal transition.* Science Signaling, 2014. **7**(344): p. re8-re8.
102. Maruthamuthu, V., et al., *Cell-ECM traction force modulates endogenous tension at cell–cell contacts.* Proceedings of the National Academy of Sciences, 2011. **108**(12): p. 4708-4713.
103. Tseng, Q., et al., *Spatial organization of the extracellular matrix regulates cell–cell junction positioning.* Proceedings of the National Academy of Sciences, 2012. **109**(5): p. 1506-1511.
104. Sakai, T., M. Larsen, and K.M. Yamada, *Fibronectin requirement in branching morphogenesis.* Nature, 2003. **423**(6942): p. 876-881.
105. Shih, W. and S. Yamada, *N-cadherin-mediated cell–cell adhesion promotes cell migration in a three-dimensional matrix.* Journal of Cell Science, 2012. **125**(15): p. 3661-3670.
106. Sander, E.E., et al., *Matrix-dependent Tiam1/Rac Signaling in Epithelial Cells Promotes Either Cell–Cell Adhesion or Cell Migration and Is Regulated by Phosphatidylinositol 3-Kinase.* Journal of Cell Biology, 1998. **143**(5): p. 1385-1398.
107. Adam, M., A.S. Potter, and S.S. Potter, *Psychrophilic proteases dramatically reduce single-cell RNA-seq artifacts: a molecular atlas of kidney development.* Development (Cambridge, England), 2017. **144**(19): p. 3625-3632.

108. O'Flanagan, C.H., et al., *Dissociation of solid tumor tissues with cold active protease for single-cell RNA-seq minimizes conserved collagenase-associated stress responses.* Genome biology, 2019. **20**(1): p. 210-210.
109. van den Brink, S.C., et al., *Single-cell sequencing reveals dissociation-induced gene expression in tissue subpopulations.* Nature Methods, 2017. **14**(10): p. 935-936.
110. Cines, D.B., et al., *Endothelial Cells in Physiology and in the Pathophysiology of Vascular Disorders.* Blood, 1998. **91**(10): p. 3527-3561.
111. Mehta, D. and A.B. Malik, *Signaling Mechanisms Regulating Endothelial Permeability.* Physiological Reviews, 2006. **86**(1): p. 279-367.
112. Jalali, S., et al., *Integrin-mediated mechanotransduction requires its dynamic interaction with specific extracellular matrix (ECM) ligands.* Proceedings of the National Academy of Sciences, 2001. **98**(3): p. 1042-1046.
113. Moy, A.B., et al., *Histamine alters endothelial barrier function at cell-cell and cell-matrix sites.* American Journal of Physiology-Lung Cellular and Molecular Physiology, 2000. **278**(5): p. L888-L898.
114. Hur, S.S., et al., *Roles of cell confluency and fluid shear in 3-dimensional intracellular forces in endothelial cells.* Proceedings of the National Academy of Sciences, 2012. **109**(28): p. 11110-11115.
115. Chien, S., et al., *Molecular basis of mechanical modulation of endothelial cell migration.* Frontiers in Bioscience-Landmark, 2005. **10**(2): p. 1985-2000.
116. Medzhitov, R., *Origin and physiological roles of inflammation.* Nature, 2008. **454**(7203): p. 428-435.
117. Park, C.O. and T.S. Kupper, *The emerging role of resident memory T cells in protective immunity and inflammatory disease.* Nature Medicine, 2015. **21**(7): p. 688-697.
118. Masopust, D., et al., *Dynamic T cell migration program provides resident memory within intestinal epithelium.* Journal of Experimental Medicine, 2010. **207**(3): p. 553-564.
119. E. Korpos, C.W.a.L.S., *Multiple Roles of the Intracellular Matrix in Inflammation.* Current Pharmaceutical Design, 2009. **15**(12).
120. Parker, A.L. and T.R. Cox, *The Role of the ECM in Lung Cancer Dormancy and Outgrowth.* Frontiers in Oncology, 2020. **10**(1766).
121. Muller, W.A., *Mechanisms of Leukocyte Transendothelial Migration.* Annual Review of Pathology: Mechanisms of Disease, 2011. **6**(1): p. 323-344.
122. Park, J., et al., *Single-cell transcriptomics of the mouse kidney reveals potential cellular targets of kidney disease.* Science (New York, N.Y.), 2018. **360**(6390): p. 758-763.
123. Rozenblatt-Rosen, O., et al., *The Human Cell Atlas: from vision to reality.* Nature, 2017. **550**(7677): p. 451-453.
124. Liao, J., et al., *Single-cell RNA sequencing of human kidney.* Scientific data, 2020. **7**(1): p. 4-4.
125. Wu, H., et al., *Advantages of Single-Nucleus over Single-Cell RNA Sequencing of Adult Kidney: Rare Cell Types and Novel Cell States Revealed in Fibrosis.* Journal of the American Society of Nephrology : JASN, 2019. **30**(1): p. 23-32.
126. Vieira Braga, F.A. and R.J. Miragaia, *Tissue Handling and Dissociation for Single-Cell RNA-Seq*, in *Single Cell Methods: Sequencing and Proteomics*, V. Proserpio, Editor. 2019, Springer New York: New York, NY. p. 9-21.
127. Wolf, F.A., P. Angerer, and F.J. Theis, *SCANPY: large-scale single-cell gene expression data analysis.* Genome Biology, 2018. **19**(1): p. 15.
128. Wagner, A., A. Regev, and N. Yosef, *Revealing the vectors of cellular identity with single-cell genomics.* Nature Biotechnology, 2016. **34**(11): p. 1145-1160.
129. Regev, A., et al., *The Human Cell Atlas.* eLife, 2017. **6**: p. e27041.

130. Bendall, S.C. and G.P. Nolan, *From single cells to deep phenotypes in cancer.* Nature Biotechnology, 2012. **30**(7): p. 639-647.
131. Bendall, S.C., et al., *Single-Cell Mass Cytometry of Differential Immune and Drug Responses Across a Human Hematopoietic Continuum.* Science, 2011. **332**(6030): p. 687-696.
132. Pollen, A.A., et al., *Low-coverage single-cell mRNA sequencing reveals cellular heterogeneity and activated signaling pathways in developing cerebral cortex.* Nature Biotechnology, 2014. **32**(10): p. 1053-1058.
133. Welch, J.D., et al., *Single-Cell Multi-omic Integration Compares and Contrasts Features of Brain Cell Identity.* Cell, 2019. **177**(7): p. 1873-1887.e17.
134. Hotze, E.M., T. Phenrat, and G.V. Lowry, *Nanoparticle Aggregation: Challenges to Understanding Transport and Reactivity in the Environment.* Journal of Environmental Quality, 2010. **39**(6): p. 1909-1924.
135. Men, Y., J. Rieger, and G. Strobl, *Role of the Entangled Amorphous Network in Tensile Deformation of Semicrystalline Polymers.* Physical Review Letters, 2003. **91**(9): p. 095502.
136. Kremer, K. and G.S. Grest, *Dynamics of entangled linear polymer melts: A molecular-dynamics simulation.* The Journal of Chemical Physics, 1990. **92**(8): p. 5057-5086.
137. Sonmez, U.M., et al., *Endothelial cell polarization and orientation to flow in a novel microfluidic multimodal shear stress generator.* Lab on a Chip, 2020. **20**(23): p. 4373-4390.
138. Matsuura, K., et al., *Adequate taylor couette flow-mediated shear stress is useful for dissociating human iPS cell-derived cell aggregates.* Regenerative Therapy, 2019. **12**: p. 6-13.
139. Chien, S., *Mechanotransduction and endothelial cell homeostasis: the wisdom of the cell.* American Journal of Physiology-Heart and Circulatory Physiology, 2007. **292**(3): p. H1209-H1224.
140. Wei, S.-Y. and J.-J. Chiu, *Mechanical Regulation of Epigenetic Modifications in Vascular Biology and Pathobiology*, in *Vascular Mechanobiology in Physiology and Disease*, M. Hecker and D.J. Duncker, Editors. 2021, Springer International Publishing: Cham. p. 241-276.
141. Gao, Y., et al., *Acoustic Microfluidic Separation Techniques and Bioapplications: A Review.* Micromachines, 2020. **11**(10): p. 921.
142. Yeo, D.C., et al., *Interference-free Micro/nanoparticle Cell Engineering by Use of High-Throughput Microfluidic Separation.* ACS Applied Materials & Interfaces, 2015. **7**(37): p. 20855-20864.
143. Liang, W., et al., *Microfluidic-based cancer cell separation using active and passive mechanisms.* Microfluidics and Nanofluidics, 2020. **24**(4): p. 26.
144. Glynne-Jones, P., et al., *Flexible Acoustic Particle Manipulation Device with Integrated Optical Waveguide for Enhanced Microbead Assays.* Analytical Sciences, 2009. **25**(2): p. 285-291.
145. Settnes, M. and H. Bruus, *Forces acting on a small particle in an acoustical field in a viscous fluid.* Physical Review E, 2012. **85**(1): p. 016327.
146. Unger, M.A., et al., *Monolithic Microfabricated Valves and Pumps by Multilayer Soft Lithography.* Science, 2000. **288**(5463): p. 113-116.
147. Mark F. Hamilton, D.T.B., *Nonlinear acoustics*. 1997.